School of Electrical Engineering, Computing and
Mathematical Sciences

Link Scheduling in Rechargeable Wireless Sensor Networks with Limited Harvested Energy

Tony
0000-0002-4284-6587

This thesis is presented for the Degree of
Doctor of Philosophy
of
Curtin University

August 2021

Declaration

To the best of my knowledge and belief this thesis contains no material previously published by any other person except where due acknowledgment has been made.

This thesis contains no material which has been accepted for the award of any other degree or diploma in any university.

Signature:

Date: ....

"*To Lely Hiryanto, Callysta Lie, and Edrick Lie*"

"*To Wahab Jie, Ervina Teh, Yenti, and Linda*"

"*To Hiryanto Balok and Mulyati Djaja*"

— AUTHOR

Abstract

Wireless Sensor Networks (WSNs) have been used in many applications of the Internet of Things. A well-known issue faced by WSNs is that nodes have limited energy. To date, rechargeable WSNs (rWSNs) are of great interest because sensor nodes are able to harvest energy from their environment, e.g., solar and wind, and store the harvested energy in rechargeable batteries. However, rWSNs have a number of limitations. First, each node can have a varying energy harvesting time, i.e., the time required to accumulate energy. Second, the battery characteristics at each node, which include capacity, leakage rate, and storage efficiency, have an impact on the operation of rWSNs. Third, the battery suffers from *memory effect* if it is partially charged and discharged. Such an effect will decrease the battery capacity, and thus will eventually shorten its lifetime. The lifetime of the battery is also affected by the total number of battery charge/discharge cycles.

Another important issue in rWSNs is channel access or link scheduling. This thesis considers a rWSN that uses a Time Division Multiple Access (TDMA) link schedule. A TDMA link scheduler ensures packet transmissions in rWSNs are interference-free. Thus, the energy used for transmission/reception is not wasted due to interference, which saves energy. A link scheduler is responsible for determining the set of transmitting and receiving nodes in each time slot. As the schedule repeats, it is important to minimise the schedule length (in terms of slots) as this allows nodes to transmit more frequently. Consequently, when links are activated more frequently, the rWSNs will have a high capacity. However, in addition to interference, a link scheduler must consider the varying energy harvesting rates of nodes. More specifically, a link can be activated only if its end nodes have sufficient energy to transmit/receive packets.

The first part of this thesis focuses on the problem of generating the shortest TDMA schedule, called Link Scheduling in Harvest Use Store (LSHUS), for use in rWSNs. This novel problem considers: 1) energy harvesting time, 2) Harvest-Use-Store protocol that allows the node to use the harvested energy immediately and stores the remaining energy in its battery for future use, and 3) battery's capacity, leakage rate, and storage efficiency. This thesis shows the problem at hand is, in general, NP-Complete. It presents analytically the optimal schedule for fixed topologies, e.g., Line, Binary Tree, and Grid. Further, it proposes a greedy heuristic algorithm, called LS-rWSN, to solve the problem. Our experiments show that harvesting time, leakage rate, and storage efficiency, significantly affect the schedule length, whereas battery capacity is an insignificant factor.

The second part of this thesis focuses on another problem of deriving the TDMA link schedule, called Link Scheduling with Memory Effect-1 (LSME-1), for rWSNs. This second problem considers: 1) energy harvesting time, 2) Harvest-Store-Use protocol that requires the harvested energy to be stored in the node's battery first before it can be used, 3) battery capacity, leakage rate, and storage efficiency, and 4) a *battery cycle* constraint which requires the battery to be charged (discharged) completely before it can be fully discharged (charged) again. The constraint is used to overcome the memory effect. This thesis shows analytically: (i) the optimal schedule in fixed topologies, and that (ii) the battery cycle constraint and leaking batteries can lead to unscheduled links. Further, it describes a greedy heuristic solution, called LSBCC, that schedules links according to when their corresponding nodes have sufficient energy. Our simulations show that enforcing the battery cycle constraint increases the schedule length. On the other hand, the constraint reduces the number of charge/discharge cycles, and hence makes the batteries last longer.

The last part of this thesis addresses a problem, called Link Scheduling with Memory Effect-2 (LSME-2). Problem LSME-2 is an extension of LSME-1 that considers nodes equipped with a dual-battery system. The dual-battery system aims to reduce the effect of using the battery cycle constraint on the schedule length. Further, it reduces the number of battery's charge/discharge cycles. This thesis presents all possible battery states and transitions for nodes. It then outlines a greedy algorithm, called LSDBS, to schedule links according to the earliest time in which batteries at the end nodes of each link can be discharged. Our results show that equipping nodes with a dual-battery system decreases the schedule length by up to 35.19% as compared to using a single battery. Such a system also reduces the number of charge/discharge cycles of the single battery by up to 13.04%. Finally, a longer energy harvesting time increases link schedules linearly, but has no impact on the number of charge/discharge cycles.

The performance of all proposed algorithms is evaluated using arbitrary networks. The results show the merits and effectiveness of the solutions proposed in this thesis.

Acknowledgements

This thesis would not have been possible without the support of many people. In particular, I would like to express my sincere gratitude and thanks to my supervisor, Dr. Sie Teng Soh, for the generous guidance, invaluable advice, support, and encouragement he has given me throughout my PhD. Without his contribution in terms of time, ideas, and hard work, I doubt I would have made it halfway through or achieved any published works. I would also like to express my thanks to my co-supervisor, Associate Professor Mihai Lazarescu, for his support. In addition, I am thankful to Associate Professor Kwan-Wu Chin at the University of Wollongong, for sacrificing his personal time to review and comment on my papers.

I also want to thank all the anonymous reviewers and editors of conferences and journals for their time, effort, and comments. Their suggestions have certainly raised the quality of my publications.

Special thanks must go to the Indonesia Lecturer Scholarship (BUDI) by Indonesia Endowment Fund for Education (LPDP), Ministry of Finance, Republic of Indonesia, for the scholarship. I would have been unable to undertake a PhD without the financial support. Thanks also to the Tarumanagara University, Jakarta, Indonesia, especially the Faculty of Information Technology, for the support to do this study.

My PhD journey at Curtin University was made wonderful because of the many friends I have made. Thanks to ISSU Curtin, Julie and Raquel, for their support during my PhD. Thanks to EECMS staff, Antoni, Robyn, Sucy, Tasneem, Simret, Ba-Tuong, and Simon, for the help in school administration. Special gratitude to Haris Sri Purwoko, Siti Nurlaela, Faiz, Adnan, Debby, Abid Halim, and Made Andik Setiawan, for their assistance when I first arrived in Perth. Thanks to Agus, Christofori MRR "Iin" Nastiti, and Cikal, for their friendship. Thanks to Kalamunda friends, Arnold Kaudin, Rebecca Santi, Sanyulandy Leowalu, Zakaria Victor Kareth, Benedicta Santoso, and Kemal Faza Hastadi, for all the joyful conversations. Thanks to Imelda Tandra, Manlika Ratchagit, Kreangkri, and Suwijak, for the adventurous road trip. Thanks to my English teacher, Elena and Reva Ramiah for teaching until I achieved the required IELTS score. Thanks to Josep and Zach in ACE Learning Centre on Lawson Street for countless conversations. Thanks also to AIPSSA and BSWA friends, for the opportunities to contribute. Thanks to my research mates in Building 314 Level 4, Quang, Linh, Lara, Yuthika, Gaurav, and Suparna, for a pleasant working environment.

Lastly, I am thankful to my wife, Lely Hiryanto, for all her support, for her cooking, and for loving and taking care of our daughter, Callysta Lie, while I spent many hours until the middle of many nights and weekends, writing this thesis and meeting the submission deadlines for conferences and journal papers.

Contents

Appendix

List of Figures

List of Tables

Published Works

This thesis is based upon several works that have been presented at conferences and published in journals over the course of the author's PhD. They are listed as follows in chronological order:

1. **Tony**, Sieteng Soh, Kwan-Wu Chin, Mihai Lazarescu, "Link Scheduling in Rechargeable Wireless Sensor Networks with Harvesting Time and Battery Constraints," in *43rd IEEE Conference on Local Computer Networks (LCN)*, Chicago, IL, USA, Oct., 2018. The paper received the Student Participation Grant. It is part of Chapter 3.

2. **Tony Tony**, Sieteng Soh, Kwan-Wu Chin, Mihai Lazarescu,"Link Scheduling in Rechargeable Wireless Sensor Networks with Imperfect Batteries," in *IEEE Access*, vol. 7, pp. 104721−104736, 2019. The paper is part of Chapter 3.

3. **Tony Tony**, Sieteng Soh, Kwan-Wu Chin, Mihai Lazarescu,"Link Scheduling in Rechargeable Wireless Sensor Networks with Battery Memory Effects," in *30th International Telecommunication Networks and Applications Conference (ITNAC)*, Melbourne, Australia, Nov., 2020. The paper received the Student Travel Grant and Best Student Paper. It is part of Chapter 4.

4. **Tony Tony**, Sieteng Soh, Kwan-Wu Chin, Mihai Lazarescu,"Link Scheduling in Rechargeable Wireless Sensor Networks with Imperfect Battery and Memory Effects," in *IEEE Access*, vol. 9, pp. 17803−17819, 2021. The paper is part of Chapter 4.

5. **Tony Tony**, Sieteng Soh, Kwan-Wu Chin, Mihai Lazarescu,"Link Scheduling in Rechargeable Wireless Sensor Networks with a Dual-Battery System," in *IEEE International Conference on Communications (ICC)*, Montreal, Canada, Jun. 2021. The paper received the Student Grant. It is part of Chapter 5.

I have obtained permission from the copyright owners to use any of my own published works in which the copyright is held by another party (publisher and co-author). The copyright information to reuse the published works has been provided in Appendix. Table 1 shows an attribution statement for all published works.

Table 1 Attribution statement for all published works

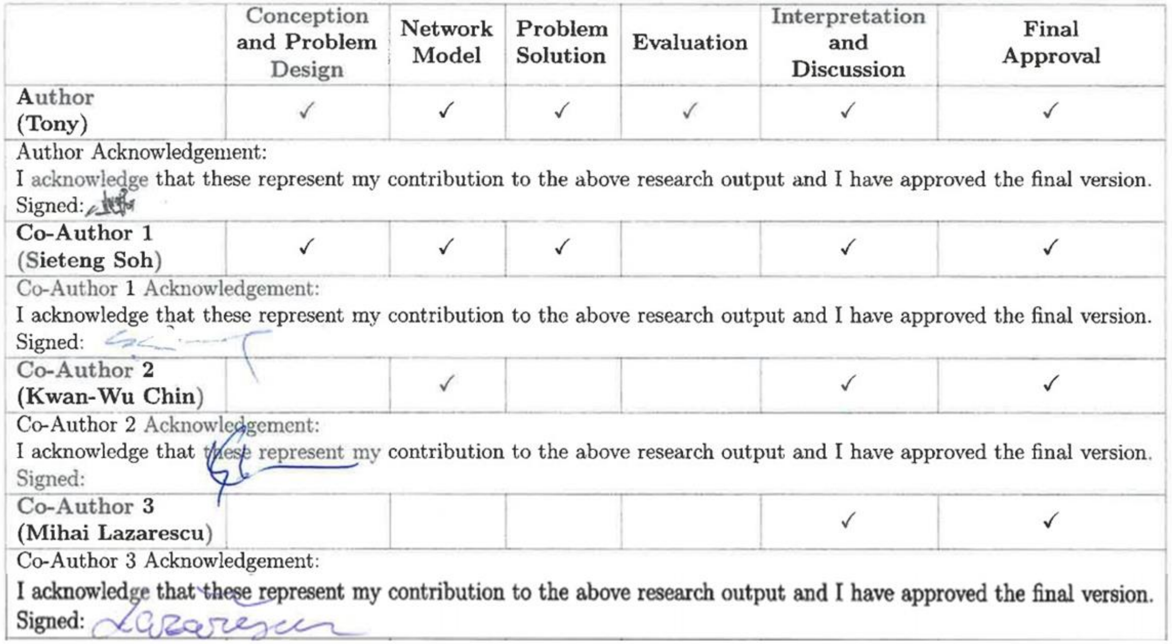

	Conception and Problem Design	Network Model	Problem Solution	Evaluation	Interpretation and Discussion	Final Approval
Author (Tony)	✓	✓	✓	✓	✓	✓
Author Acknowledgement: I acknowledge that these represent my contribution to the above research output and I have approved the final version. Signed:						
Co-Author 1 (Sieteng Soh)	✓	✓	✓		✓	✓
Co-Author 1 Acknowledgement: I acknowledge that these represent my contribution to the above research output and I have approved the final version. Signed:						
Co-Author 2 (Kwan-Wu Chin)		✓			✓	✓
Co-Author 2 Acknowledgement: I acknowledge that these represent my contribution to the above research output and I have approved the final version. Signed:						
Co-Author 3 (Mihai Lazarescu)					✓	✓
Co-Author 3 Acknowledgement: **I acknowledge that these represent my contribution to the above research output and I have approved the final version.** **Signed:** Lazarescu						

Acronyms

WSNs	Wireless Sensor Networks
IoTs	Internet of Things
rWSNs	rechargeable Wireless Sensor Networks
WPT	Wireless Power Transfer
DoD	Depth of Discharge
TDMA	Time Division Multiple Access
MAC	Medium Access Control
CSMA	Carrier Sense Multiple Access
POMDP	Partially Observable Markov Decision Process
EH	Energy Harvesting
RF	Radio Frequency
HU	Harvest Use
HSU	Harvest Store Use
HUS	Harvest Use Store
RTS	Request To Send
CTS	Clear To Send
LSHUS	Link Scheduling in Harvest Use Store
LSME-1	Link Scheduling with Memory Effect-1
LSME-2	Link Scheduling with Memory Effect-2
LS-rWSN	Link Scheduler for a rechargeable Wireless Sensor Network
LSBCC	Link Scheduler with Battery Cycle Constraint
LSNBC	Link Scheduler with No Battery Cycle Constraint
LSCC	Link Scheduler with Charging Constraint
LSDC	Link Scheduler with Discharging Constraint
LSDBS	Link Scheduler with a Dual-Battery System

Notation

Notation	Definition
$G(V, E)$	A directed graph with $\|V\|$ nodes and $\|E\|$ links.
$C_G(V', E')$	A conflict graph for a graph $G(V, E)$.
V	The set of sensor nodes.
v_i	A sensor node i.
E	The set of directional links.
$l_{i,j}$	A directed link from node v_i to node v_j.
$w_{i,j}$	The link weight for each incident link $l_{i,j}$ at a node v_i.
$\mathcal{R}_i$	The transmission range of each node v_i.
r_i	Time for the harvester in a node v_i to accumulate 1ϵ unit of energy.
b_i	The battery capacity of a node v_i.
μ_i	The battery leakage rate of a node v_i.
η_i	The battery storage efficiency of a node v_i.
$b_{i,t}$	The battery level of a node v_i at time t.
$A_{i,t}$	The amount of energy that a node v_i can use at time t.
t_i	The most recent time the battery at a node v_i was used.
τ_i	The time span between time t_i and t, i.e., $\tau_i = t - t_i$.
ρ_i	When $A_{i,t_i} < 1$, $\rho_i = t - t_i$ is the amount of time (in slots) for a node v_i to accumulate energy such that $A_{i,t} \geq 1$.
$t_{i,j}$	The earliest time in which the end nodes of a link (i, j) have sufficient energy.
$\alpha_{i,t}$	A binary variable that indicates whether a node v_i is able to transmit/receive one packet at time t.
T_i	The earliest timeslot when a node v_i has sufficient energy to transmit/receive one packet.
$\tilde{b}_{i,t}$	The energy level of the battery in charging mode at a node v_i at time slot t.
$b_{i,max}$	The upper limit capacity of the battery at a node v_i.
$b_{i,min}$	The lower limit capacity of the battery at a node v_i.

Notation	**Definition**
$\hat{b}_i$	The battery usable energy at a node v_i.
$\tilde{t}_{i,k}^{+}$	The start time of charging cycle k of the battery at a node v_i.
$\tilde{t}_{i,k}^{-}$	The end time of charging cycle k of the battery at a node v_i.
$t_{i,k}^{+}$	The start time of discharging cycle k of the battery at a node v_i.
$t_{i,k}^{-}$	The end time of discharging cycle k of the battery at a node v_i.
$\tilde{\tau}_{i,k}$	The charging time interval of the battery at a node v_i at cycle $k \geq 1$.
$\tau_{i,k}$	The discharging time interval of the battery at a node v_i at cycle $k \geq 1$.
b_{i,t_i}	The energy level of the battery at a node v_i at timeslot t_i.
σ_{i,t_i}	A binary variable that indicates whether the battery at a node v_i can be discharged at time t_i.
$\mathcal{T}_{i,k}$	The latest timeslot when the battery at a node v_i can be discharged in a discharging cycle k.
B_i^z	The dual battery at a node v_i for $z \in \{1, 2\}$.
B_i^1	The first battery at a node v_i.
B_i^2	The second battery at a node v_i.
b_i^z	The capacity of the battery z at a node v_i.
$\hat{b}_i^z$	Each battery's usable energy.
$\tilde{t}_i^{z+}$	The start charging time of the battery z at a node v_i.
$\tilde{t}_i^{z-}$	The end charging time of the battery z at a node v_i.
t_i^{z+}	The start discharging time of the battery z at a node v_i.
t_i^{z-}	The end discharging time of the battery z at a node v_i.
$\tilde{\tau}_i^z$	The charging time interval of the battery z at a node v_i.
τ_i^z	The discharging time interval of the battery z at a node v_i.
$\tilde{b}_{i,t}^z$	The amount of energy stored in the battery z at a node v_i at the start of slot t for a charging cycle.
$b_{i,t}^z$	The amount of energy stored in the battery z at a node v_i at the start of slot t for a discharging cycle.
$\|\mathcal{S}\|$	The superframe or schedule length.
τ	The length of each timeslot.
ϵ	Energy needed to transmit/receive a packet.

Chapter 1

Introduction

Wireless Sensor Networks (WSNs) are of great interest to the Internet of Things (IoTs) community [3]. They have been used in many applications [4], e.g., military [5], habitat [6][7][8] or environment [9][10][11][12][13], health [14][15], home [16][17][18][19], industry [20][21][22], and commercial applications [23]. They consist of various numbers (tens to thousands) of small devices (nodes) embedded with sensors that have the ability to collect useful information from their surroundings and forward it to one or more base/central/sink locations via wireless communications [24][25][26]. Each sensor node is composed of four subsystems [27]: (i) sensing unit to collect data, (ii) processing unit to deal with data, (iii) wireless communication unit to transfer data, and (iv) power unit to activate the sensor node.

A well-known issue faced by WSNs is that nodes have limited energy. In some implementations, it is impractical to replace the batteries of nodes due to energy depletion, especially when there are a large number of sensor nodes and they are deployed in difficult-to-reach locations. Based on the battery type used by their sensor nodes, WSNs can be classified into two categories: *non-rechargeable* and *rechargeable*. The non-rechargeable WSNs will stop their operations once the batteries are depleted−each battery has only a limited amount of energy. To maximise the battery's lifetime, researchers have proposed various techniques, e.g., energy-efficient link scheduling and routing protocols [28] that minimise energy usage while optimising network quality of service (QoS), e.g., throughput, delay, and fairness. In contrast, the rechargeable WSNs (rWSNs) use batteries that can be recharged by harvesting energy from their environment, e.g., solar, wind, and/or some types of wireless power transfer (WPT) techniques [29], such as Witricity [30]. Thus, rWSNs potentially can be immortal [31]. Nevertheless, those energy-efficient techniques are still relevant in the context of rWSNs due to limited energy sources by the existing energy harvesting technology and limited battery capacity.

To this end, rWSNs are now of great interest because sensor nodes are able to harvest energy from their environment. However, they have a number of operational issues. *First*, the energy arrivals of nodes exhibit spatio-temporal properties. This means nodes may experience time-varying energy arrivals. When a node exhausts its energy, it will have to spend time for harvesting energy before it continues executing tasks. Thus, a node that has a greater energy consumption rate than its energy harvesting rate can operate perpetually, but with delays. The time used to harvest a given amount of energy is affected by the type of energy source as well as a node's location [32]. For instance, assuming a solar panel has a power density of $15,000$ μW/cm^3 and 20 μW/cm^3 for outdoor and indoor settings, respectively [33], hence, a node with a 50 cm^3 solar panel will have a corresponding energy harvesting rate of 300 mJ/s (outdoor) and 0.4 mJ/s (indoor). A Mica2 mote [34], which requires 30 mJ of energy to transmit/receive a packet, will need to spend 0.1s (outdoor) or 75s (indoor) for harvesting energy before it can transmit/receive one packet.

The *second* important issue of interest recently is the lifetime of rechargeable batteries. Among others, one contributing factor to the battery's lifetime is *memory effect* [35], which decreases its usable capacity if the battery is charged and discharged repeatedly, after a partial discharge and charge, respectively. This degradation can be avoided by enforcing a so-called *battery cycle* constraint, i.e., a node must charge (or discharge) its battery completely before fully discharging (or charging) its battery again [36]. In addition, the degradation can be reduced by equipping the rWSNs with a dual-battery system [37], in which the batteries are charged and discharged alternately. Another factor is the percentage of discharged energy relative to a battery's overall capacity which is also called as battery's *Depth of Discharge (DoD)* [38]. Further, frequent charging and discharging also affects a battery's lifetime [39].

The *third* issue is channel access or *link scheduling* [40], which determines when nodes activate their link(s), and thus governs the network capacity of an rWSN. To this end, this thesis considers Time Division Multiple Access (TDMA) to ensure that nodes do not experience collisions nor waste energy, and that they only need to be active during the allocated timeslot. Specifically, a link scheduler is responsible for determining the set of transmitting and receiving nodes in each time slot. As the TDMA schedule repeats, it is important that the schedule length (in terms of slots) is short as this allows nodes to transmit frequently; consequently, as links are activated frequently, they will have a high capacity. The schedule governs the active time of a node; therefore, a node only needs to become active if its neighbours are active. In other words, such schedule minimises idle listening [41]. It is evident that a link scheduler plays a *critical* role in an rWSN. Past works on link scheduling assumed nodes have no energy harvesting constraint [42]. In contrast, in an rWSN, link schedulers must consider the varying energy harvesting rates of sensor nodes. Specifically, they must consider the *energy harvesting time* of nodes, i.e., the time interval in which a sensor node accumulates sufficient energy to either transmit/receive a packet. Without this consideration, a link scheduler may allocate slots to nodes that have insufficient energy to transmit/receive a packet. Another important factor to consider are battery characteristics, namely: (i) limited capacity, i.e., *battery capacity*, (ii) leakage, and (iii) storage efficiency. These characteristics can result in a longer link schedule. Our work in this thesis considers all of the above factors. It is important to note that link scheduling problem in general is known to be NP-hard [43]. Further, our problem is the general version of the link scheduling problem that assumes nodes have no energy constraint. Thus, all problems addressed in this thesis are in NP-hard.

Our research hypothesis are as follows: (i) the harvesting time can significantly effect the link schedule; as each node has to wait for its harvesting time to accumulate sufficient energy before it can transmit/receive a packet, (ii) the imperfect battery characteristics can lead to a longer link schedule; since the battery will take longer time to have energy due to leakage and/or storage efficiency, and (iii) the battery cycle constraint can significantly increase the link schedule length; the reason is the battery can only be charged (discharged) if its energy level reaches the minimum (maximum) level.

1.1 Aim and Approach

The aims of our works are as follows.

Aim 1 – To propose and analyse a novel TDMA link scheduling problem for rWSNs with energy harvesting time and battery capacity constraints. This thesis proposes a heuristic approach, called Link Scheduler in a rechargeable Wireless Sensor Network (LS-rWSN). The greedy approach selects non-interfering links starting from the link whose end nodes have sufficient energy to transmit/receive one packet at the earliest time.

Aim 2 – To propose and analyse a novel TDMA link scheduling problem for rWSNs that consider battery memory effect. Note that this problem extends that in **Aim 1** to reduce the impact of memory effect that is caused by repeated charge/discharge cycles of batteries. Our proposed heuristic approach, called Link Scheduler with Battery Cycle Constraint (LSBCC), requires each battery to be charged (discharged) completely before it can be discharged (charged) again. In addition, the greedy heuristic schedules all non-interfering links at the earliest possible timeslot when the batteries at their end nodes can be used.

Aim 3 – To propose and analyse a novel problem to reduce the negative effect of enforcing the battery cycle constraint of **Aim 2** on a TDMA link schedule length. Our proposed approach, called Link Scheduler with a Dual-Battery System (LS-DBS), uses a dual-battery system; each of which is subjected to the battery cycle constraint. Further, the heuristic greedily schedules all non-interfering links at the earliest possible timeslot.

Our proposed link schedulers, i.e., LS-rWSN, LSBCC, and LSDBS, are to be deployed in a centralised manner.

1.2 Significance and Contributions

The main significance and contributions of this thesis are threefold.

1. It addresses a *novel* TDMA link scheduling problem, called Link Scheduling in Harvest-Use-Store (LSHUS), and proposes a solution called LS-rWSN,

to maximise the throughput of rWSNs where: (i) sensor nodes have different energy harvesting times, (ii) sensor nodes have a battery with a finite capacity, and each battery has a less-than-ideal storage efficiency and leaks over time, and (iii) each link i has a weight $w_i \geq 1$ that specifies that it must be scheduled at least w_i times in the resulting schedule. To the best of our knowledge, no link schedulers have simultaneously considered factors (i)-(iii). The authors of [44] considered factors (i) and (iii) and they assumed nodes used the Harvest-Store-Use (HSU) model with unlimited battery capacity. More specifically, the work in [44] assumed batteries that were leakage free and had 100% storage efficiency. This thesis, particularly Chapters 3 and 4, also consider different leakage rates and storage efficiencies. Furthermore, it outlines an efficient greedy technique to generate TDMA link schedules and contains analysis of its time complexity. In addition, it presents proof to show that LSHUS is NP-Complete and contains analysis of the optimal schedule length for the following topologies: *Line*, *Tree*, and *Grid*. The proposed technique does not require an *extended* conflict graph, as in [44], and thus, it is more efficient. The results in Chapter 3 show that imperfect batteries increase the schedule length. The conclusion is justified by our simulation results in Chapter 3.

2. It presents a TDMA link scheduling problem, called Link Scheduling with Memory Effect-1 (LSME-1), that considers: (i) sensor nodes with different energy harvesting times and a finite battery capacity, (ii) battery operation governed by a *battery cycle* constraint, (iii) batteries with a leakage rate and storage efficiency, and (iv) activation of each link (i, j) at least $w_{i,j}$ times. It analyses the optimal schedule length for three fixed topologies: *Line*, *Tree*, and *Grid*. Further, it develops a *novel* heuristic technique, called LSBCC,

that greedily schedules links that can be activated according to when their end nodes are able to transmit/receive a packet. In addition, it analytically shows that some links cannot be scheduled for networks that contain batteries with a non-negative leakage rate. This conclusion is supported by our simulation results in Chapter 4.

3. It proposes a new TDMA link scheduling problem, called LSME-2, to maximise throughput in rWSNs where: (i) sensor nodes have a different energy harvesting time, (ii) each node is equipped with a dual-battery system, (iii) each battery has a finite capacity, (iv) each battery has a *battery cycle* constraint, and (v) each link i has a weight $w_i \geq 1$ and must be scheduled at least w_i times. It presents battery states and their state transitions in the dual-battery system. Further, it develops a heuristic algorithm called LSDBS, to generate a TDMA link schedule, where it schedules links that can be activated at the earliest time when one of the dual battery at their end nodes can be discharged to transmit/receive a packet. The simulation results in Chapter 5 show that using two batteries at each node reduces the schedule length and number of battery charge/discharge cycles.

The impact of our research projects in this thesis are as follows: (i) the economic impact: our work contributes to decreasing the energy cost as it utilizes energy harvesting, (ii) the environmental impact: since our research is related to renewable energy, it helps to reduce global greenhouse gas emission [45], and (iii) the research communities impact: this work has a potential interdisciplinary research collaboration.

1.3 Thesis Organisation

The contents of each chapter in this thesis are as follows.

Chapter 2: Background

Chapter 2 discusses the background, network model, and notations that are used in this thesis. It describes three protocols of energy harvesting and battery usage. Further, it addresses interference models. It covers an overview of TDMA link scheduling. A review of related works on link scheduling problems is also discussed. Lastly, the chapter presents the simulation environment used to evaluate the performance of all proposed algorithms in this thesis.

Chapter 3: Link Scheduling in rWSNs with Harvesting Time and Battery Capacity Constraints

Chapter 3 formally defines the LSHUS problem and describes our proposed solution to the problem, i.e., LS-rWSN. The chapter includes a proof of the problem and the analytical analysis of optimal schedule length for three fixed topologies. Finally, the chapter evaluates our LS-rWSN algorithm using simulation.

Chapter 4: Link Scheduling in rWSNs with Battery Memory Effect

Chapter 4 formulates the LSME-1 problem and presents our proposed solution, i.e., LSBCC. This chapter presents analytically the optimal schedule length for fixed topologies. It also shows the feasibility study of LSME-1. Finally, Chapter 4 includes simulations to evaluate the LSBCC algorithm.

Chapter 5: Link Scheduling in rWSNs with a Dual-Battery System

Chapter 5 addresses the LSME-2 problem and shows our proposed solution, i.e., LSDBS. The chapter describes battery states and state transitions in a dual-battery system. We perform simulations to evaluate our solution.

Chapter 6: Conclusion

Chapter 6 summarises this thesis and discusses possible areas of future research.

This thesis includes one Appendix that contains copyright information from IEEE conferences and journals in which the author has published.

Chapter 2

Background

This chapter is divided into seven sections. It contains all the theory and materials that are used in Chapters 3, 4, and 5. Section 2.1 describes the network model and notations that are used throughout this thesis. Additional notations that are used only in specific chapters will be described in their corresponding chapters. Section 2.2 discusses energy harvesting and battery usage protocols. Section 2.3 introduces interference models for WSNs. Section 2.4 addresses an overview of MAC layer, including TDMA link scheduling. Section 2.5 reviews the literature related to this thesis. Section 2.6 presents the network topologies and platform used in the thesis. Finally, Section 2.7 summarises this chapter.

2.1 Network Model

A rWSN is modelled as a directed graph $G(V, E)$, where each node $v_i \in V$ is a sensor node and each link $l_{i,j} \in E$ denotes a directed link from node v_i to node v_j. Each node v_i has a transmission range of $\mathcal{R}_i$. Let $||v_i - v_j||$ be the Euclidean distance between nodes v_i and v_j. A node v_i can transmit/receive packets to/from node v_j if $||v_i - v_j|| \leq \mathcal{R}_i$. Each link $l_{i,j} \in E$ has weight of

$w_{i,j} \geq 1$, meaning the link must be activated at least $w_{i,j}$ times in the generated schedule to transmit/receive data packets in networks with continuous traffic model. We assume each node has a fixed location in a network.

A sensor node consumes energy when sensing the environment, computing collected samples, and communicating with its neighbours, which includes transmitting, receiving, listening for messages on the radio channel, sleeping, and switching state [46]. This work assumes that communication is the only source of energy expenditure. The assumption is reasonable because as shown in [46], the energy consumption of nodes for communications is significantly larger than the other operations, e.g., 180.10 mJ, 17.242 mJ, and 5.2 mJ for communication, sensing, and computing, respectively. Similar to [47], we assume the energy usage for transmission and reception is equal. Let ϵ (in Joule) be the energy consumed when transmitting or receiving one packet. For example, assuming a TI CC2420 transceiver uses 226 nJ/bit for transmission [48] and a packet size of 125 bytes or 1,000 bits, then we have $\epsilon = 226$ μJ.

A node v_i is equipped with a harvester that scavenges energy from its environment, e.g., solar, and a rechargeable battery with capacity of b_i (in a unit of ϵ). Note that our work does not make any specific assumption about any energy harvesting model used by nodes; i.e., the problem is *independent* of any specific energy harvesting model. That is, it assumes each node has a known energy arrival rate that arrives *after* energy conversion. In addition, it is independent of any specific signal propagation models and spread spectrum technology. Let $r_i \geq 1$ (in slots) be the *harvesting time* or total number of slots that is required by a node v_i to accumulate 1ϵ of energy. Thus, the harvesting rate of a node v_i is $\frac{\epsilon}{r_i}$ per time slot. Let $0 < \eta_i \leq 1$ be the storage efficiency and $0 \leq \mu_i < 1$ be the battery leakage factor (per time slot) of a node v_i. This work omits the following cases. First, when $\eta_i = 0$ and $\mu_i = 1$, the battery of nodes cannot store any harvested energy and retain its energy, respectively. Second, in each slot, the amount of harvested energy must be greater than the battery's leakage rate μ_i. Otherwise, any harvested energy will be lost immediately due to battery leakage. In both cases, nodes will have no energy to activate links.

2.2 Energy Harvesting and Battery Usage Protocols

Energy harvesting techniques utilise energy from ambient environments or other energy sources (body heat, foot strike, and finger strokes) and convert it to electrical energy to power the sensor nodes in rWSNs [27][32]. The harvested energy which is large and periodically available can power a sensor node continuously [32]. Energy harvesting offers a promising solution to extend the lifetime of energy-constrained wireless networks, such as rWSNs [49].

Energy harvesting sources consist of two main categories: ambient environments and external sources [27]. Ambient environments provide readily accessible energy in nature at no cost, such as radio frequency (RF), solar, thermal, and flow (wind or hydro). Meanwhile, external sources, like mechanical and human, are dispersed explicitly in the environments for energy harvesting purposes. There are different types of rechargeable batteries whose characteristics are dependent on their internal chemistries to power the energy harvester [50]. Batteries that use Nickel-Cadmium (NiCd), Nickel-Metal-Hydride (NiMH), and Lithium-ion (Li-ion) have high discharge rates [50]. Table 2.1 shows the specifications of the rechargeable batteries.

Table 2.1 Specifications of rechargeable batteries [2].

Specifications	NiCd	NiMH	Li-ion
Nominal voltage (V)	1.2	1.2	3.7
Capacity (mAH)	1100	2500	740
Energy (Wh)	1.32	3.0	2.8
Self-discharge per month (%)	10	30	<10
Charge-discharge efficiency (%)	70-90	66	99.9

There are three commonly used energy harvesting and battery usage protocols [51]:

1. Harvest-Use (HU) [52]: The harvested energy at slot t directly powers the sensor node at slot t. There is no device to store the unused energy for future use.

2. Harvest-Store-Use (HSU) [53]: The harvested energy at slot t is first stored in the battery for use in subsequence slots, i.e., it can only be used starting at slot $t + 1$. There is a storage device to save the harvested energy.

3. Harvest-Use-Store (HUS) [54][55]: The harvested energy at slot t that is temporarily stored in a supercapacitor, can be used by sensor nodes immediately, i.e., also at slot t, and any unused energy is stored in a rechargeable battery for future use. This protocol requires two energy storage devices. A supercapacitor has a faster charging efficiency but also a larger energy leakage than a battery [56]. Additionally, HUS has a higher achievable harvesting rate and lower energy loss as compared to HSU [51].

Our work in Chapter 3 considers HUS protocol, while in Chapters 4 and 5, we use the HSU model. Note that it is possible to revise the HSU model to apply in the HUS model.

2.3 Interference Models

Cardieri [57] presented a complete survey of interference models for wireless ad hoc networks. The author classified three groups of models: (i) statistical interference, (ii) effects of interference, and (iii) graph-based interference. The first uses random process to model the statistical characterisation of interference signal. The author [57] discussed two of the most used interference models in the groups (ii): protocol interference and physical interference. The protocol interference considers the effects of interference based on a pairwise interference relationship between two links. Also, it can be used to solve more complex problems in the communication protocols of WSNs [57]. In contrast, the physical interference examines the aggregate interference affecting the receiver. Both models can be defined as a graph-based interference model, which is categorised as the third model. This thesis employs the protocol interference.

Ramanathan [58] categorised the protocol interference model into 11 atomic constraints in terms of: (i) their vertex or edge in a graph to be coloured, (ii) the forbidden separation between them, and (iii) the direction of the constraint (transmitter or receiver). More specifically, constraint c is denoted as $c = \langle \epsilon \rangle_{\langle d \rangle}^{\langle s \rangle}$, where $\epsilon \in \{N, E\}$, $s \in \{0, 1\}$, $d \in \{tr, tt, rr, rt\}$. Here, ϵ is the entity (<u>N</u>ode or <u>E</u>dge) being constrained, s is the forbidden separation between two vertices or edges, and d qualifies the separation by specifying its direction with respect to the transmitter (t) and receiver (r). A separation of 0 between two vertices or edges indicates the vertices or edges are adjacent, and a separation of 1 between two vertices or edges is indicative of one vertex or edge between them. For instance, if $c = V_{tt}^{1}$, then two vertices u and v that are separated by another vertex w (i.e., $s = 1$) with an edge from the transmitters (i.e., $d = tt$) of u, v to w are constrained.

Djukic and Valaee [1] used five of eleven interference types in [58], i.e., (i) transmitter-transmitter $(t - t)$, (ii) receiver-receiver $(r - r)$, (iii) transmitter-receiver $(t - r)$, (iv) transmitter-receiver-transmitter $(t - r - t)$, and (v) receiver-transmitter-receiver $(r - t - r)$; see Figure 2.1. These interferences are based on the distance model [1] where two edges interfere with each other at a receiver, if the receiver cannot decode packets from either link. Types (i) to (iii) are called the *primary* conflicts and the last two are the *secondary* conflicts. As discussed in [1][44][58], the first four conflicts need to be considered in a TDMA network, while the fifth one exists when a request-to-send (RTS)/clear-to-send (CTS) model is used.

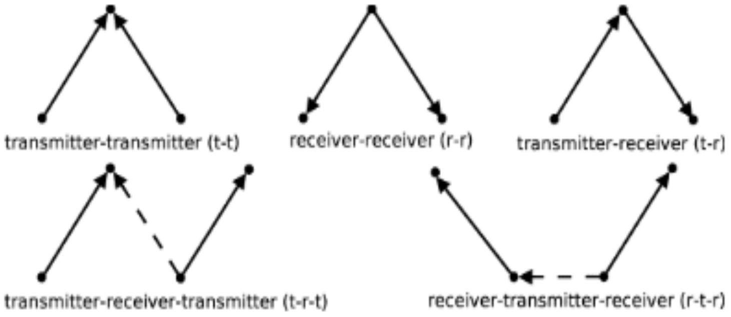
transmitter-transmitter (t-t)
receiver-receiver (r-r)
transmitter-receiver (t-r)
transmitter-receiver-transmitter (t-r-t)
receiver-transmitter-receiver (r-t-r)

Figure 2.1 Interference models [1].

Our work in this thesis uses the protocol interference model [58] which considers: (i) primary interference, where each node is half-duplex, and (ii) secondary interference, where a receiver, say A, that is receiving a packet from a transmitter, say B, is interfered by another transmitter, say C. The interference between links is modeled by a conflict graph $C_G(V', E')$ [59], which can be constructed for a graph $G(V, E)$ as follows: (i) each vertex in V' represents a link in E, i.e., $|V'| = |E|$, and (ii) each edge in E' represents two links of G that experience primary or secondary interference if they are active together.

2.4 MAC Layer

Data transmissions from a node in rWSNs will be received by all nodes within its range and can possibly cause interferences to some non-intended receivers [60]. There are two main approaches to address interference in the medium access control (MAC) layer [61]: (i) use a random access scheme or contention-based protocol, e.g., Carrier Sense Multiple Access (CSMA) and (ii) derive link schedules, e.g., Time Division Multiple Access (TDMA). This thesis considers a TDMA protocol that offers these benefits [40][62]: (i) concurrency of transmissions, (ii) high reliability of communications, and (iii) energy conservation. Note that to further conserve energy, a node in TDMA can switch off its transceiver when it is neither transmitting nor receiving.

In a TDMA, time is split into equal intervals called *superframe*. A superframe consists of a number of slots with equal length called *timeslots*. Each timeslot contains non-interfering links, and thus links at the same slot can transmit/receive packets interference-free. Since the schedule in a superframe is repeated, a shorter superframe results in higher throughput because nodes can transmit more frequently [63]. Further, TDMA gives guaranteed fairness and provides bounds on per-hop latency [40]. Sgora *et al.* [64] presented a comprehensive survey of TDMA scheduling algorithms. The algorithms can be classified into centralised, e.g., [1][44][65][66][67], and distributed, e.g., [40][68][69][70][71]. Our work only considers a centralised scheduler.

A TDMA superframe or a link schedule, is defined as a collection of consecutive, equal-sized timeslots. All links in each slot do not experience primary and secondary interference. Indeed, after colouring a conflict graph, all links with the same colour can be placed in a slot. Let $\mathcal{S}$ represent the superframe and $|\mathcal{S}|$ denote its length (in slots). Each slot is either *empty* or contains one or more non-interfering, concurrently active links. A slot is empty when all sensor nodes experience an energy outage. Note that prior link schedulers assumed nodes always have energy when they are scheduled to transmit/receive; our work relaxes this assumption.

2.5 Related Works

To the best of our knowledge, except for references [44] and [72], there are no works that solve a similar problem to ours. The authors in [72] proposed three link scheduling algorithms to activate links with the maximum weight. The weight of a link represents the amount of consumed energy when it is active. They aimed to minimise the amount of stored energy and reduce energy waste.

Sun *et al.* [44] considered the HSU model [51], whereby harvested energy must be first stored in a battery before it can be used. Each battery has a *recharging time* that determines when a node has sufficient energy to transmit/receive one packet. The authors assumed nodes have a perfect battery, i.e., nodes used batteries with unlimited capacity, 100% storage efficiency, and are leakage-free. The links in [44] can be scheduled only if the batteries of their end nodes have accumulated sufficient energy to transmit/receive one data packet. Each node with insufficient energy thus must wait for at least one recharging cycle before it can activate one link. The authors proposed two link schedulers to maximise network throughput: (i) without link weight (or $w_{i,j} = 1$), and (ii) with link weight ($w_{i,j} > 1$). For (i), they generated a *conflict graph* $C_G(V', E')$ from $G(V, E)$ according to the protocol interference model. For (ii), their scheduler required an *extended* conflict graph $C'_G(V', E")$, which is generated from C_G and $w_{i,j}$ of each link such that each link (i, j) appears $w_{i,j}$ times in C'_G.

Recently, there were works that considered HUS, but those works did not consider the problem in this thesis. More specifically, in [73], Yuan *et al.* investigated the HUS architecture for point-to-point data transmission with a rechargeable battery over two channels: (i) static, and (ii) block fading. They aimed to maximise throughput and proposed optimal energy policies based on a discrete-time energy model. They then extended their work in [74], whereby the aim was to minimise the energy used for transmissions subject to a delay constraint. However, these papers assumed perfect batteries, i.e., batteries with zero leakage and 100% storage efficiency.

The work in [75][76] and [77] considered batteries with leakage and storage efficiency, i.e., imperfect batteries. The authors in [75] proposed a framework to maximise the amount of data transmission by adjusting the transmit power in an energy harvesting system with battery limitation, such as leakage constraint. Biason *et al.* [76] proposed a framework based on a Partially Observable Markov Decision Process (POMDP). The goal was to optimise the throughput of energy-harvesting-capable devices. Further, they considered the effects of imperfect batteries. In [77], Tutuncuoglu *et al.* studied two policies: (i) optimal offline, and (ii) online to maximise the average transmission rate in an energy harvesting network with an inefficient finite capacity battery that loses a constant fraction of its stored energy. However, none of these papers considered link scheduling.

Liu *et al.* [78] aimed to optimise the throughput and transmission time in many-to-one networks. The authors considered two cases: (i) infinite, and (ii) finite battery capacity. Kapoor and Pillai [79] aimed to find efficient schedulers for energy harvesting nodes operating over a multiple access channel. Lenka *et al.* [80] designed a hybrid MAC protocol for WSNs that minimises latency and collisions. He *et al.* [81] presented link scheduling, data routing, and energy sharing in rWSNs to maximise the minimum source or sensing rate of nodes. On the other hand, Li *et al.* [82] studied a scheduling optimisation problem for an Energy Harvesting (EH) mobile WSN. They aimed to maximise the amount of data collected from sensors by scheduling the transmission per time slot according to the energy harvested by sensor nodes and link quality. The authors of [83] investigated a joint data gathering and EH problem in rWSNs with a mobile sink. The goal was to maximise the network utility by jointly considering the relay selection, power/energy allocation and time scheduling problems. Further, the authors in [84], [85], and [86] included multi-user channel access and radio channel model in their link scheduling. However, none of these works considered the recharging time of batteries at the end nodes of active links.

In summary, there are no prior works on *link scheduling* for rWSNs that consider all of the following factors: battery recharging time, capacity, leakage, and storage efficiency. Sun *et al.* [44] considered recharging time and assumed unlimited battery capacity. The authors considered the HSU model [51] that requires the harvested energy at slot t to be used no earlier than slot $t + 1$, resulting in a longer schedule length. On the other hand, Chapter 3 uses the HUS model such that nodes can use their harvested energy immediately, and hence, reduce energy loss and produce a shorter link schedule. This means a larger throughput than a link schedule that uses the HSU model. The approach in our work only requires a conflict graph, unlike the solution in [44] in which an extended conflict graph was also required. Our approach is advantageous as the extended conflict graph becomes computationally expensive to use with a large link weight $w_{i,j}$. In addition, the work in [44] did not consider battery leakage and storage efficiency. Note that a Ni-MH rechargeable battery can only store 70% of the harvested energy [51]. As a result, some valuable energy is lost due to energy storage efficiency and leakage. Henceforth, this thesis extends the work in [44] to include these two important factors. Further, it considers a battery cycle constraint to cope with memory effect in Chapter 4 and employs a dual-battery system in Chapter 5.

2.6 Simulation Environments

This section describes the network topologies used in simulations performed in Chapters 3 through 5.

2.6.1 Topologies

The performance of the proposed algorithms in Chapters 3 and 4 are evaluated using two sets of networks: (i) fixed topology, and (ii) arbitrary network. On the other hand, the proposed solution in Chapter 5 is only evaluated on the arbitrary network.

2.6.1.1 Fixed Topologies

The fixed topologies consist of *Line*, *Binary Tree (BTree)*, and *Grid* topologies. Specifically, all three topologies are bipartite graphs [87]. Briefly, a graph is bipartite if its nodes can be placed into two sets, namely, Set-1 and Set-2, with links between nodes in Set-1 and Set-2 only. The fixed topologies range from 20 to 100 nodes, with an increment of 10. Hence, there are nine *Line*, nine *Binary Tree (BTree)*, and nine *Grid* topologies. The following describes the details of each fixed topology.

1. *Line* (see Figure 2.2): Assume a line graph with n nodes. The nodes are labeled consecutively from 1 to n. Following the protocol interference model, a node cannot transmit and receive at the same time. Further, any nodes within two hops away are not allowed to transmit in the same

slot when at least one of them transmits to their common neighbour. For example, there are interferences between links $(2,1)$ and $(4,3)$, and links $(2,3)$ and $(4,5)$ at node 3, but links $(2,1)$ and $(4,5)$ are interference-free.

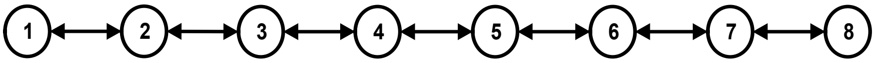

Figure 2.2 A line graph with eight nodes.

2. *BTree* (see Figure 2.3): Consider a *BTree* with $L \geq 2$ levels, n nodes and bidirectional links between nodes. A *BTree* with n nodes has $L = \lceil log_2\ n \rceil + 1$ levels, e.g., for $n = 30$, the resulting *BTree* has $L = 5$ levels. Thus, each *BTree* is not a complete binary tree; its lowest level may not be fully populated. We consider a complete binary tree, i.e., $n = 2^L - 1$. Thus, for $2^{L-1} \leq n < 2^L - 1$, we include some dummy nodes to form a complete tree. The root node is at level $k = 1$. Its two children are at level $k = 2$. We label nodes consecutively from left to right level by level, e.g., the root node is node 1, and the rightmost node at the lowest level $k = L$ is node $2^k - 1$. Thus, level k contains 2^{k-1} nodes; the nodes are labeled $2^{k-1}, 2^{k-1} + 1, \cdots, 2^k - 1$. As a bipartite graph, Set-1 contains nodes at odd levels of the *BTree*, and Set-2 has nodes at even levels. The secondary interference in the *BTree* can occur only between (i) a pair of nodes from different levels having a common neighbour, e.g., nodes 1 and 4 activating links $(1,2)$ and $(4,8)$, and (ii) a pair of nodes with the same parent, e.g., nodes 4 and 5 with links $(4,2)$ and $(5,10)$.

3. *Grid* (see Figure 2.4): Let $(row \times col)$ *Grid* be a bidirectional grid topology that contains $n = row \times col$ nodes. We consider $row \geq col$ such that $(row - col)$ is minimum, e.g., for $n = 20$ and $n = 80$, we have (5×4) and (10×8) *Grid*, respectively. We label the nodes, starting from number one,

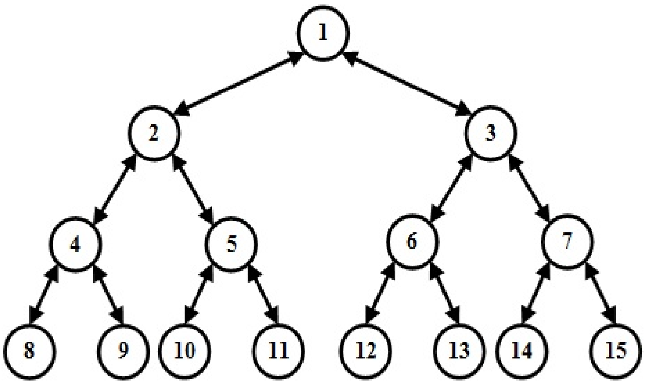

Figure 2.3 A binary tree with four levels.

sequentially from left-to-right in a row-wise manner. For example, for the $(4{\times}3)$ *Grid* in Figure 2.4, $row = 1$ contains nodes $\{1, 2, 3\}$, and $col = 3$ has nodes $\{3, 6, 9, 12\}$. One can consider a $(row{\times}col)$ *Grid* is constructed from row (col) *Line* graphs, each of which has col (row) nodes. We label each **row** *Line* graphs as R_1, R_2, $\ldots$, R_{row}, and each **col** *Line* graph as C_1, C_2, $\ldots$, C_{col}. The secondary interference in a *Grid* can occur only between pair of nodes from a different row or column that share a common neighbour. For example, consider nodes 1 and 5 in Figure 2.4 where node 2 is their common neighbour. It is indicative of an interference at node 2 when links $(1, 2)$ and $(5, 8)$ are activated simultaneously in the same slot.

2.6.1.2 Arbitrary Network

We consider arbitrary networks from 20 to 50 (10 to 50) nodes randomly deployed on a 40×40 m^2 area in Chapter 3 (Chapters 4 and 5). Each node has a transmit and interference range of 15 and 30 meters, respectively. The average number of links $|E|$ are 28, 125, 273, 470, and 758 for 10, 20, 30, 40, and 50 nodes, respectively. As in [44], the interference range is two times the transmit range. Note that additional parameter values, which are used only in specific chapters, will be described in their corresponding chapters.

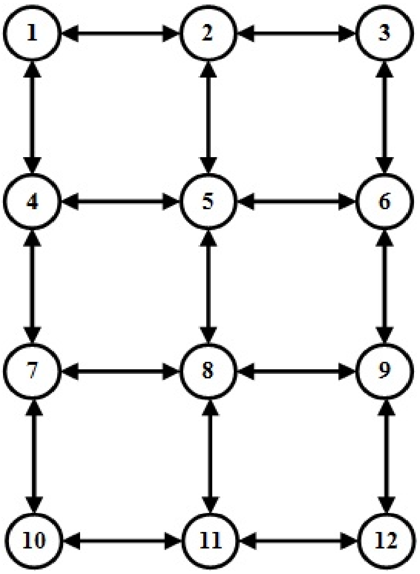

Figure 2.4 A (4×3) grid.

2.6.2 Platform

All proposed algorithms were implemented in C++ and all experiments were conducted on a computer with an Intel Core i7-9700T CPU @2.00 GHz and 16GB of RAM, running Windows 10 Enterprise.

2.7 Chapter Summary

This chapter covered the background for this thesis. Section 2.1 described our network model and its notations. Section 2.2 described three energy harvesting and battery usage protocols. Section 2.3 showed the interference model. Section 2.4 addressed MAC layer, including TDMA link scheduling. Section 2.5 discussed the related literature. Section 2.6 summarised the network topologies and platform used in this thesis. In the following three chapters, we propose three link scheduling algorithms that schedule links according to the earliest activation time.

Chapter 3

Link Scheduling in rWSNs with Harvesting Time and Battery Capacity Constraints

This chapter considers the problem of generating the shortest TDMA schedule for use in rWSNs with varying energy harvesting times. This *novel* problem considers: (i) the time required by nodes to harvest sufficient energy to transmit/receive a packet, (ii) Harvest-Use-Store (HUS) energy harvesting and battery usage protocol, and (iii) battery imperfections, i.e., leakage, storage efficiency, and capacity. This chapter shows that the problem at hand, Link Scheduling in Harvest-Use-Store (LSHUS), is, in general, NP-Complete. Further, it presents a greedy heuristic, called LS-rWSN, to solve LSHUS.

Here we discuss the link scheduling problem with the aid of an example. Figures 3.1a and 3.1b show two rWSN examples with four nodes and three directed links; the number next to each link refers to its activation timeslot. Links (v_1, v_2), (v_3, v_2), and (v_4, v_2) interfere with each other and thus cannot be scheduled to transmit concurrently. Assume links (v_1, v_2), (v_3, v_2) and (v_4, v_2) are to be activated in timeslots $t = 1$, $t = 2$, and $t = 3$, respectively. Therefore, the resulting TDMA schedule or *superframe* is three slots in length. The key assumption for the example in Figure 3.1a is that nodes have sufficient energy to transmit and receive in their allocated timeslots. Next, consider the case where sensor nodes have different energy harvesting cycles. Figure 3.1b shows that node v_1 is able to transmit/receive every five slots; denoted as $v_1|5$. This causes the schedule length to exceed three slots as each node must now wait for its battery to recharge. Notice that node v_2 has sufficient energy at timeslot $t = 2$. However, none of its incoming links can be activated at time $t = 2$ because its neighbours have insufficient energy to transmit a packet. Specifically, link (v_1, v_2) can be scheduled no earlier than slot $t = 5$ because node v_1 can only transmit after time $t = 5$.

The battery capacity of sensor nodes is also a key factor that affects the schedule length. Consider the case where at time $t = 3$, node v_2 continues to accumulate energy, and hence at time $t = 5$ and $t = 7$, it has sufficient energy to receive two and three consecutive packets, respectively. For this case, links (v_1, v_2), (v_3, v_2), and (v_4, v_2) can be scheduled at time $t = 5$, $t = 6$, and $t = 7$, respectively, giving a schedule length of seven. Now assume the battery capacity of node v_2 is only sufficient to store the energy required to receive one packet. Consequently, the battery of node v_2 can be recharged only after it is used at time $t = 5$, and it is fully recharged at time $t = 5 + 2 = 7$. Thus, node v_2 can receive the second and third packet no earlier than at time $t = 7$ and $t = 9$, respectively, e.g., link (v_3, v_2) can be scheduled at time $t = 7$, and link (v_4, v_2) at time $t = 9$, which yields a schedule length of nine; see Figure 3.1b. This example shows that battery capacity affects the schedule length.

Two additional factors that can affect the schedule length are battery leakage and storage efficiency. The typical value of storage efficiency can be as low as 66% [77] depending on the battery technology. Similarly, the leakage rate of a battery depends on its type, age, usage, and/or temperature [75]. As an example, the leakage rate of a Li-ion battery is 8% per month [88], which is lower than a Nickel-based battery. Further, the leakage rate changes over time and has the highest leakage right after being charged [75]. To illustrate the effect of these factors on the link schedule, reconsider the previous example depicted in Figure 3.1b. Assume sensor nodes have a battery with a capacity of one unit of energy (1ϵ). Now assume the battery of nodes leaks at a rate of 5% per slot and has a storage efficiency of 90%. Given this imperfect battery, the schedule length becomes 12 slots instead of 9 slots. This is because links (v_1, v_2), (v_3, v_2), and (v_4, v_2) are scheduled at time $t = 6$, $t = 9$, and $t = 12$, respectively. Moreover, nodes v_1, v_2, and v_3 require more than five, six, and seven timeslots, respectively, to accumulate sufficient energy to transmit/receive a packet due to battery leakage and storage efficiency.

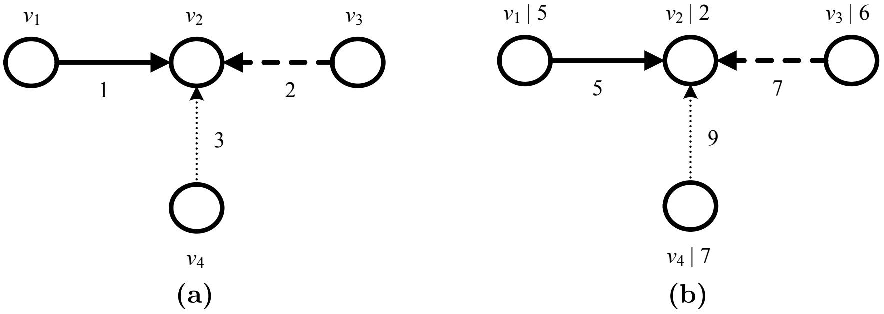

Figure 3.1 Example (a) with only protocol interference constraint and (b) with protocol interference, harvesting time, and battery capacity constraints. The number next to each link denotes its activation time, and $v_x|z$ denotes node x requires z time slots to recharge its battery to a level before the next transmission or reception is possible.

The preliminary work of this chapter has been presented in [89], and the full version has been published in [90]. Specifically, reference [89] addressed LSHUS problem without considering battery leakage and storage efficiency, while reference [90] extended [89] to include these two important factors and described

LS-rWSN. Note that the proposed LS-rWSN algorithm in this chapter was called Algo-1 in [89].

The layout of this chapter is as follows. Section 3.1 discusses the network model and formulates the LSHUS problem. Then, it analyses the problem in fixed topology networks. Section 3.2 describes our proposed algorithm to solve LSHUS. Section 3.3 presents the simulation results. Finally, Section 3.4 concludes this chapter.

3.1 Preliminaries

Section 3.1.1 first describes the rWSN model under consideration. It then introduces key notations used in this chapter. Section 3.1.2 formally presents the problem at hand and shows that the said problem is NP-Complete. Section 3.1.3 presents an analysis of how factors such as harvesting time, battery leakage, and storage efficiency impact the schedule length for fixed topology networks.

3.1.1 Network Model

This chapter considers nodes that use the HUS model [51], where the harvested energy is first stored in a capacitor for immediate use and any unused energy is stored in a rechargeable battery for use in future slots. A node v_i contains a harvester that generates energy from its environment, e.g., the sun, and two energy storage types: (i) a super capacitor with a capacity of c_i and (ii) a rechargeable battery with a capacity of b_i; both capacities are in a unit of ϵ. Let $r_i > 0$ (in slots) be the total number of slots or *harvesting time* required by a node v_i to accumulate 1ϵ amount of energy. Thus, a node has a harvesting rate of $\frac{\epsilon}{r_i}$ per time slot. Each capacitor for a node v_i is assumed to have sufficient capacity to store all harvested energy in each slot, i.e., $c_i \geq 1/r_i$. The energy level of each capacitor is zero at the start of each time slot. Any unused energy that the harvester receives at slot t, e.g., any excess energy when $r_i < 1$ or node v_i is not active, is stored in a rechargeable battery for use in slot $t+1$ and thereafter. The battery of a node is initially empty.

The rechargeable battery of a node supports *shallow recharging* [32], meaning it can be recharged even though it is partially discharged. Let $b_{i,t}$ be the energy level of a node v_i's battery at time t. For each node v_i, $A_{i,t}$ (in unit of ϵ) represents the amount of energy that a node v_i is allowed to use in slot t; note, $\frac{1}{r_i} \leq A_{i,t} \leq b_{i,t} + \frac{1}{r_i}$. The value of $A_{i,t}$ is the sum of the energy level of a node v_i's battery and capacitor at time t, i.e., $A_{i,t} = b_{i,t} + \frac{1}{r_i}$. As the capacitor has a high leakage rate [51], the energy level in each capacitor is always equal to the energy harvested in each slot, i.e., $\frac{1}{r_i}$. This chapter considers the capacitor of a node has 100% energy storage efficiency. When $A_{i,t} < 1\epsilon$, a node v_i cannot transmit/receive packets at time t. In contrast, if $r_i \leq 1$ or $A_{i,t} \geq 1\epsilon$, a node can transmit/receive at any time, assuming there is an available packet. The available energy $A_{i,t}$ is a function of a node v_i's battery capacity (b_i), energy harvesting rate (r_i), storage efficiency (η_i), leakage rate (μ_i), and energy usage. Let t_i be the time in which node v_i last draws energy from its battery. When $A_{i,t_i} < 1$, it takes $\rho_i = t - t_i$ slots for a node v_i to accumulate energy such that it has $A_{i,t} \geq 1$. As explained later in Section 3.2.1, ρ_i is affected by the harvesting time r_i, storage efficiency η_i, leakage rate μ_i, and energy level b_{i,t_i}.

A battery cannot be charged and discharged simultaneously [91]. However, its energy level may increase when a node uses energy at the same time slot t. This case occurs when $r_i < 1$. On the other hand, when $r_i > 1$ and $b_{i,t} \geq 1 - \frac{1}{r_i}$, then a node v_i will draw the fraction $1 - \frac{1}{r_i}$, i.e., an energy shortfall from its battery. Finally, since the amount of leaked energy can never be larger than the energy stored in a node's battery, we have the amount of energy that a node v_i uses at time $t + 1$ is greater than or equal to the energy at time t; i.e., $A_{i,t+1} \geq A_{i,t}$.

Let T_i denote the earliest time slot when a node v_i has at least 1ϵ of energy to transmit/receive one packet. In other words, T_i is the earliest slot such that $A_{i,T_i} \geq 1\epsilon$. The earliest time link $l_{i,j}$ can be scheduled is thus at time $t_{i,j} = \mathbf{max}(T_i, T_j)$. Note that a link can be scheduled only when each of its end nodes have at least 1ϵ amount of energy. Let t_i be the most recent time a node v_i transmits/receives a packet.

Consider Figure 3.2a to illustrate the aforementioned notation. The batteries at the nodes in Figure 3.2a have energy levels of $b_1 = 3$, $b_2 = b_3 = b_4 = 2$, and harvesting time of $r_1 = 2$, $r_2 = 6$, $r_3 = 5$, and $r_4 = 7$ timeslots. Assume $\eta_i = 1$ and $\mu_i = 0$ for all batteries. At time $t = 1$, the available energy of node 1 is $A_{1,1} = 0.5\epsilon$, while at time $t = 2$, it increases to $A_{1,2} = 1\epsilon$. Thus, the earliest time node v_1 can transmit/receive is $T_1 = 2$. For the other nodes, Figure 3.2a shows $T_2 = 6$, $T_3 = 5$, and $T_4 = 7$. The earliest time in which nodes v_1 and v_2 can transmit/receive is therefore $t_{1,2} = \mathbf{max}(2, 6) = 6$. The other two nodes have $t_{3,1} = 5$ and $t_{4,3} = 7$. Notice that the first four slots in schedule $\mathcal{S}$ are empty because the smallest $t_{i,j}$ is five. Assume a scheduler selects link $l_{1,2}$ first, at time 6; thus, $t_1 = t_2 = 6$ and the next earliest time nodes v_1 and v_2 can transmit/receive is at slot $T_1 = 6 + 2 = 8$ and $T_2 = 12$, respectively. Figure 3.2b shows the conflict graph C_G for the rWSN in Figure 3.2a. In Figure 3.2b, there are two primary interferences, i.e., link $l_{4,3}$ with $l_{3,1}$ and $l_{3,1}$ with $l_{1,2}$. Also shown is the secondary interference at node v_3 that is caused by node v_1.

3.1.2 Problem Statement

For a given rWSN, the **Link Scheduling in Harvest-Use-Store (LSHUS)** problem is to generate a TDMA link schedule $\mathcal{S}$ with the shortest length $|\mathcal{S}|$ such

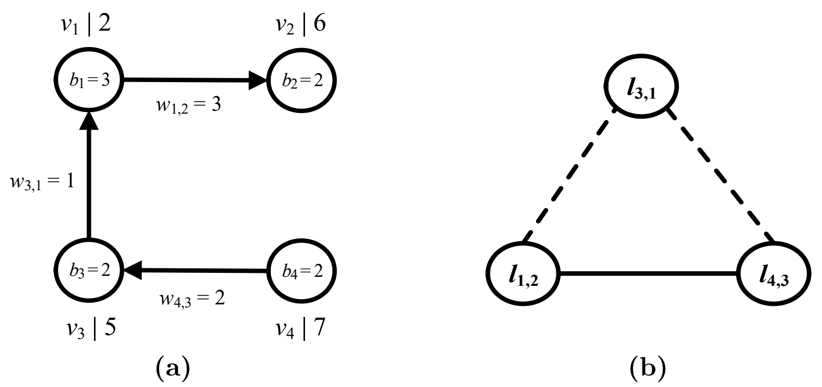

Figure 3.2 A rWSN model: (a) graph G, and its (b) conflict graph C_G. Also shown are primary (dashed lines) and secondary (solid line) interference.

that: (i) each link $l_{i,j}$ that is allocated a time slot t satisfies $A_{i,t} \geq 1\epsilon$ and $A_{j,t} \geq 1\epsilon$, and (ii) each link $l_{i,j} \in E$ is scheduled at least $w_{i,j}$ times in $\mathcal{S}$. For example, in Figure 3.2a, link $l_{3,1}$ can be scheduled no earlier than $t = 5$; and link $l_{1,2}$ needs to be scheduled three times because $w_{1,2} = 3$.

To illustrate the effect of link scheduling on $|\mathcal{S}|$, consider the example in Figure 3.2 with equal $\mu_i = 0$ and $\eta_i = 1$. Figure 3.3a shows one *feasible* schedule. A schedule is called *feasible* if it satisfies constraints (i) and (ii). The optimal solution can be found in Figure 3.3b. Note that the figure shows only non-empty slots, i.e., each empty slot is represented as "…". The problem aims to generate a schedule $\mathcal{S}$ with the shortest length, e.g., the schedule in Figure 3.3b has length of $|\mathcal{S}| = 18$.

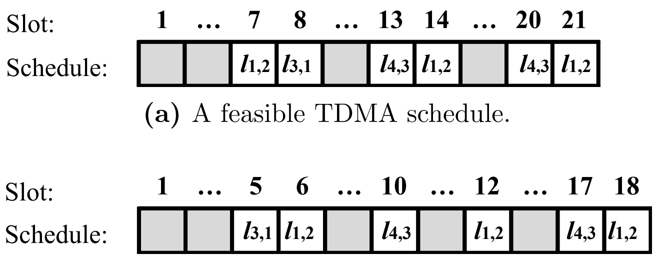

Slot:	1	…	7	8	…	13	14	…	20	21
Schedule:			$l_{1,2}$	$l_{3,1}$		$l_{4,3}$	$l_{1,2}$		$l_{4,3}$	$l_{1,2}$

(a) A feasible TDMA schedule.

Slot:	1	…	5	6	…	10	…	12	…	17	18
Schedule:			$l_{3,1}$	$l_{1,2}$		$l_{4,3}$		$l_{1,2}$		$l_{4,3}$	$l_{1,2}$

(b) The optimal TDMA schedule.

Figure 3.3 TDMA schedules for the rWSN in Figure 3.2. Gray coloured slots indicate no transmissions/receptions.

Let $\mathcal{S}_{\mathcal{E}}$ represent the superframe generated when there is no interference. In this case, the activation of links is delayed by insufficient energy as opposed to interference. One can use $|\mathcal{S}_{\mathcal{E}}|$ as the lower bound of the superframe length for LSHUS, computed as

$$|\mathcal{S}_{\mathcal{E}}| = \mathbf{max}\left(\rho_i\left(\sum_{j\epsilon N(i)} w_{i,j} + \sum_{j\epsilon N(i)} w_{j,i}\right)\right) \tag{3.1}$$

where $N(i)$ is the set of node v_i's neighbours.

The following theorem states that the LSHUS problem is intractable.

Theorem 3.1. *LSHUS is NP-Complete.*

Proof. In [65], Ergen *et al.* addressed the following NP-Complete scheduling problem, referred to as *ScheduleEV*: consider a WSN $G(V, E)$ that forms a tree in which each node v_i except the root node, generates $\omega_i > 0$ packets. The scheduling problem is to find a superframe with the minimum length such that all nodes can send their packets to the root node. Note that ScheduleEV and LSHUS use the same conflict graph. The proof is by reduction from ScheduleEV to LSHUS. Specifically, an instance of WSN $G(V, E)$ for ScheduleEV can be mapped into an instance of WSN $G'(V', E')$ for LSHUS as follows. Firstly, set $G' = G$, i.e., $V' = V$, and $E' = E$. Secondly, for each node v_i in G', compute its weight w_i as follows. For each leaf node in G', set $w_i = \omega_i$. Then, compute the weight of each parent node v_j by summing the weight of all its children and ω_j. Note that one can interpret each weight w_i as the total number of packets that each node v_i in G' must transmit to the root node; further, nodes forward their own packets as well as those generated by their descendant nodes. Finally, compute the weight $w_{i,j}$ of each link (i, j) in G' from node weight w_i, i.e., set $w_{i,j} = w_i$, where node v_j is the parent of node v_i. Note that each link weight $w_{i,j}$ in G' represents the total number of times a link (i, j) must be activated in the superframe such that a node v_i can forward w_i packets to its parent node v_j until all packets reach the root node. Figure 3.4a shows an example of WSN G [65] while Figure 3.4b gives its mapping graph G'; the number next to a node and a link shows its node and link weight, respectively. Note that G' can be constructed from G in polynomial time. Now, we show how the solution for LSHUS, for instance G' gives the solution for ScheduleEV on instance of G. Consider two cases: (i) $r_i = 1$, and (ii) $r_i > 1$. For both cases, consider each battery has a capacity of $b_i = 1$, a storage efficiency of $\eta_i = 1$, and a leakage rate of $\mu_i = 0$.

For case (i), where each node always has sufficient energy to transmit or receive one packet, the superframe $\mathcal{S}_1$ of LSHUS for instance G', generated by an optimal scheduler Opt_1, is exactly the solution for instance G of ScheduleEV. For case (ii), due to the energy harvesting constraint, each node v_i must wait for at least r_i slots after each transmission or reception before the node is able to transmit or receive another packet. Consider a scheduler Opt_2 that uses Opt_1 to generate superframe $\mathcal{S}_2$. More specifically, Opt_2 utilizes Opt_1 only when all nodes have sufficient energy to transmit or receive packets. First, Opt_2 sets τ_0 to the maximum r_i among all nodes in G' and sets the first τ_0 slots in $\mathcal{S}_2$ to be empty slots. Then, it calls Opt_1 to schedule links in slot $\tau_0 + 1$. Note that in slot $\tau_0 + 1$, all nodes have sufficient energy to transmit or receive a packet, and thus Opt_1 generates exactly the same set of links in slot $\tau_0 + 1$ of $\mathcal{S}_2$ as the links in slot 1 of $\mathcal{S}_1$. After that, Opt_2 (a) computes the maximum time τ_1 such that each end node of the scheduled links in $\tau_1 + 1$ of $\mathcal{S}_2$, and thus those in slot 1 of $\mathcal{S}_1$, has at least 1ϵ of energy, (b) sets each slot from $\tau_0 + 2$ to τ_1 to empty, and (c) calls Opt_1 to generate another set of links for slot $\tau_1 + 1$. Thus, the links in $\tau_1 + 1$ of $\mathcal{S}_2$ are exactly the same as those in slot 1 of $\mathcal{S}_1$. Scheduler Opt_2 repeats steps (a) to (c) each time after it calls Opt_1 until each link (i, j) is scheduled $w_{i,j}$ times.

Following the said steps, there is a one-to-one mapping between each non-empty slot in $\mathcal{S}_2$ and one slot in $\mathcal{S}_1$, i.e., the corresponding slots contain the same links since they are generated by the same scheduler Opt_1 when all nodes have no energy constraint. Thus, one can obtain superframe $\mathcal{S}_1$ for ScheduleEV from $\mathcal{S}_2$ by removing all empty slots. We now conclude that for both cases, LSHUS is at least as hard as ScheduleEV, i.e., LSHUS is also an NP-Complete problem. □

It is important to note that while Opt_2 produces the optimal solution for ScheduleEV, it cannot, in general, be used to produce the optimal solution for LSHUS for two main reasons. First, Opt_2 inserts an excessive number of empty slots, and thus its solution is likely much longer than the optimal solution. Second, LSHUS is more complex than ScheduleEV because the former considers any arbitrary topologies, not only tree topologies in the latter problem. Moreover, we consider $\mu_i \geq 0$ and $\eta_i \leq 1$.

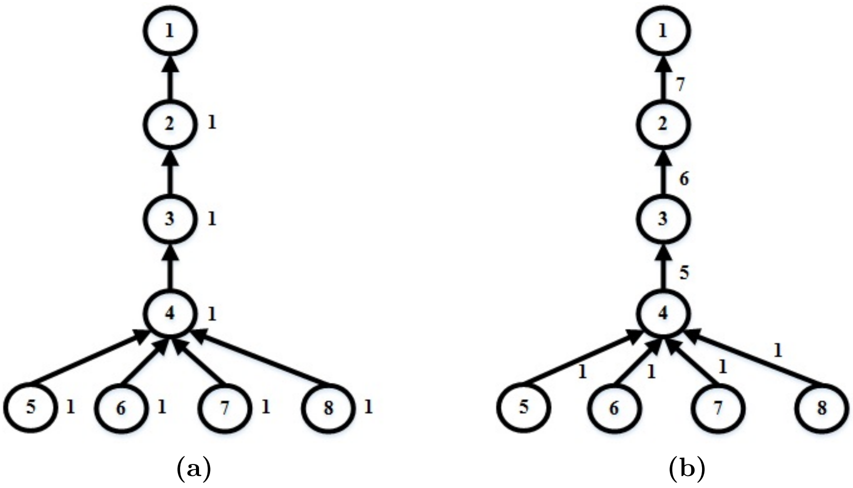

Figure 3.4 An instance of (a) graph G, and its mapping (b) graph G'.

3.1.3 Problem Analysis

This section analyses the effects of harvesting time, battery storage efficiency, leakage, and capacity on the schedule length on the three fixed topologies described in Section 2.6.1.1, i.e., *Line*, *Binary Tree* (*BTree*), and *Grid*. Consider each node has an equal harvesting time $r > 0$, battery capacity $b \geq 1$, and link weight $w \geq 1$. Further, the storage efficiency is set to $\eta = 1$ and the leakage rate is set to $\mu = 0$; thus $\rho = r$. Recall that ρ_i is the number of slots for a node i to accumulate energy to reach at least 1ϵ worth of energy, starting from the time the node has $A_{i,t} < 1\epsilon$.

Proposition 3.1. *The optimal link schedule for Line topology with $n \geq 3$ has superframe length $|\mathcal{S}| = 4wr$.*

Proof. This proof first describes how to construct a link schedule with $4wr$ time slots, for two cases: $r = 1$ and $r > 1$. Then, it shows that the result is optimal.

Consider each link has weight $w = 1$. For $r = 1$, schedule links in the set $\{(2 + 4i, 3 + 4i), (5 + 4i, 4 + 4i)\}$ in Slot-1, for $i = 0, 1, \cdots, \lfloor (n - 2) \ / \ 4 \rfloor$; e.g., for $n = 9$, Slot-1 contains links $\{(2, 3), (5, 4), (6, 7), (9, 8)\}$. Then, reverse the direction of each link in Slot-1, and schedule the reversed link in Slot-2; e.g., Slot-2 contains links $\{(3, 2), (4, 5), (7, 6), (8, 9)\}$. Next, schedule links in the set $\{(1 + 4i, 2 + 4i), (4 + 4i, 3 + 4i)\}$ in Slot-3, for $i = 0, 1, \cdots, \lfloor (n - 2) \ / \ 4 \rfloor$; e.g., links $\{(1, 2), (4, 3), (5, 6), (8, 7)\}$, and finally reverse the links for Slot-4; e.g., links $\{(2, 1), (3, 4), (6, 5), (7, 8)\}$. For $r > 1$, use the same link schedule described above for case $r = 1$ each time all nodes have sufficient energy. Thus, this case will have four non-empty slots. The first $r - 1$ slots are empty as all nodes have insufficient energy. Therefore, the first non-empty slot is slot r, which is followed by $r - 1$ empty slots. After that the scheduler can activate other links in slot $2r$. Similarly, the third and fourth non-empty slots are slot $3r$ and $4r$, respectively.

When each link has weight $w \geq 1$, repeat the schedule w times, and thus, the link schedule has $4wr$ slots, which is optimal for a *Line* with $n \geq 3$ for the following reason. For $n \geq 3$, some nodes in the *Line* have four bidirectional links;

each of which can be activated no earlier than every r slots. Further, each link has to be activated w times, and thus the schedule requires $4wr$ slots. □

Proposition 3.2. *The optimal link schedule for a BTree with $L \geq 3$ levels has $|\mathcal{S}| = 6wr$ time slots.*

Proof. This proof first outlines the steps used to obtain a link schedule with $6wr$ time slots for the following cases: (i) $r = 1$ and (ii) $r > 1$. Then, it shows that the result is optimal.

For $r = 1$, links in a *BTree* with three levels can be scheduled in six slots: Slot-1 $= \{(1,2),(3,6)\}$, Slot-2 $= \{(2,1),(6,3)\}$, Slot-3 $= \{(1,3),(2,4)\}$, Slot-4 $= \{(3,1),(4,2)\}$, Slot-5 $= \{(2,5),(3,7)\}$, and Slot-6 $= \{(5,2),(7,3)\}$. The link schedules for a four-level *BTree*, see Figure 2.3, can be generated from the schedules of two *BTree* with three levels as follows. Denote the larger tree as T with root R, and the two smaller trees as $T1$ and $T2$ with root $R1$ and $R2$, respectively. Tree T is constructed from $T1$ and $T2$ by connecting R to $R1$ with two bidirectional links, and R to $R2$ with two other links, i.e., $T1$ and $T2$ are the left and right subtrees of T, respectively. Thus, renumbering the nodes in T, the label of nodes R, $R1$, and $R2$ are 1, 2, and 3 respectively. Links in T are scheduled as follows. First, combine the links of $T1$ scheduled in one slot with the corresponding links of $T2$ that are scheduled in the same slot number. Notice that no links in $T1$ interfere with any links in $T2$, and vice versa. Then, insert each of the four incident links at R into a slot that does not contain any link that interferes with it. More specifically, links $(1,2)$, $(2,1)$, $(1,3)$, and $(3,1)$ are inserted into a slot that contains links $(8,4)$, $(4,8)$, $(12,24)$, and $(24,12)$, respectively. Using the same steps, one can schedule links in a five-level tree using the six slot schedules of its two four-level subtrees. Repeating the process, one can always generate the link schedules of a tree with k levels in six slots from the schedules of its two subtrees with $(k-1)$ levels, for any $k \geq 4$.

For $r > 1$, the first $r-1$ slots contain no links because each node requires a harvesting time r. Then, use the same link schedules described for case $r = 1$, except after scheduling the first set of links at slot r, each node can transmit or receive only after every r slots, i.e., there are $r-1$ empty slots in between every non-empty slot. Thus, $|\mathcal{S}| = 6r$ for $w = 1$.

When $w \geq 1$, one can repeat the above schedule w times, and thus the link schedule uses $6wr$ slots. The optimality of the schedule is shown as follows. For $L \geq 3$, some nodes in a *BTree* have six bidirectional links, each of which can be activated no earlier than every r slots of harvesting time. Since each link must be activated w times, the schedule requires $6wr$ slots. □

Proposition 3.3. *The optimal link schedule length for a Grid of size row* ≥ 3 *and col* ≥ 3 *is* $|\mathcal{S}| = 8wr$.

Proof. From *Proposition 3.1*, the link schedule of each *Line* graph requires $4wr$ slots. The following describes how to produce the schedule for a *Grid* with length $8wr$. Finally, the length is shown to be optimal.

Consider the schedule of links in **row** *Line* graphs. One can observe that links in *odd* rows can be activated in $4wr$ slots. Same rules apply for links in *even* rows. Except for links in two consecutive rows, there is no other interference. Without loss of generality, consider the links in R_2 and R_3 in Figure 2.4. Note that there is an interference only between nodes in each (2×2) *Grid*, e.g., nodes $\{4,5\}$ at R_2 and $\{7,8\}$ at R_3, and when their links are in opposite directions, e.g., links $(4,5)$ and $(8,7)$ that incur interference at nodes 5 and 7. To prevent any interference, each slot must contain links of the same directions, e.g., links $(4,5)$ and $(7,8)$. Thus, links in all rows can be scheduled in $4wr$ slots. As an example, for Figure 2.4 with $r = w = 1$, the four slots are: Slot-1 = $\{(1,2)$, $(4,5)$, $(7,8)$,

$(10, 11)\}$, Slot-2 $= \{(2, 1), (5, 4), (8, 7), (11, 10)\}$, Slot-3 $= \{(2, 3), (4, 5), (8, 9), (11, 12)\}$, and Slot-4 $= \{(3, 2), (6, 5), (9, 8), (12, 11)\}$. The same construction for links is used in all columns. More specifically, these links are scheduled in $4wr$ slots. Thus, all links in a *Grid* can be scheduled in $4wr + 4wr = 8wr$ slots. The constructed schedules are optimal because for $row \geq 3$ and $col \geq 3$, some nodes in a $(row \times col)$ *Grid* have eight bidirectional links, e.g., node 5 and 8 in Figure 2.4. Since each node can be activated no earlier than every r slots of harvesting time for w times, the link schedule of a *Grid* requires $8wr$ slots. □

Propositions 3.1, *3.2*, and *3.3* show the effect of energy harvesting time and link weight on the schedule length. These propositions indicate that, for $r > 1$ and $w \geq 1$, there are $4w(r-1)$, $6w(r-1)$, and $8w(r-1)$ empty slots in the TDMA schedules for *Line*, *BTree*, and *Grid*, respectively, and thus the schedule lengths increase as much. Further, all propositions show that the battery capacity of nodes and the network size do not affect the schedule length for the *Line*, *BTree*, and *Grid*. In addition, the lower bound in Eq. (3.1) is tight for the fixed topologies when $\mu = 0$ and $\eta = 1$.

3.2 Solution

Section 3.2.1 describes three propositions relied upon by the proposed greedy algorithm, namely, **Link Scheduler for a rechargeable WSN (LS-rWSN)**, to solve LSHUS. The details of LS-rWSN are presented in Section 3.2.2.

3.2.1 Key Properties

Algorithm LS-rWSN schedules links according to the earliest time in which they have sufficient energy. It relies on the following *Propositions 3.4*, *3.5*, and *3.6*.

Let t_i be the time in which a node v_i last draws energy from its battery and b_{i,t_i} be the energy level of the battery at a node v_i at time t_i.

Proposition 3.4 computes $A_{i,t}$, the amount of energy at node v_i that can be used to transmit/receive packets at time $t \geq 1$, computed as $A_{i,t} = b_{i,t} + 1/r_i$. For brevity, in the following propositions, we define $\hat{r}_i = r_i/\eta_i$ and $\hat{\mu}_i = 1 - \mu_i$. Further, we use τ_i to denote the time span between time t_i and t, i.e., $\tau_i = t - t_i$.

Proposition 3.4. *The amount of energy (in unit of ϵ) that a node v_i can use at timeslot $t > t_i$ is*

$$A_{i,t} = \mathbf{min}(b_i + 1/r_i, \hat{\mu}_i^{\tau_i} b_{i,t_i} + \sum_{k=0}^{\tau_i - 2} \frac{\hat{\mu}_i^k}{\hat{r}_i} + 1/r_i) \tag{3.2}$$

Proof. The stored energy at time t_i+1, i.e., b_{i,t_i+1}, is computed by subtracting the energy due to leakage from the battery, i.e., $\mu_i b_{i,t_i}$ and adding energy harvested at slot t_i, i.e., $1/\hat{r}_i$. However, for HUS with $r_i > 1$, a node v_i spends all the energy harvested at time t_i by slot t_i; i.e., $1/\hat{r}_i = 0$. Thus, $b_{i,t_i+1} = (1 - \mu_i)b_{i,t_i}$. Similarly, one can compute the amount of energy available at the battery at time slot $t_i + 2$ from the stored energy at $t_i + 1$, minus the amount of energy that has leaked between time $t_i + 1$ and $t_i + 2$, plus the stored energy from the energy harvested in time slot $t_i + 1$. Thus, the result is $b_{i,t_i+2} = (1 - \mu_i)b_{i,t_i+1} + 1/\hat{r}_i$. Substituting b_{i,t_i+1} with $(1 - \mu_i)b_{i,t_i}$ gets $b_{i,t_i+2} = (1 - \mu_i)[(1 - \mu_i)b_{i,t_i}] + 1/\hat{r}_i$ $= (1 - \mu_i)^2 b_{i,t_i} + 1/\hat{r}_i$. Next, for time $t_i + 3$, this case obtains $b_{i,t_i+3} = (1 - \mu_i)^3 b_{i,t_i} + (1 - \mu_i)/\hat{r}_i + 1/\hat{r}_i$. Repeating the step for time $t_i + 4, \cdots, t - 1, t$, one can generate the stored energy at the battery at the beginning of time t, i.e., $b_{i,t} = (1 - \mu_i)^{t - t_i} b_{i,t_i} + \sum_{k=0}^{t-t_i-2} (1 - \mu_i)^k/\hat{r}_i$. Note that for the HUS model, the available energy at a node v_i at time t is the sum of its available energy at the beginning of time t and the energy harvested at time t. In particular, the model has $A_{i,t} = b_{i,t} + 1/r_i$ or $A_{i,t} = (1 - \mu_i)^{\tau_i} b_{i,t_i} + \sum_{k=0}^{\tau_i - 2} (1 - \mu_i)^k/\hat{r}_i + 1/r_i$. However,

$b_{i,t}$ is bounded by the battery capacity b_i, which implies $A_{i,t} \leq b_i + 1/r_i$. □

Consider the following terms in Eq. (3.2): (i) $\hat{\mu}_i^{\tau_i} b_{i,t_i}$, (ii) $\sum_{k=0}^{\tau_i - 1} \frac{\hat{\mu}_i^k}{\hat{r}_i}$, and (iii) $1/r_i$. Term (i) represents the amount of energy stored in the battery of a node v_i up to time t_i after accounting for energy leakage. Term (ii) shows the amount of energy that can be added to the battery from time t_i to the start of time t. The last term shows the amount of harvested energy, in the capacitor, at time t that is available for use by a node v_i.

Consider four possible tuples $(\eta_i,\ \mu_i)$ in Eq. (3.2): (i) $(\eta_i = 1,\ \mu_i = 0)$, (ii) $(0 < \eta_i \leq 1,\ \mu_i = 1)$, (iii) $(\eta_i = 0,\ 0 \leq \mu_i < 1)$, and (iv) $(0 < \eta_i < 1,\ 0 < \mu_i < 1)$. For case (i), the battery has 100% storage efficiency and no leakage, and hence, Eq. (3.2) reduces to the following equation:

$$A_{i,t} = \mathbf{min}(b_i + 1/r_i, A_{i,t_i} + (\tau_i - 1)/r_i) \tag{3.3}$$

In case (ii), the battery cannot retain its stored energy. One can see that when $\hat{\mu}_i = 0$, Eq. (3.2) reduces to $A_{i,t} = 1/r_i$. In case (iii), when $\eta_i = 0$, no harvested energy can be stored in the battery. For this case, the harvesting time is set to $\hat{r}_i = \infty$. Thus, the value of the aforementioned term (ii) in Eq. (3.2) becomes 0. Cases (ii) and (iii) represent a possibly faulty battery. Finally, case (iv) considers the effects of battery storage efficiency and leakage on the available energy of each node.

Our work considers $0 \leq \mu_i < 1$ and $0 < \eta_i \leq 1$, i.e., only case (i) and (iv). On the other hand, the work in [89] considered only case (i), and thus, our work generalises the battery model in [89] to also consider battery storage efficiency and leakage. *Proposition 3.5* computes the number slots $\rho_i = t - t_i$ needed such that $A_{i,t} = 1\epsilon$. The condition $A_{i,t_i} < 1$ means that the amount of available energy at a node v_i at time t_i is insufficient to transmit/receive one packet. Note that

$A_{i,t_i} < 1$ implies $r_i > 1$ and $b_{i,t} < 1 - 1/r_i$.

Proposition 3.5. *Given $A_{i,t_i} < 1$, the number of slots $\rho_i = t - t_i$ before a node v_i has $A_{i,t} = 1$ is given as*

Case (i): $\eta_i = 1$ *and* $\mu_i = 0$

$$\rho_i = \lceil r_i(1 - A_{i,t_i}) + 1\rceil \tag{3.4}$$

Case (ii): $0 < \eta_i < 1$ *and* $0 < \mu_i < 1$

$$\rho_i = \lceil \frac{log(\frac{\mu_i - \mu_i r_i + \eta_i}{\eta_i - b_{i,t_i}\mu_i r_i(1-\mu_i)})}{log(1-\mu_i)} + 1\rceil \tag{3.5}$$

Proof. A node v_i needs at least $(1 - A_{i,t_i})\epsilon$ extra energy to reach 1ϵ unit of energy. Eq. (3.2) is used to compute the time span $\rho_i = t - t_i$ such that $A_{i,t} \geq 1$. More specifically, to compute the smallest ρ_i that satisfies the following:

$$\hat{\mu}_i^{\rho_i} b_{i,t_i} + \sum_{k=0}^{\rho_i - 2} \frac{\hat{\mu}_i^k}{\hat{r}_i} + 1/r_i \geq 1 \tag{3.6}$$

For case (i), setting $\hat{\mu}_i = 1$ and $\hat{r}_i = r_i$ in Eq. (3.6) obtains $b_{i,t_i} + \rho_i/r_i \geq 1$. Since $A_{i,t_i} = b_{i,t_i} + 1/r_i$, case (i) produces $A_{i,t_i} - 1/r_i + \rho_i/r_i \geq 1$. Thus, $\rho_i = \lceil r_i(1 - A_{i,t_i} + 1)\rceil$ as shown in Eq. (3.4). In case (ii), $\hat{\mu}_i \neq 1$, and thus one can use the geometric series to produce $\sum_{k=0}^{\rho_i-1} \frac{\hat{\mu}_i^k}{\hat{r}_i} = \frac{1}{\hat{r}_i}\frac{\hat{\mu}_i^{\rho_i}-1}{\hat{\mu}_i-1}$. Thus, Eq. (3.6) becomes $\hat{\mu}_i^{\rho_i} b_{i,t_i} + \frac{1}{\hat{r}_i}(\frac{\hat{\mu}_i^{\rho_i}-1}{\hat{\mu}_i-1} - \hat{\mu}^{\rho_i-1}) + 1/r_i \geq 1$, which is used to obtain ρ_i in Eq. (3.5). □

Recall that Eq. (3.4) and Eq. (3.5) apply only when $A_{i,t_i} < 1$, which implies $r_i > 1$ and $b_{i,t} < 1 - 1/r_i$. For $b_{i,t} = 0$, Eq. (3.4) has $\rho_i = r_i$, which is consistent with the fact that when the battery is leakage free and has perfect storage efficiency, it takes r_i slots to accumulate 1ϵ of energy. In addition, Eq. (3.5) requires $\eta_i - b_{i,t_i}\mu_i r_i > 0$, or $\frac{\eta_i}{r_i} > \mu_i b_{i,t_i}$. In other words, the amount of harvested energy to be stored in the battery must be greater than the energy leakage from the battery. Otherwise, the battery is always empty. Eq. (3.5) also requires $\mu_i - \mu_i r_i + \eta_i > 0$, or $\frac{\eta_i}{r_i - 1} > \mu_i$. Let $\mathcal{T}(b_{i,t_i}, r_i, \eta_i, \mu_i)$ be a function to compute the value of ρ_i for Eq. (3.6). Specifically, for ($\eta_i = 1$, $\mu_i = 0$) and ($\eta_i \neq 1$, $\mu_i \neq 0$), the function produces Eq. (3.4) and Eq. (3.5), respectively.

The following *Proposition 3.6* computes the next value of T_i after a node v_i transmits/receives one packet at time t_i. Let α_{i,t_i} be a Boolean variable such that $\alpha_{i,t_i} = 1$ ($\alpha_{i,t_i} = 0$) if at time t_i, a node v_i has $A_{i,t_i} < 1\epsilon$ ($A_{i,t_i} \geq 1\epsilon$). Further, set $\sigma_i = t_i$ ($\sigma_i = t_i + 1$) when $A_{i,t_i} < 1\epsilon$ ($A_{i,t_i} \geq 1\epsilon$).

Proposition 3.6. *The next earliest time slot when a node v_i has sufficient energy to transmit/receive one packet is*

$$T_i = \sigma_i + \alpha_{i,t_i}\rho_i \tag{3.7}$$

Proof. The next value of T_i depends on the remaining available energy in a node v_i, i.e., A_{i,t_i}, harvesting time r_i, the battery's storage efficiency η_i, and leakage rate μ_i. Eq. (3.7) considers two cases. First, when $A_{i,t_i} < 1\epsilon$, a node v_i needs $(1 - A_{i,t_i})\epsilon$ extra energy to transmit/receive the next packet. Proposition 3.5, i.e., Eq. (3.4) and (3.5), is used to compute the number of slots ρ_i for a node v_i to accumulate the extra energy. Thus, $T_i = t_i + \rho_i$, and in Eq. (3.7), $\alpha_{i,t_i} = 1$, and $\sigma_i = t_i$. Second, when $A_{i,t_i} \geq 1\epsilon$, after a node v_i uses 1ϵ of energy at time t_i, the node still has sufficient energy to transmit/receive another packet at time t_i. However, the primary interference does not allow a node to transmit/receive more than one packet at the same timeslot. Thus, the earliest time the node can transmit/receive a packet is in the next slot, i.e., $T_i = t_i + 1$. For this case, in Eq. (3.7), $\alpha_{i,t_i} = 0$ and $\sigma_i = t_i + 1$. □

Our work in [89] considered batteries with 100% storage efficiency and zero leakage, i.e, $\eta_i = 1$ and $\mu_i = 0$. For this case, using Eq. (3.4), Eq. (3.7) becomes

$T_i = \sigma_i + \alpha_{i,t}(r_i(1 - A_{i,t}))$, as given in [89]. Further, this case produces $T_i = r_i$ for $b_{i,t} = 0$ or $t = 0$ because each battery is initially empty.

3.2.2 LS-rWSN

This section provides the details of the new algorithm, i.e., LS-rWSN in Algorithm 1. The algorithm selects each non-interfering link with end nodes that have sufficient energy to transmit/receive one packet at the earliest time. It uses the conflict graph C_G to check for interfering links.

LS-rWSN first initialises t_i to the last timeslot a node v_i draws energy from its battery, and A_{i,t_i} to the amount of energy that a node v_i can use at time t_i to zero; see *Lines 1–5* of LS-rWSN. It also sets T_i to ρ_i slots, i.e., the solution for Eq. (3.6). Recall that T_i is the earliest time a node v_i has 1ϵ energy. LS-rWSN starts at $t = 0$ and the battery is initially empty. *Lines 6–8* compute the earliest time a link (i, j) can be scheduled, while *Line 9* generates a set K to record a link (i, j) that has the earliest activation time. *Line 10* uses function ORDER(K) to sort links in K. It aims to maximise the number of links that can be scheduled at time t without interference. The function greedily schedules links closer to each other when there is no interference. More specifically, function ORDER(K) performs the following steps: (i) Select a link $(i, j) \in K$; (ii) Move a link (i, j) from set K into a set K'; (iii) Find a link $(m, k) \in K$ that does not interfere with any link in K', where k is node v_j's neighbour. Note that there is no interference between links (i, j) and (m, k); (iv) Move (m, k) from K to K'; (v) Set $j = k$ and repeat (iii) until no such link can be found in K; (vi) repeat step (i) until K is empty. Without loss of generality, when there is more than one candidate link for selection in steps (i) and (iii), select a link (u, v), where u is a node with the smallest label, and v is node u's neighbour with the smallest label.

Algorithm 1 LS-rWSN: a greedy algorithm that schedules links according to the earliest activation time

Input: $G(V, E)$, r_i, b_i, μ_i, η_i of each node $i \in V$, weight $w_{i,j}$ of each link $l_{i,j} \in E$, and conflict graph C_G

Output: Superframe $\mathcal{S}$

```
 1: for each node $i \in V$ do
 2:     $t_i \leftarrow 0$
 3:     $A_{i,t_i} \leftarrow 0$
 4:     $T_i \leftarrow \mathcal{T}(0, r_i, \eta_i, \mu_i)$
 5: end for
 6: for each link $l_{i,j} \in E$ do
 7:     $t_{i,j} \leftarrow \mathbf{max}(T_i, T_j)$
 8: end for
 9: $K = \{$node $l_{i,j}$ in $C_G$ with $\mathbf{min}\{t_{i,j}\}\}$
10: $K' = \mathrm{ORDER}(K)$
11: $t \leftarrow \mathbf{min}\{t_{i,j}\}$
12: for each $l_{i,j} \in K'$ do
13:     if NOT $CONFLICT(l_{i,j}, \mathcal{S}[t])$ then
14:         $\mathcal{S}[t] \leftarrow \mathcal{S}[t] \cup l_{i,j}$
15:         $w_{i,j} \leftarrow w_{i,j} - 1$
16:         if $w_{i,j} = 0$ then
17:             remove node $l_{i,j}$ from $C_G$
18:         end if
19:         $A_{i,t} \leftarrow COMPUTE\_A_{\alpha,t}(t, i, \mu_i, \eta_i)$
20:         $A_{j,t} \leftarrow COMPUTE\_A_{\alpha,t}(t, j, \mu_j, \eta_j)$
21:         $t_i \leftarrow t_j \leftarrow t$
22:         $T_i \leftarrow COMPUTE\_T_{\alpha}(t, i, \mu_i, \eta_i)$
23:         $T_j \leftarrow COMPUTE\_T_{\alpha}(t, j, \mu_j, \eta_j)$
24:         $UPDATE\_t_{cd}(T_i, T_j)$
25:     end if
26: end for
27: repeat Lines 9−26 until all $w_{i,j} = 0$
```

Line 11 initialises t with the earliest slot. *Lines 12–26* repeatedly schedule each link $l_{i,j} \in K'$ in order. Each selected link in *Line 14* does not cause interference or is interfered by links that have been scheduled in slot t; see the condition in *Line 13*. Each slot in $\mathcal{S}$ is initially empty. Note that function *CONFLICT()* uses a matrix M of size $|E|^2$ that contains Boolean variables to represent the conflict graph of the network; i.e., $M[a,b]$ is set to "1" if there is an interference between links a and b. *Line 15* decrements the weight of each selected link $l_{i,j}$ by one. Once the weight reaches zero, *Line 17* removes the link from contention. Further, *Lines 19–20* use function $COMPUTE\_A_{\alpha,t}()$ that implements Eq. (3.2) to recompute the available energy $A_{i,t}$ and $A_{j,t}$ at each end node of the selected link. *Line 21* then sets the last time that the end nodes of the selected link use energy to the current time, and $COMPUTE\_T_{\alpha}()$ in *Lines 22–23* use Eq. (3.7) to recompute the T_i and T_j of the two end nodes. Finally, function $UPDATE\_t_{cd}()$ in *Line 24* recomputes the earliest time schedule of each link that has v_i or v_j as one of its end nodes. The steps from *Line 9* are repeated until all links have $w_{i,j} = 0$.

As an example, consider the rWSN and conflict graph C_G shown in Figure 3.2. *Lines 1–5* of LS-rWSN set $t_1 = t_2 = t_3 = t_4 = 0$, $A_{1,t_1} = A_{2,t_2} = A_{3,t_3} = A_{4,t_4} = 0$, $T_1 = \mathcal{T}(0, r_1, \eta_1, \mu_1) = \mathcal{T}(0, 2, 1, 0) = 2$, $T_2 = 6$, $T_3 = 5$, and $T_4 = 7$. *Lines 6-8* compute $t_{1,2} = \mathbf{max}(2, 6) = 6$, $t_{3,1} = 5$, and $t_{4,3} = 7$. *Line 9* places link $l_{3,1}$ into the set K, and thus *Line 10* obtains $K' = l_{3,1}$. *Line 11* sets $t = 5$. *Line 13* finds that $l_{3,1}$ has no conflict with other links, and thus *Line 14* inserts the link into $\mathcal{S}[5]$. *Line 15* reduces $w_{3,1}$ by 1 and hence it becomes 0. *Lines 19–20* compute $A_{3,5} = 0.2$ and $A_{1,5} = 2$, while *Line 21* sets $t_3 = t_1 = t = 5$. *Lines 22–23* obtain $T_3 = 11$ and $T_1 = 6$. *Line 24* updates the earliest time that links can be scheduled, i.e., $t_{1,2} = \mathbf{max}(6,\, 6) = 6$, $t_{3,1} = 11$, and $t_{4,3} = 7$. *Line 27* repeats the steps from *Line 9* until all links have $w_{i,j} = 0$. Figure 3.3b shows the schedule generated by LS-rWSN, i.e., $\mathcal{S} = [\mathcal{S}[5] = \{l_{3,1}\}, \mathcal{S}[6] = \{l_{1,2}\}, \mathcal{S}[10] = \{l_{4,3}\}, \mathcal{S}[12] = \{l_{1,2}\}, \mathcal{S}[17] = \{l_{4,3}\}, \mathcal{S}[18] = \{l_{1,2}\}]$. The generated schedule contains 12 empty slots as nodes are unable to transmit/receive due to insufficient energy.

Proposition 3.7. *The time complexity of LS-rWSN is* $O(W|E|^2)$, *where* $W = \sum_{(i,j)\in|E|}(w_{i,j})$.

Proof. *Lines 1–5* require $O(|V|)$, while *Lines 6–8* require $O(|E|)$. *Line 9* inserts at most $|E|$ links and thus takes $O(|E|\ log\ |E|)$. *Line 10* requires at most $O(|E|^2)$ to sort links in K using the function ORDER(K). *Line 11* takes $O(1)$. *Line 13* uses a matrix M to represent the conflict graph C_G. It takes $O(|E|^2)$ to build the C_G and M. Note that LS-rWSN constructs C_G and M only once. The function in *Line 13* needs to access the matrix $|\mathcal{S}[t]|$ times or $O(|E|)$ to check for interference between a selected link (i, j) and the already scheduled links in $\mathcal{S}[t]$. *Lines 14–23* take $O(1)$ each. *Line 24* requires $O(|V|)$. Thus, the for loop in *Lines 12–26* takes, at most, $O(|E|^2)$ since $|V| \leq |E|$. Finally, *Line 27* repeats *Lines 9–26* W times and hence, the time complexity of LS-rWSN is $O(W|E|^2)$. □

3.3 Evaluation

Section 3.3.1 compares the performance between HSU and HUS in terms of superframe length. Section 3.3.2 analyses the effect of energy harvesting time, battery leakage, and storage efficiency on the superframe length $|\mathcal{S}|$. Then, Section 3.3.3 shows the effect of battery capacity on $|\mathcal{S}|$. Section 3.3.4 contains an evaluation of LS-rWSN versus the theoretical bounds of $|\mathcal{S}|$. Finally, Section 3.3.5 discusses the running time of LS-rWSN. Our evaluation encompasses two types of networks: (i) fixed topologies, namely, *Line*, *BTree*, and *Grid*, with 20 to 100 nodes, and (ii) arbitrary networks with 20 to 50 nodes deployed uniformly on a 40 ×

40 m^2 area. This is sufficient since each node has a fixed location. Further, each presented result is an average over 100 random node deployments. Table 3.1 lists the parameter values used in our evaluation.

Table 3.1 Parameter values used in the evaluation.

Parameter	***Value(s)***
Network size	40×40 m^2
Transmit range	15 m
Interference range	30 m
$\|V\|$ in arbitrary networks	20, 30, 40, 50
$\|V\|$ in fixed topologies	20−100
r_i	$1, 5, 10, 15, 20$
μ_i	$0.0, 0.01, 0.02, 0.03, 0.04$
η_i	$0.6, 0.7, 0.8, 0.9, 1.0$
b_i	3
$w_{i,j}$	3

3.3.1 HSU *versus* HUS

We consider various r_i values; namely, 1, 5, 10, 15, and 20, in a rWSN with 50 nodes. We randomly fix the battery capacity b_i and link weight $w_{i,j}$, each to a value between 1 and 5. As shown in Figure 3.5, harvesting time significantly affects the link schedules in both models. Specifically, when r_i increases from 1 to 20, $|\mathcal{S}|$ jumps from 769 to 2995 slots in HUS and from 990 to 3744 slots in HSU, an increase of 289.5% and 278.2%, respectively. Note that when $r_i = 1$, each node in HUS has sufficient energy to transmit/receive one packet in any slots. Thus, the required number of slots is due to link interference only. The figure also shows that increasing harvesting time consistently creates longer $|\mathcal{S}|$, i.e., when $r_i = 5$, 10, and 15, HUS produces 870, 1506, and 2250 slots, while HSU generates 1508, 2253, and 2998 slots, respectively.

Figure 3.5 shows that the superframe length $|\mathcal{S}|$ when using HSU is longer than HUS. For example, when $r_i = 1$, HSU results in 221 more slots as compared to when using HUS; i.e., 28.74% longer. The results are consistent for other harvesting times, i.e., $r_i = 5$, 10, 15, and 20. The difference between $|\mathcal{S}|$ ranges from 600 to 800 slots. HSU produces superframes that are 73.33%, 49.6%, 33.24%, and 25.01% longer, respectively, than those by HUS. Recall that the work in [44] considered HSU protocol. HUS generates shorter superframes as compared to HSU because the former can directly use harvested energy without storing it first. In the following experiments, we only consider HUS because HSU generates similar trends but longer superframes.

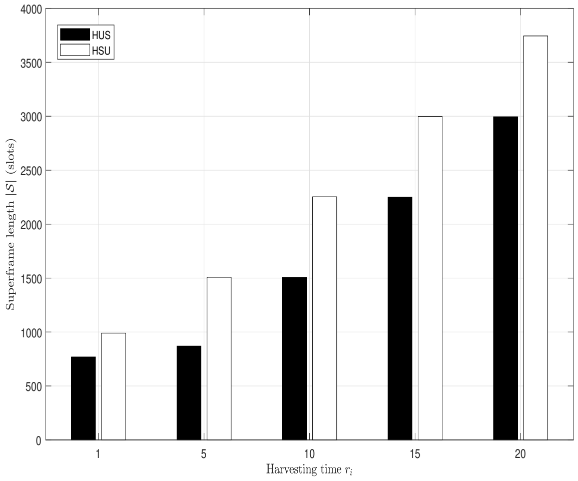

Figure 3.5 HUS versus HSU in rWSNs of 50 nodes.

To further analyse the effect of harvesting time on $|\mathcal{S}|$, we classify slots in the $\mathcal{S}$ into two categories: (i) all slots α in which the end nodes of links have sufficient energy, and (ii) all slots α in which the end nodes of at least one link has insufficient energy, and thus the link can be activated only at slot $\beta > \alpha$ after its end nodes have harvested energy. Thus, due to insufficient energy, $|\mathcal{S}|$ is increased by $\beta - \alpha$ slots.

In this experiment we investigate the effect of insufficient energy for case (ii). As shown in Figure 3.6, when $r_i = 1$, the superframe length $|\mathcal{S}|$ of case (ii) is zero because each node has sufficient energy at any slot. When we increase r_i to 5, some links must be scheduled in later slots because their nodes have no energy. Thus, those links increase $|\mathcal{S}|$ by 47 slots from 815 slots. Further, Figure 3.6 shows that increasing the value of r_i will increase the number of slots under case (ii) because more nodes need a longer time to harvest energy. We see that $|\mathcal{S}|$ for this case is increased by 217, 711, and 1418 slots when $r_i = 10$, 15, and 20, respectively.

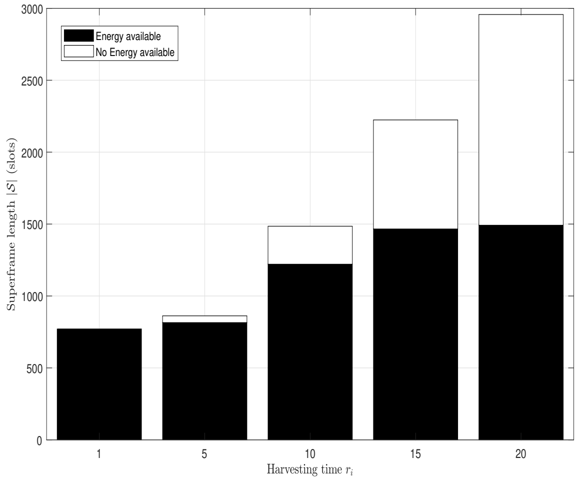

Figure 3.6 The effect of energy unavailability on $|\mathcal{S}|$.

3.3.2 Effect of r_i, μ_i, and η_i on $|\mathcal{S}|$

The following experiments consider three factors: (i) harvesting time, (ii) battery leakage, and (iii) storage efficiency, with the following corresponding values: (i) $r_i = 1, 5, 10, 15, 20$, (ii) $\mu_i = 0.0, 0.01, 0.02, 0.03, 0.04$, and (iii) $\eta_i = 0.6, 0.7, 0.8, 0.9, 1.0$. Further, the battery capacity is $b_i = 3$. Each link has weight $w_{i,j} = 3$. These experiments use the HUS battery usage protocol. Note that Section 3.3.1 has shown that the HUS model produces shorter superframe length as compared to the HSU model.

3.3.2.1 Effect of Harvesting Time

Figure 3.7 shows the resulting superframe length $|\mathcal{S}|$ for various energy harvesting times r_i and leakage values μ_i when the storage efficiency is $\eta_i = 1$. Specifically, from left to right, each bar for each harvesting time is the result for network sizes of 20, 30, 40, or 50 nodes, respectively. Further, each bar shows the average $|\mathcal{S}|$ value when the μ_i is gradually increased from 0 to 0.04. For example, the left (right) most bar for $r_i = 15$ shows five results of $|\mathcal{S}|$ for networks with 20 (50) nodes for each of the five values of μ_i. Recall that $\mu_i = 0$ means the battery has no leakage.

As shown in in Figure 3.7, for $\mu_i = 0$, increasing the energy harvesting time of nodes significantly affects the schedule length. The figure shows that for $r_i = 1$ and $|V| = 20$, the superframe length is $|\mathcal{S}| = 196$. However, as the harvesting time increases, the length increases steadily, reaching $|\mathcal{S}| = 1305$ for $r_i = 20$; this is an increase of 565.82%. This is because more nodes need a longer time to harvest energy. Recall that $r_i = 1$ means each node which uses the HUS mode always has sufficient energy to transmit/receive one packet in any slot. Therefore, there is no constraint on harvesting time. The negative effects of having larger r_i values are similar for each of the tested network sizes; namely, $|V| = 30$, 40, and 50.

3.3.2.2 Effect of Leakage Rate

Figure 3.7 shows when the energy harvesting time of nodes is $r_i = 1$, increasing μ_i from 0 to 0.04 has no effect on the schedule length. That is, $|\mathcal{S}|$ remains at 196, 334, 591, and 820 for networks with 20, 30, 40, and 50 nodes, respectively. However, with a longer harvesting time $r_i > 1$, e.g., $r_i = 15$, increasing μ_i from 0 to 0.04 significantly affects the superframe length $|\mathcal{S}|$. In particular, we see that $|\mathcal{S}|$ increases from 2223 to 3187 slots for $|V| = 50$, an increase of 43.36%. The results are consistent for other tested network sizes, i.e., an increase of 44.54% (from 979 to 1415 slots), 44.24% (1372 to 1979), and 43.92% (1719 to 2474) for networks with 20, 30, and 40 nodes, respectively. Figure 3.7 also shows that, in general, increasing the leakage rate creates longer superframe length $|\mathcal{S}|$. For example, for an energy harvesting time of $r_i = 20$, the link schedule increases by 16.6% (from 1639 to 1911 slots) for 20 nodes, 16.71% (from 2298 to 2682 slots) for 30 nodes, 16.76% (from 2876 to 3358 slots) for 40 nodes, and 16.47% (from 3703 to 4313 slots) for 50 nodes when we increase the value of the leakage rate μ_i from 0.02 to 0.03. The superframe length increases because when $r_i > 1$, a node v_i needs to first accumulate energy until $A_{i,t} = 1\epsilon$. However, due to storage leakage, it requires longer time to accumulate sufficient energy to transmit/receive a packet.

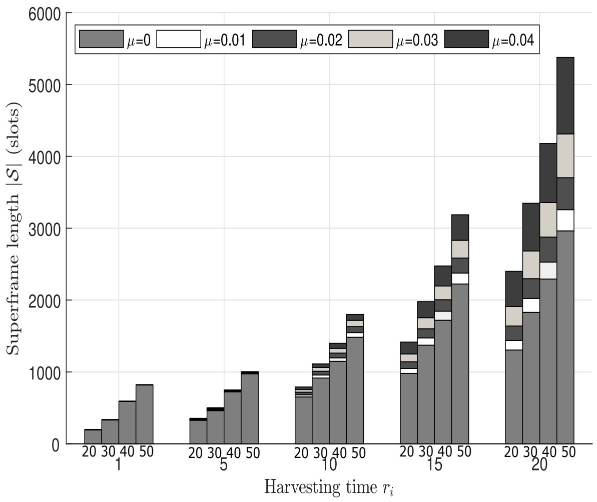

Figure 3.7 The effect of harvesting time and leakage rate on $|\mathcal{S}|$.

3.3.2.3 Effect of Storage Efficiency

To study the effect of storage efficiency η_i, in this section the leakage rate μ_i is set to zero. Figure 3.8 shows the resulting schedule length $|\mathcal{S}|$ for $r_i = 1, 5, 10, 15, 20$ and five values of storage efficiency η_i. Similar to Figure 3.7, from left to right, each bar for each harvesting time is the result for network sizes of 20, 30, 40, or 50 nodes, respectively. Further, each bar shows the average value of $|\mathcal{S}|$ when η_i gradually decreases from 1 to 0.6. As shown in Figure 3.8, when nodes require one slot to harvest energy, i.e., $r_i = 1$, decreasing η_i from 1 to 0.6 has no effect on the superframe length $|\mathcal{S}|$, i.e., $|\mathcal{S}|$ remains at 196, 334, 591, and 820 for networks with 20, 30, 40, and 50 nodes, respectively. This is because when nodes use the HUS model, and $r_i = 1$, each node has 1ϵ worth of harvested energy in each slot that can be directly used irrespective of the energy level of its battery. However, for $r_i > 1$, decreasing η_i has a significant negative effect on $|\mathcal{S}|$. For example, when $r_i = 15$ and η_i drops from 1 to 0.6, the superframe length $|\mathcal{S}|$ increases by 62.21% (from 979 to 1588 slots) when there are 20 nodes, 62.17% (1372 to 2225) for 30 nodes, 62.77% (1719 to 2798) when there are 40 nodes and 61.72% (2223 to 3595) for 50 nodes. Figure 3.8 also shows that decreasing storage efficiency consistently creates longer superframe lengths $|\mathcal{S}|$. Specifically, for $r_i = 20$, decreasing η_i from 0.9 to 0.8 increases the link schedule by 11.92% (from 1443 to 1615 slots) for 20 nodes, 11.8% (from 2026 to 2265 slots) for 30 nodes, 12.28% (from 2532 to 2843 slots) for 40 nodes, and 11.62% (from 3278 to 3659) slots for 50 nodes. The superframe length $|\mathcal{S}|$ increases because when $r_i > 1$, nodes need time to harvest energy before they have $A_{i,t} = 1\epsilon$ worth of energy to transmit. However, due to storage efficiency, nodes take a longer time to reach the said minimum amount of energy to transmit/receive.

3.3.2.4 Effect of Leakage Rate and Storage Efficiency

This section aims to investigate the effect of battery leakage rate together with storage efficiency on the schedule length. It compares the schedule length for two cases: (i) $\mu_i = 0$ and $\eta_i = 1$, and (ii) $\mu_i = 0.01$ and $\eta_i = 0.7$. Note that the schedule length in case (i) is affected only by the energy harvesting time of

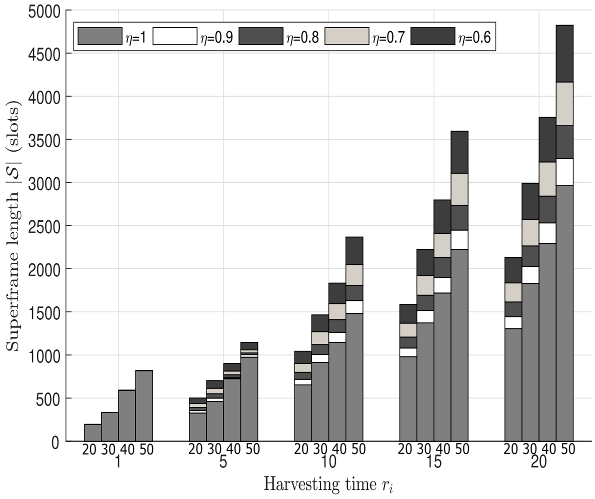

Figure 3.8 The effect of harvesting time and storage efficiency on $|\mathcal{S}|$.

nodes and interference. The results for case (i) are used to benchmark against the results for case (ii).

As shown in Figure 3.9, an imperfect battery for case (ii) has a significant effect on the schedule length $|\mathcal{S}|$ for all network sizes. More specifically, for a rWSN with 20 nodes, the $|\mathcal{S}|$ increases by 37.61% (from 327 in case (i) to 450 slots in case (ii)), 47.78% (653 to 965), 55.46% (979 to 1522), and 63.68% (1305 to 2136), for $r_i = 5, 10, 15$, and 20, respectively. A similar negative effect is also noticed for larger sized rWSNs. For example, when there are 50 nodes, the $|\mathcal{S}|$ increases by 10.46% (975 to 1077), 47.44% (1482 to 2185), 55.24% (2223 to 3451), and 63.21% (2963 to 4836) for $r_i = 5, 10, 15, 20$, respectively. The $|\mathcal{S}|$ is longer because as nodes have an imperfect battery, they require a longer time to accumulate energy. Figure 3.9 also shows that the increase in $|\mathcal{S}|$ is more noticeable in denser networks; see the results for 100 nodes.

One can observe that leakage rate and storage efficiency together cause more severe negative effects on the superframe length $|\mathcal{S}|$ as compared to the effect of leakage rate (Figure 3.7) or storage efficiency (Figure 3.8) separately. As an example, consider the result for a network with 50 nodes and $r_i = 20$. For

$\mu_i = 0.01$ and $\eta_i = 1$, as per Figure 3.7, we find that the $|\mathcal{S}| = 3258$, while in Figure 3.8, the $|\mathcal{S}| = 4166$ for $\eta_i = 0.7$ and $\mu_i = 0$. On the other hand, as shown in Figure 3.9, setting $\eta_i = 0.7$ together with $\mu_i = 0.01$ results in $|\mathcal{S}| = 4836$, which increases the length by 48.43% (from 3258 to 4836) and 16.08% (4166 to 4836) as compared to considering only leakage rate and storage efficiency, respectively.

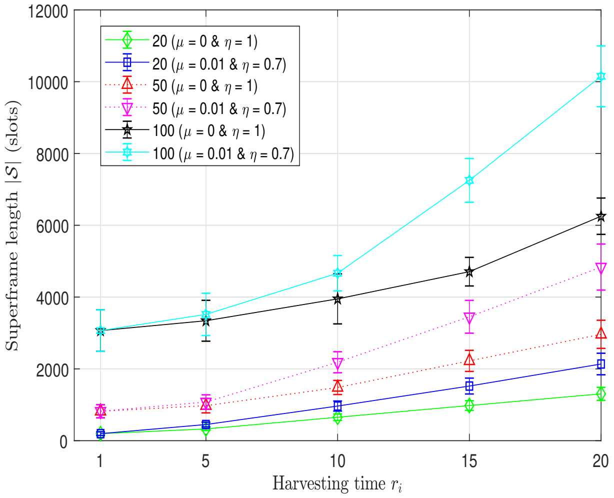

Figure 3.9 Effect of network sizes with varying r_i on $|\mathcal{S}|$.

3.3.3 Effect of b_i, μ_i, and η_i on $|\mathcal{S}|$

This section considers rWSNs with 40 nodes and set $w_{i,j} = 3$, $r_i = 5$, and battery capacity $b_i = 1$, 5, 10, 15, and 20. The following sections discuss the effect of: 1) battery capacity only, 2) battery capacity and leakage rate, and 3) battery capacity and storage efficiency.

3.3.3.1 Effect of Battery Capacity

To see the effect of battery capacity on the schedule length $|\mathcal{S}|$, we set $\mu_i = 0$ and $\eta_i = 1$. As shown in Figure 3.10, when $\mu_i = 0$, increasing b_i from 1 to 20 only slightly reduces the $|\mathcal{S}|$; there is only a 6.5% decrease (from 769 to 719 slots).

The main reason for the insignificant effect of battery capacity on $|\mathcal{S}|$ is explained as follows.

Consider a node v_i with $r_i > 1$ that needs to activate multiple links to/from its m neighbours that have a harvesting time of at least $r_j > r_i$. Assume one neighbour has harvesting time r_j while each of the others has a harvesting time of $r_j + k$, $r_j + 2k$, $\ldots$, $r_j + mk$, for $k \geq 0$. In this case, a node v_i needs to activate m consecutive links, one every k slots. Assume the current time is $t = 0$. One can observe that $|\mathcal{S}|$ is minimised if a node v_i can accumulate energy in its battery at time $t = r_j$ such that it is sufficient to activate one link every k slots. Specifically, to minimise $|\mathcal{S}|$, it is necessary that (i) $r_i \leq k$ or, (ii) when $r_i > k$, b_i must contain more than 1ϵ energy at time r_j, i.e., $b_i > 1$. Thus, one can see that $b_i > 1$ is needed for case (ii). As an example, node 2 in Figure 3.1b receives three consecutive packets from its neighbours in three consecutive slots, i.e., $k = 1$ and $r_2 = 2 > k$ and increasing b_i from 1 to 3 reduces $|\mathcal{S}|$ from 9 to 7. It is important to note that a node v_i can accumulate more than 1ϵ energy only if $r_i < r_j$ for each neighbour v_j; in the example, r_2 is the smallest. Otherwise, if $r_i > r_j$, the battery at a node v_i will never accumulate more than 1ϵ of energy because a node v_i will consume it immediately to activate one of its links. Thus, for this case $b_i = 1$ is sufficient, i.e., a larger b_i does not reduce $|\mathcal{S}|$.

3.3.3.2 Effect of Leakage Rate

To analyse the effect of battery capacity b_i and leakage rate μ_i on the $|\mathcal{S}|$, we set the storage efficiency η_i to 1. From Figure 3.10, we see that increasing the battery capacity for $\mu_i = 0$, 0.01, 0.02, 0.03, and 0.04 has an insignificant effect on the $|\mathcal{S}|$. As an example, when $\mu_i = 0.01$, increasing b_i from 1 to 20 reduces the $|\mathcal{S}|$ by 6.61%, i.e., from 772 to 721 slots; subsection 3.3.3.1 explains the reason. Similarly, there is only a decrease of 4.26% (775 to 742 slots), 3.59% (779 to 751

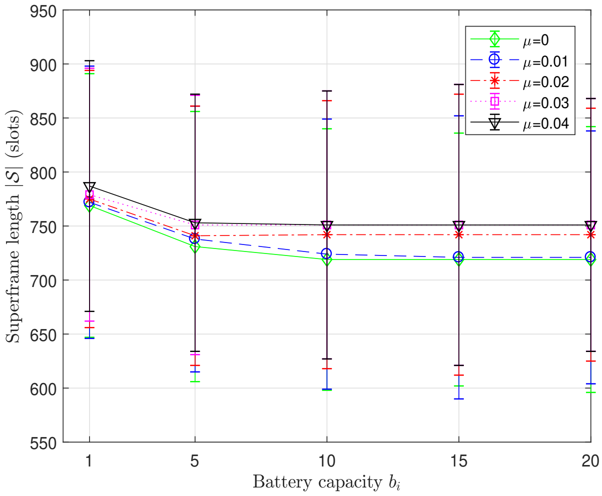

Figure 3.10 The effect of battery capacity and leakage rate in a rWSN with 40 nodes.

slots), and 4.57% (787 to 751 slots) for μ_i values of 0.02, 0.03, 0.04, respectively, when b_i increases from 1 to 20. Note that the standard deviation values of $|\mathcal{S}|$ range between 117 and 131.

3.3.3.3 Effect of Storage Efficiency

To evaluate the effect of battery capacity and storage efficiency, consider the leakage rate $\mu_i = 0$. As shown in Figure 3.11, increasing the battery capacity for $\eta_i = 1$, 0.9, 0.8, 0.7, and 0.6 does not affect the superframe length $|\mathcal{S}|$ significantly. For example, when $\eta_i = 0.9$, increasing b_i from 1 to 20 only reduces the $|\mathcal{S}|$ from 792 to 721 slots. This is a decrease of only 8.96%. Note that the standard deviation values of $|\mathcal{S}|$ range between 84 to 126.

The results shown in Figure 3.10 and Figure 3.11 indicate that increasing the capacity of imperfect batteries can only slightly reduce the schedule length. The results are consistent to rWSNs where nodes have a battery with perfect storage, i.e., $\mu_i = 0$ and $\eta_i = 1$.

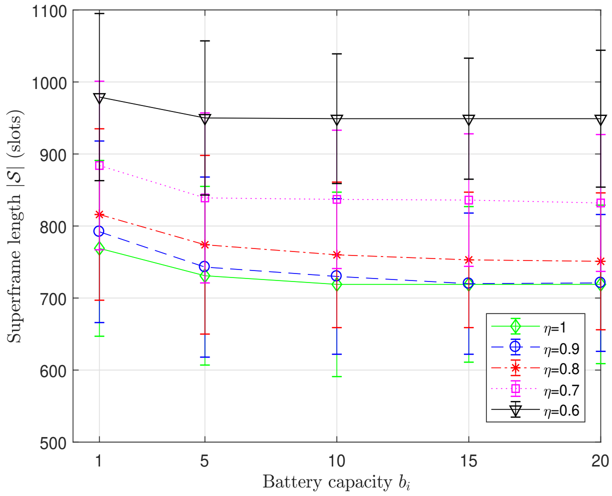

Figure 3.11 The effect of battery capacity and storage efficiency in a network with 40 nodes.

3.3.4 Effectiveness of LS-rWSN

To analyse the performance of LS-rWSN, Section 3.3.4.1 computes the ratio $\mathcal{R}_1 \geq 1$ between its generated $|\mathcal{S}|$ and the optimal bound as per *Propositions 3.1*, *3.2*, and *3.3* for *Line*, *BTree*, and *Grid*, respectively, for nodes with a perfect battery, i.e., $\eta = 0$ and $\mu = 1$. Recall that the optimal $|\mathcal{S}|$ is $4wr$, $6wr$, and $8wr$ for *Line*, *BTree*, and *Grid*, respectively. Note that when nodes have a perfect battery, the value of ρ is equal to the nodes' harvesting time r. Apart from these networks, Section 3.3.4.2 computes $\mathcal{R}_2$ to further evaluate LS-rWSN on arbitrary networks, where $\mathcal{R}_2$ is the ratio between its generated $|\mathcal{S}|$ and the lower bound $|\mathcal{S}_{\mathcal{E}}|$ in Eq. (3.1). For both types of networks, we set $w_{i,j} = 3$, $b_i = 3$, and $r_i = 1$, 5, 10, 15, and 20.

3.3.4.1 Fixed Topologies

This experiment considers rWSNs with nodes from 20 to 100, with an increment of 10 for the *Line*, *BTree*, and *Grid* topologies. As shown in Figure 3.12, LS-rWSN always produced the optimal superframe for *Line* for any values of r_i. On the other hand, for $r_i = 1$, *BTree* and *Grid* produce $\mathcal{R}_1 = 1.28$ and $\mathcal{R}_1 = 1.42$, respectively. However, LS-rWSN has better performance for larger values of r_i. Specifically, when $r_i \geq 5$, LS-rWSN has a performance ratio $\mathcal{R}_1$ of 1.04 and 1.02 for *BTree* and *Grid*, meaning the superframe length is only 4% and 2%, respectively, away from the optimal value for rWSNs with 20 to 100 nodes.

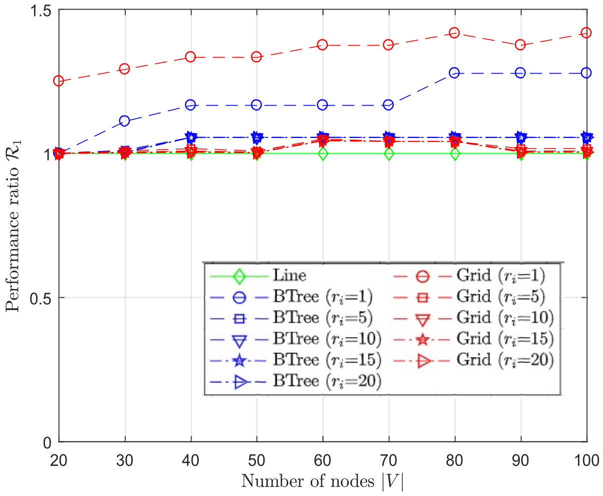

Figure 3.12 The performance of LS-rWSN in fixed topologies with a various number of nodes for $\mu_i = 0$ and $\eta_i = 1$.

3.3.4.2 Arbitrary Networks

For each network, consider $\mu_i = 0.01$, and $\eta_i = 0.7$. The average ratio $\mathcal{R}_2$ in Figure 3.13 is obtained by averaging 100 random node deployments. As shown in Figure 3.13, for a rWSN with 20 nodes and $r_i = 1$, i.e., when nodes always have energy, LS-rWSN achieves an average performance ratio $\mathcal{R}_2$ of 3.01. However, when nodes have a lower energy harvesting constraint, i.e., $r_i > 1$ the performance of LS-rWSN improves significantly. Specifically, for $r_i \geq 5$ and $|V| = 20$, LS-rWSN on average produces superframes with $\mathcal{R}_2 = 1.07$, i.e., only 7% longer than the lower bound computed using Eq. (3.1). Figure 3.13 also shows that except for $r_i = 1$, increasing the network size does not reduce the performance of LS-rWSN. Further, it shows that increasing the network size from 20 to 50 reduces the performance due to the high level of interference. The standard deviation values of the performance ratio in Figure 3.13 range between 0.01 and 0.98.

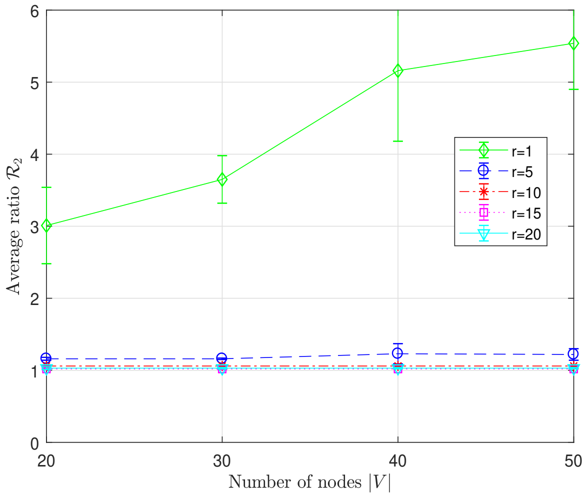

Figure 3.13 The performance of LS-rWSN in arbitrary networks for $\mu_i = 0.01$ and $\eta_i = 0.7$.

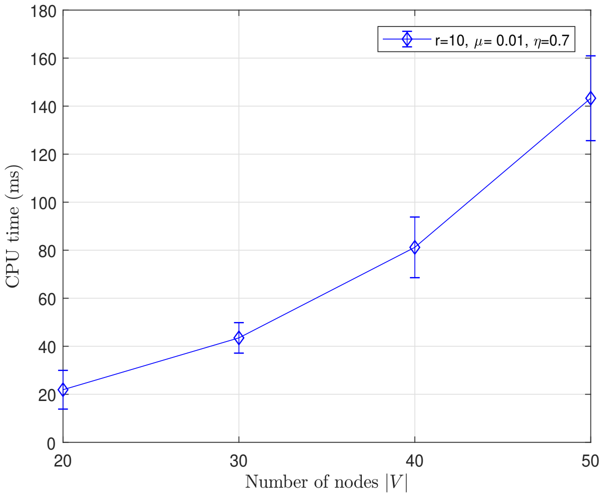

Figure 3.14 The running time of LS-rWSN in arbitrary networks for $r_i = 10$, $\mu_i = 0.01$, and $\eta_i = 0.7$.

3.3.5 Running Time

To measure the running time of LS-rWSN, this experiment considers rWSN with 20 to 50 nodes with $r_i = 10$, $\mu_i = 0.01$ and $\eta_i = 0.7$. Each node has battery capacity $b_i = 3$ and each link has weight $w_{i,j} = 3$. Figure 3.14 shows that the running time of LS-rWSN becomes longer when the number of nodes increases. More specifically, the running time of LS-rWSN is 21.9 ms for $|V| = 20$, and gradually increases to 143.3 ms when $|V|$ reaches 50 nodes. This is because there are more links when $|V|$ increases. The running time is thus increasing, which is consistent with *Proposition 3.7*. Note that there are on average 125 (from 104 to 152 links), 273 (from 236 to 312), 470 (from 420 to 556), and 758 (from 670 to 854) links when there are 20, 30, 40, and 50 nodes, respectively. The standard deviation of the running time in Figure 3.14 ranges between 6.35 and 17.66.

3.4 Chapter Summary

This chapter addressed link scheduling in rWSNs. It considered the following factors: (i) energy harvesting time of nodes, (ii) battery capacity, (iii) imperfect battery storage, i.e., leakage and storage inefficiency, and (iv) activation frequencies w_i. It presented a novel problem called LSHUS that aimed to produce a link schedule $\mathcal{S}$ with the minimum length subject using the HUS protocol. This chapter formally showed that LSHUS is NP-Complete and presented analytical results for the optimal length for three bipartite topologies: *Line*, *BTree*, and *Grid*. A greedy algorithm, called LS-rWSN, was proposed to solve LSHUS. Extensive simulations showed that factors such as harvesting time, battery leakage, and storage efficiency significantly affected the schedule length. These factors increased the length by up to 63.21%. On the other hand, battery capacity is an insignificant factor, i.e., increasing the schedule length no more than 6.5%.

LS-rWSN produced the optimal superframe length for *Line*, and up to 1.28 and 1.42 times longer superframe lengths as compared to the theoretical superframe length bound for *BTree* and *Grid*, respectively, for $r_i > 1$. In Chapters 4 and 5, we investigate using a battery cycle constraint to overcome the memory effect of batteries.

Chapter 4

Link Scheduling in rWSNs with Battery Memory Effect

This chapter considers the novel problem of deriving a TDMA link schedule for rWSNs. Unlike past works, it considers: (i) the energy harvesting time of nodes, (ii) Harvest-Store-Use (HSU) energy harvesting and battery usage protocol, (iii) battery imperfections, and (iv) a *battery cycle* constraint that is used to overcome the *memory effect*. Recall that such effect will reduce the battery's usable capacity if it is charged and discharged repeatedly after a partial discharge and charge, respectively. This chapter shows analytically that the battery cycle constraint and leaky batteries lead to unscheduled links. Further, it presents a greedy heuristic that schedules links according to when their corresponding nodes have sufficient energy.

This chapter considers a *novel* research aim: deriving a short TDMA link schedule that considers nodes with a varying energy harvesting rate and battery memory effect. To achieve this aim, solutions must address a number of problems. Consider Figures 4.1a, 4.1b, and 4.1c. Note that links (v_1, v_2), (v_1, v_3), and (v_1, v_4) interfere with each other and thus cannot be scheduled concurrently. Consider the HSU battery usage protocol [32], where the harvested energy in slot t can only be used in slot $t+1$, $t+2, \ldots$. Node v_1 needs to wait for three timeslots to accumulate one unit of energy, denoted as $v_1|3$, and this energy can only be used after slot $t = 3$. First, consider the case where nodes have unlimited battery capacity; denoted by $\sim$ in Figure 4.1a. Node v_1 can use its stored energy in timeslot $t = 4$. However, none of its links can be scheduled at time $t = 4$ because its neighbours have insufficient energy to receive a packet. For example, link (v_1, v_2) can be scheduled no earlier than at slot $6 + 1 = 7$. After node v_1 transmits a packet to node v_2 at time $t = 7$, its remaining energy is sufficient to transmit a packet to node v_3. Thus, link (v_1, v_3) is scheduled at time $t = 8$. Then, node v_1 needs to accumulate energy before it can transmit a packet to node v_4. Thus, link (v_1, v_4) is scheduled at slot $t = 8+3+1 = 12$, producing the schedule length of 12.

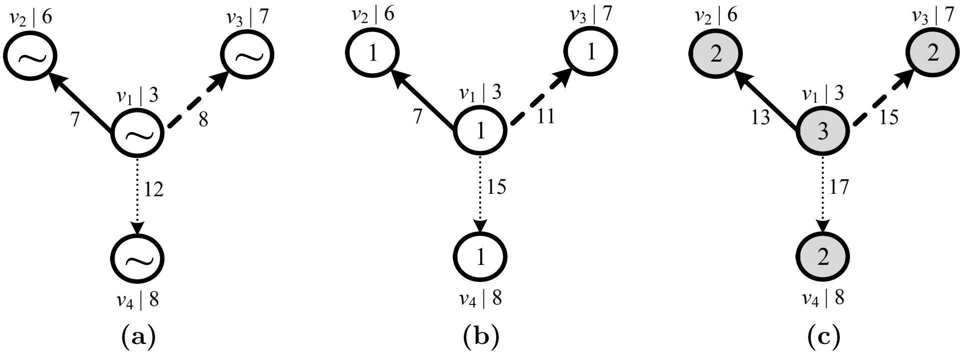

Figure 4.1 An example (a) with interference and harvesting time, (b) plus battery capacity, and (c) plus battery cycle constraints. The number inside each node shows the capacity of its battery. The number next to each link denotes its activation time, and $v_x|z$ represents node x requiring z time slots to accumulate one unit of energy.

Next, consider the case where each battery has a capacity of one unit; see Figure 4.1b. This means the battery at node v_1 can be recharged only after it is used at time $t = 7$. Thus, node v_1 can transmit the second packet no earlier than at time $t = 7+3+1 = 11$, i.e., after it has harvested sufficient energy. Further, it can transmit the third packet no earlier than time $t = 11 + 4 = 15$. Hence, the schedule length is 15.

Lastly, consider the case where each battery has a *battery cycle* constraint; see Figure 4.1c. Node v_1 has a battery with three units of energy and nodes v_2, v_3, and v_4 each have a battery with two units of capacity. Thus, v_1 needs to wait until slot $t = 3 \times 3 + 1 = 10$ to fully recharge its battery before it can transmit one packet. However, it cannot do so because its neighbours' battery is yet to be fully recharged. That is nodes v_2, v_3, and v_4 have to wait until slot $t = 6 \times 2 + 1 = 13$, $t = 15$, and $t = 17$, respectively, before their battery can be discharged. The schedule length in this case is 17.

The preliminary version of the work in this chapter has been presented in [92], while its full version has been published in [93]. More specifically, reference [92] described the problem and its solution for perfect batteries, while reference [93] included imperfect batteries.

The layout of this chapter is as follows. Section 4.1 shows our network model and formulates the problem. Section 4.2 consists of four subsections; it addresses key properties of our proposed algorithm in Section 4.2.1, the feasibility study in Section 4.2.2, a proposed method to shorten superframe length in Section 4.2.3, and a proposed algorithm in Section 4.2.4. Section 4.3 provides simulation results to show the performance of our approaches. Finally, Section 4.4 concludes the chapter.

4.1 Preliminaries

Section 4.1.1 formalises our rWSN model and key notations used in this chapter. After that, Section 4.1.2 formalises the problem of interest.

4.1.1 Network Model

A node v_i is equipped with a harvester that scavenges energy from its environment, e.g., solar, and it is equipped with a rechargeable battery with capacity b_i (in unit of ϵ). It uses the HSU battery usage protocol [32], where the harvested energy at timeslot t must first be stored before it is used in later slots. Recall that it is possible to revise the HSU model to apply in the HUS model. Let $r_i \geq 1$ (in slots) be the *harvesting time* or total number of slots that is required by a node v_i to accumulate 1ϵ of energy. Thus, the harvesting rate of a node is $\frac{\epsilon}{r_i}$ per time slot. Let $0 < \eta_i \leq 1$ be the storage efficiency and $0 \leq \mu_i < 1$ be the battery's leakage factor (per time slot) of a node v_i. This work omits the following cases. First, when $\eta_i = 0$ and $\mu_i = 1$, the battery of nodes cannot store any harvested energy and retain its energy, respectively. Second, in each slot, the amount of harvested energy must be larger than the battery leakage rate μ_i. Otherwise, any harvested energy will be lost immediately due to battery leakage. In both cases, nodes will have no energy to activate links.

All nodes have a minimum battery capacity, i.e., for a node v_i, we have $b_i \geq 1\epsilon$. They have a single rechargeable battery with a *battery cycle* constraint [36]. This constraint requires the battery of a node v_i to be: (i) charged to its maximum capacity $b_{i,max}$ before it can be used/discharged, for $2 \leq b_{i,max} \leq b_i$, and (ii) discharged to its minimum capacity, $b_{i,min} \geq 1$, before it can be charged. We call (i) and (ii) respectively as the discharging and charging constraint. Consequently, the battery at each node v_i can be in one of two modes: (i) *charging*, or (ii) *discharging*. More specifically, the battery cannot be in the charging and discharging mode at the same time. Without loss of generality, we assume each battery has an initial energy level of $b_{i,min}$. Further, we assume $b_{i,min}$ and $b_{i,max}$ are integers, where $b_{i,min} < b_{i,max}$.

For a node v_i, let $\tilde{t}^{+}_{i,k}$ and $\tilde{t}^{-}_{i,k}$ respectively, be the start and end time of its k-th charging cycle. Similarly, for discharging cycle k at a node v_i, its start and end time are denoted respectively as $t^{+}_{i,k}$ and $t^{-}_{i,k}$. Further, $\tilde{\tau}_{i,k}$ and $\tau_{i,k}$ respectively are the *charging* and the *discharging* time intervals of the battery at a node v_i in cycle $k \geq 1$; these quantities are computed as $\tilde{\tau}_{i,k} = \tilde{t}^{-}_{i,k} - \tilde{t}^{+}_{i,k}$ and $\tau_{i,k} = t^{-}_{i,k} - t^{+}_{i,k}$. In other words, the battery at a node v_i is being charged during time interval $\tilde{\tau}_{i,k}$ and being discharged during time interval $\tau_{i,k}$ for each cycle k. As illustrated in Figure 4.2, each battery follows a sequence of a charge-discharge cycle. Thus, we have $t^{+}_{i,k} = \tilde{t}^{-}_{i,k} + 1$ and $\tilde{t}^{+}_{i,k} = t^{-}_{i,k} + 1$. Note that for each cycle k, the value of $\tilde{\tau}_{i,k}$ is dependent on r_i, η_i as well as $b_{i,max}$, while the length of $\tau_{i,k}$ is affected by $b_{i,min}$ and the number of times the battery is used to transmit/receive packets at each cycle k, denoted by $u_{i,k}$. In addition, both times are affected by the battery's leakage factor μ_i. Note that as r_i, μ_i, η_i, and $b_{i,max}$ are constants, all intervals $\tilde{\tau}_{i,k}$ have equal length. In contrast, the value of $\tau_{i,k}$ may vary at different cycles because $u_{i,k}$ varies according to the number of transmitted/received packets. In the remainder of this chapter, the cycle number k is omitted if the context is clear.

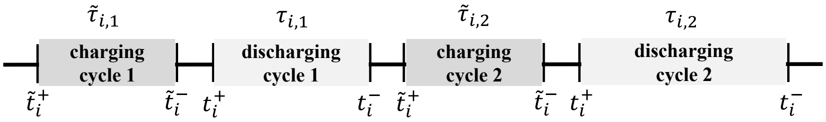

Figure 4.2 Charge-discharge cycles at a node v_i at cycle $k = 1$ and $k = 2$.

Let $\tilde{b}_{i,t}$ and $b_{i,t}$ (in unit of ϵ) denote the energy level of the battery at a node v_i during a charging and discharging cycle at time slot t, respectively. Thus, we have $\tilde{b}_{i,\tilde{t}_i^-} = b_{i,max}$ and $b_{i,t_i^-} = b_{i,min}$. The battery level of a node v_i at the beginning of each *charging* cycle, i.e., at time $\tilde{t}_i^+$, is

$$\tilde{b}_{i,\tilde{t}_i^+} = b_{i,min} - \mu_i b_{i,min} = (1 - \mu_i) b_{i,min}. \tag{4.1}$$

This is because: (i) the battery stops discharging at time $t_i^- = \tilde{t}_i^+ - 1$ when the amount of energy reaches $b_{i,min}$, and (ii) there is energy leakage of $\mu_i b_{i,min}$ from time $\tilde{t}_i^+ - 1$ to $\tilde{t}_i^+$. On the other hand, the battery level of a node v_i at the start of *discharging* cycle t_i^+ is

$$b_{i,t_i^+} = b_{i,max} - \mu_i b_{i,max} = (1 - \mu_i) b_{i,max} \tag{4.2}$$

This is because: (i) the battery stops charging at time $\tilde{t}_i^- = t_i^+ - 1$ when its battery level reaches its maximum capacity, i.e., $b_{i,max}$, and (ii) there is energy leakage of $\mu_i b_{i,max}$ from time $t_i^+ - 1$ to t_i^+.

Let T_i be the earliest time slot when the battery at a node v_i is in discharging mode. The earliest time in which a link $l_{i,j}$ can be scheduled is at time $t_{i,j} = \mathbf{max}(T_i, T_j)$, i.e., when the end nodes of a link $l_{i,j}$ can discharge their battery. For each node v_i, we initialise T_i to $\tilde{\tau}_i + 1$. It is updated when the battery at a node v_i is discharged to transmit/receive a packet.

Figure 4.3a presents a rWSN with four nodes to illustrate our network model. It shows values of $b_{i,min}$, $b_{i,max}$, b_i, μ_i, η_i, and r_i for each node v_i as well as the weight of each link $l_{i,j}$. The battery level of each node v_i in charging and discharging mode is computed using Eq. (4.1) and (4.2), e.g., $b_{1,t_1^+} = b_{1,max} \times \hat{\mu_1} = 5 \times 0.99 = 4.95$ and $\tilde{b}_{1,\tilde{t}_1^+} = b_{1,min} \times \hat{\mu_1} = 1 \times 0.99 = 0.99$, respectively. As shown later in Section 4.2, one can compute the charging time and discharging time intervals for each battery to obtain $\tilde{\tau}_1 = 9$, $\tilde{\tau}_2 = 12$, $\tilde{\tau}_3 = 20$, and $\tilde{\tau}_4 = 10$. Thus, we have $T_1 = \tilde{\tau}_1 + 1 = 10$, $T_2 = 13$, $T_3 = 21$, and $T_4 = 11$. Therefore, the earliest time each link $l_{i,j}$ can be scheduled is computed as $t_{1,2} = \mathbf{max}(10, 13) = 13$, $t_{2,4} = 13$, and $t_{3,1} = 21$. In Figure 4.3b, there are two links that experience primary interference, namely, link $l_{3,1}$ with $l_{1,2}$ and $l_{1,2}$ with $l_{2,4}$. Also shown is secondary interference at node v_1 that is caused by node v_2, i.e., link $l_{3,1}$ with $l_{2,4}$.

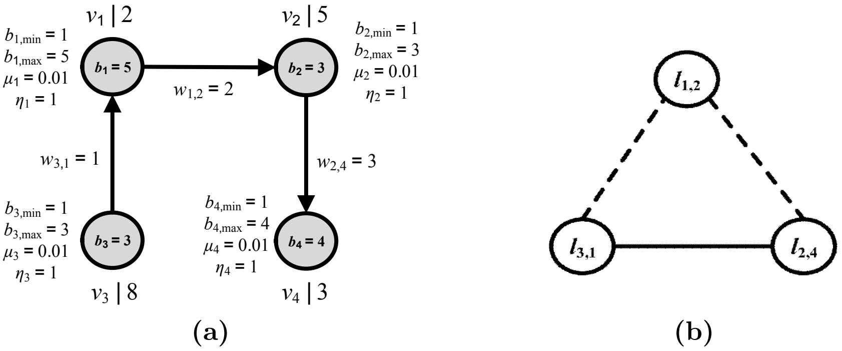

Figure 4.3 A rWSN as a (a) graph G, and its (b) conflict graph C_G.

4.1.2 Problem Statement

Given a rWSN, our problem, called **Link Scheduling with Memory Effect-1 (LSME-1)**, is to generate the TDMA link schedule $\mathcal{S}$ with minimum length $|\mathcal{S}|$ that satisfies the following constraints: (i) the battery at each node $v_i \in V$ satisfies the *battery cycle* constraint, (ii) each link $l_{i,j} \in E$ can be scheduled at timeslot t only if its end nodes are in discharging mode, (iii) each link $l_{i,j} \in E$ is scheduled at least $w_{i,j}$ times in $\mathcal{S}$.

Figure 4.4 shows two example of link schedules. Figure 4.4a presents a *feasible* link schedule with 320 slots which satisfies constraints (i), (ii), and (iii). Figure 4.4b gives a shorter *feasible* schedule with $|\mathcal{S}| = 307$ slots. Note that link scheduling is known to be NP-hard; works such as [59] and [43] assumed nodes with unlimited energy. This is simply a special case of **LSME-1**. Thus, our problem is also NP-hard.

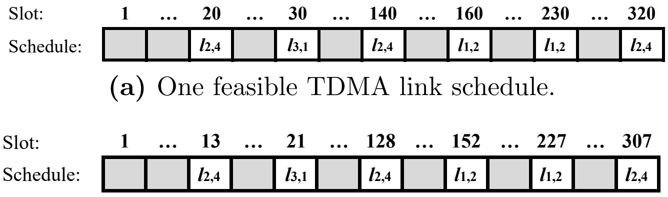
Slot: 1 ... 20 ... 30 ... 140 ... 160 ... 230 ... 320
Schedule: $l_{2,4}$ $l_{3,1}$ $l_{2,4}$ $l_{1,2}$ $l_{1,2}$ $l_{2,4}$
Slot: 1 ... 13 ... 21 ... 128 ... 152 ... 227 ... 307
Schedule: $l_{2,4}$ $l_{3,1}$ $l_{2,4}$ $l_{1,2}$ $l_{1,2}$ $l_{2,4}$

(a) One feasible TDMA link schedule.

(b) The optimal TDMA link schedule.

Figure 4.4 TDMA link schedules for the rWSN in Figure 4.3 with a battery cycle constraint. Gray coloured slots show no transmissions/receptions. Note that the figure shows only non-empty slots with empty slot represented as "...".

4.1.3 Problem Analysis

We now analyse the effect of a battery cycle constraint on the schedule length for three fixed topologies, i.e., *Line*, *Binary Tree* (*BTree*), and *Grid*; see Section 2.6.1.1 for their detailed configurations. We consider that each node has equal harvesting time of $r > 0$, that a battery's usable energy $\hat{b} \geq 1$, and the link weight $w \geq 1$. Note that $\hat{b}$ is equal to $b_{max} - b_{min}$. The following *Propositions 4.1*, *4.2*, and *4.3* show the effect of a battery cycle constraint on the schedule length for *Line*, *BTree*, and *Grid*, respectively.

Proposition 4.1. *The optimal link schedule for a Line topology with $n \geq 3$ has superframe length*

$$|\mathcal{S}| = \left\lceil \frac{4w}{\hat{b}} \right\rceil \times r\hat{b} + 4w \tag{4.3}$$

Proof. We first describe by construction how to derive a link schedule for *Line* when each node *always* has energy to transmit/receive packets. For this case with $w = 1$, we can schedule links in four different slots as follows. Links in the set $\{(2+4i, 3+4i), (5+4i, 4+4i)\}$ can be scheduled in a slot A, for $i = 0, 1, \cdots, \lfloor (n-2) \ / \ 4 \rfloor$; e.g., for $n = 9$, slot A contains links $\{(2,3), (5,4), (6,7), (9,8)\}$. Then, reverse the direction of each link in slot A, and schedule the reversed link in slot B; e.g., slot B contains links $\{(3,2), (4,5), (7,6), (8,9)\}$. Next, schedule links in the set $\{(1+4i, 2+4i), (4+4i, 3+4i)\}$ in slot C for $i = 0, 1, \cdots, \lfloor (n-2) \ / \ 4 \rfloor$; e.g., links $\{(1,2), (4,3), (5,6), (8,7)\}$. Finally reverse the links in slot C for slot D; e.g., links $\{(2,1), (3,4), (6,5), (7,8)\}$. For $w > 1$, repeat the described four-slot link schedule, in the same order, for $w - 1$ times. Thus, we have $|S| = 4w$. For example, for $w = 2$, the following sequence of $4 \times 2 = 8$ slots are constructed: $\mathcal{S} = (A, B, C, D, A, B, C, D)$.

Next, consider the case where each battery follows the battery cycle constraint. Notice that each node requires $r \times \hat{b}$ slots to charge its battery to the maximum level before it can be used to transmit/receive $\hat{b}$ packets with no additional charging. In other words, there are $r \times \hat{b}$ empty slots, at which time each node charges its battery to the maximum level, before the battery can be used to activate, at most, $\hat{b}$ number of links. Thus, in general, there are in total $4w$ non-empty slots where links are activated, and $\lceil \frac{4w}{\hat{b}} \rceil \times r\hat{b}$ empty slots where batteries are being charged. For example, consider $r = 2$, and $\hat{b} = 3$ for the aforementioned eight slot schedules $\mathcal{S}$. Due to the battery cycle constraint, there are $2 \times 3 = 6$ empty slots before links in slot A can be activated at Slot-7. Links in slot B and C are activated at Slot-8 and Slot-9, respectively. Then, nodes need to recharge their battery to the maximum level, i.e., there are other $2 \times 3 = 6$ empty slots, before links in slots D, A, and B can be activated at Slot-16, Slot-17, and Slot-18, respectively. Finally, following the other six empty slots, links in slot C and D are activated at Slot-25 and Slot-26, respectively. Thus, for this example, $|\mathcal{S}| = \lceil \frac{4\times 2}{3} \rceil \times 2 \times 3 + 4 \times 2 = 26$. The schedule length is optimal for the following two reasons. Firstly, for $n \geq 3$, some nodes in *Line* have four bidirectional links. Thus, the schedule must contain at least $4w$ non-empty slots. Secondly, each node needs $r\hat{b}$ empty slots before it can schedule $\hat{b}$ links. In other words, there are at least $\lceil \frac{4w}{\hat{b}} \rceil \times r\hat{b}$ number of empty slots. Thus, the schedule length of $\lceil \frac{4w}{\hat{b}} \rceil \times r\hat{b} + 4w$ slots, shown in Eq. (4.3), is optimal. □

Proposition 4.2. *The optimal link schedule for a BTree with $L \geq 3$ levels has superframe length*

$$|\mathcal{S}| = \left\lceil \frac{6w}{\hat{b}} \right\rceil \times r\hat{b} + 6w \tag{4.4}$$

Proof. We first outline the steps to construct a link schedule for a *BTree* when each of its nodes *always* have energy. Links in a *BTree* with three levels can be scheduled in six slots: Slot-1 = $\{(1,2),(3,6)\}$, Slot-2 = $\{(2,1),(6,3)\}$, Slot-3 = $\{(1,3),(2,4)\}$, Slot-4 = $\{(3,1),(4,2)\}$, Slot-5 = $\{(2,5),(3,7)\}$, and Slot-6 =

$\{(5,2),(7,3)\}$. The link schedules for a four-level *BTree* can be generated from the schedules of two *BTree* with three levels as follows. Denote the larger tree as T with root R, and the two smaller trees as $T1$ and $T2$ with root $R1$ and $R2$, respectively. Tree T is constructed from $T1$ and $T2$ by connecting R to $R1$ with two bidirectional links, and R to $R2$ with two other links, i.e., $T1$ and $T2$ are the left and right subtrees of T, respectively. Thus, renumbering the nodes in T, the label of nodes R, $R1$, and $R2$ are 1, 2, and 3, respectively. Links in T are scheduled as follows. First, combine the links of $T1$ scheduled in one slot with the corresponding links of $T2$ that are scheduled in the same slot number. Notice that no links in $T1$ interfere with any links in $T2$, and vice versa. Then, insert each of the four incident links at R into a slot that does not contain any link that interferes with it. More specifically, links $(1,2)$, $(2,1)$, $(1,3)$, and $(3,1)$ are inserted into a slot that contains links $(8,4)$, $(4,8)$, $(12,24)$, and $(24,12)$, respectively. Using the same steps, one can schedule links in a five-level tree using the six-slot schedules of its two four-level subtrees. Repeating the process, one can always generate the link schedules of a tree with k levels in six slots from the schedules of its two subtrees with $(k-1)$ levels, for any $k \geq 4$. For $w > 1$, repeat the described six-slot link schedule in the same order for $w-1$ times. Thus, we have $|S| = 6w$.

Next, consider the case where each battery follows the battery cycle constraint. Notice that each node requires $r \times \hat{b}$ slots to charge its battery to the maximum level before it can be used to transmit/receive $\hat{b}$ packets with no additional charging. In other words, there are $r \times \hat{b}$ empty slots, at which time each node charges its battery to the maximum level, before the battery can be used to activate, at most, $\hat{b}$ number of links. Thus, in general, there are in total $6w$ non-empty slots where links are activated, and $\lceil \frac{6w}{\hat{b}} \rceil \times r\hat{b}$ empty slots where batteries are being charged.

The schedule length is optimal for the following two reasons. Firstly, for $L \geq 3$, some nodes in a *BTree* have six bidirectional links. Thus, the schedule must contain at least $6w$ non-empty slots. Secondly, each node needs $r\hat{b}$ empty slots before it can schedule $\hat{b}$ links. In other words, there are at least $\lceil \frac{6w}{\hat{b}} \rceil \times r\hat{b}$ number of empty slots. Thus, the schedule length of $\lceil \frac{6w}{\hat{b}} \rceil \times r\hat{b} + 6w$ slots, shown in Eq. (4.4), is optimal. □

Proposition 4.3. *The optimal link schedule length for a Grid of size row* ≥ 3 *and col* ≥ 3 *is*

$$|\mathcal{S}| = \left\lceil \frac{8w}{\hat{b}} \right\rceil \times r\hat{b} + 8w \tag{4.5}$$

Proof. We first outline the steps to construct a link schedule for a *Grid* when each of its nodes *always* has energy. From *Proposition 4.1*, the link schedule of each *Line* graph requires $4w$ non-empty slots. Next, the following describes how to produce the schedule for a *Grid* with length $8w$. Further, the length is shown to be optimal.

Consider the schedule of links in **row** *Line* graphs. One can observe that links in *odd* rows can be activated in $4w$ slots. Similar rules apply for links in *even* rows. Further, except for links in two consecutive rows, there is no other interference. Without loss of generality, consider links in R_2 and R_3 in Figure 2.4. Note that there is an interference only between nodes in each (2×2) *Grid*, e.g., nodes $\{4, 5\}$ at R_2 and $\{7, 8\}$ at R_3, and when their links are in opposite directions, e.g., links $(4, 5)$ and $(8, 7)$ that incur interference at nodes 5 and 7. To prevent any interference, each slot must contain links of the same directions, e.g., links $(4, 5)$ and $(7, 8)$. Thus, links in all rows can be scheduled in $4w$ slots. As an example, for Figure 2.4 with $w = 1$, the four slots are: Slot-1 = $\{(1, 2), (4, 5), (7, 8), (10, 11)\}$, Slot-2 = $\{(2, 1), (5, 4), (8, 7), (11, 10)\}$, Slot-3 = $\{(2, 3), (4, 5), (8, 9), (11, 12)\}$, and Slot-4 = $\{(3, 2), (6, 5), (9, 8), (12, 11)\}$. Use the same construction for links in all columns. More specifically, these links are scheduled in $4w$ slots. Thus, all links in a *Grid* can be scheduled in $4w + 4w = 8w$ slots. Next, consider the case where each battery follows the battery cycle constraint. Notice that each node requires $r \times \hat{b}$ slots to charge its battery to the maximum level before it can be used to transmit/receive $\hat{b}$ packets with no additional charging. In other words, there are $r \times \hat{b}$ empty slots, at which time each node charges its battery to the maximum level, before the battery can be used to activate at most $\hat{b}$ number of links. Thus, in general, there are in total $8w$ non-empty slots where links are activated, and $\lceil \frac{8w}{\hat{b}} \rceil \times r\hat{b}$ empty slots where batteries are being charged.

The schedule length is optimal for the following two reasons. First, for $row \geq 3$ and $col \geq 3$, some nodes in $(row \times col)$ *Grid* have eight bidirectional links, e.g., node 5 and 8 in Figure 2.4. Thus, the link schedule of a *Grid* requires at least $8w$ non-empty slots. Secondly, each node needs $r\hat{b}$ empty slots before it can schedule $\hat{b}$ links. In other words, there are at least $\lceil \frac{8w}{\hat{b}} \rceil \times r\hat{b}$ number of empty slots. Thus, the schedule length of $\lceil \frac{8w}{\hat{b}} \rceil \times r\hat{b} + 8w$ slots shown in Eq. (4.5) is optimal. □

4.2 Solution

This section first describes eight propositions relied upon by our greedy algorithm. It then provides two propositions to show that **LSME-1** might not have a feasible solution when the battery of each node has a non-negative leakage rate, i.e., $\mu_i > 0$. Finally, the details of the proposed greedy algorithm are presented in Section 4.2.4.

4.2.1 Key Properties

Propositions 4.4 and *4.5* relate to batteries in a charging cycle, and *Propositions 4.6* to *4.11* relate to batteries in a discharging cycle. For brevity, we define

$\hat{r}_i = r_i/\eta_i$, and $\hat{\mu}_i = 1 - \mu_i$.

Proposition 4.4. *The energy level (in ϵ) of a battery in the charging mode at a node v_i at time slot t, for $\tilde{t}_i^+ \leq t \leq \tilde{t}_i^-$, is*

$$\tilde{b}_{i,t} = \mathbf{min}\left(b_{i,max}, b_{i,min} \times \hat{\mu_i}^{t-\tilde{t}_i^+ +1} + \sum_{p=0}^{t-\tilde{t}_i^+ -1} \frac{\hat{\mu_i}^p}{\hat{r}_i}\right) \tag{4.6}$$

Proof. The stored energy at time $\tilde{t}_i^+ + 1$ is computed by subtracting the energy lost due to battery leakage, i.e., $\mu_i \tilde{b}_{i,\tilde{t}_i^+}$ plus the energy harvested at slot $\tilde{t}_i^+$, i.e., $1/\hat{r}_i$. Thus, $\tilde{b}_{i,\tilde{t}_i^+ +1} = (1-\mu_i)\tilde{b}_{i,\tilde{t}_i^+} + 1/\hat{r}_i$. The energy level $\tilde{b}_{i,\tilde{t}_i^+ +2}$ is computed from $\tilde{b}_{i,\tilde{t}_i^+ +1}$ by (i) subtracting the energy leakage that occurs from time $\tilde{t}_i^+ + 1$ to $\tilde{t}_i^+ + 2$, (ii) adding the energy harvested in time slot $\tilde{t}_i^+ + 1$, and (iii) substituting $\tilde{b}_{i,\tilde{t}_i^+ +1}$ with $(1-\mu_i)\tilde{b}_{i,\tilde{t}_i^+} + 1/\hat{r}_i$. Steps (i) and (ii) obtain $\tilde{b}_{i,\tilde{t}_i^+ +2} = (1-\mu_i)\tilde{b}_{i,\tilde{t}_i^+ +1} + 1/\hat{r}_i$. Step (iii) substitutes $\tilde{b}_{i,\tilde{t}_i^+ +1}$ with $(1-\mu_i)\tilde{b}_{i,\tilde{t}_i^+} + 1/\hat{r}_i$ to produce $\tilde{b}_{i,\tilde{t}_i^+ +2} = (1 - \mu_i)[(1-\mu_i)\tilde{b}_{i,\tilde{t}_i^+}] + 1/\hat{r}_i = (1-\mu_i)^2\tilde{b}_{i,\tilde{t}_i^+} + (1-\mu_i)/\hat{r}_i + 1/\hat{r}_i$. Then, using energy level $\tilde{b}_{i,\tilde{t}_i^+ +2}$, steps (i) to (iii) are used to compute the energy level at time $\tilde{t}_i^+ + 3$, i.e., $\tilde{b}_{i,\tilde{t}_i^+ +3} = (1-\mu_i)^3\tilde{b}_{i,\tilde{t}_i^+} + (1-\mu_i)^2/\hat{r}_i + (1-\mu_i)/\hat{r}_i + 1/\hat{r}_i$. Repeating steps (i) to (iii) for time $\tilde{t}_i^+ + 4, \ldots, t-1, t$, we obtain the stored energy at the beginning of time t, i.e., $\tilde{b}_{i,t} = (1-\mu_i)^{t-\tilde{t}_i^+}\tilde{b}_{i,\tilde{t}_i^+} + \sum_{p=0}^{t-\tilde{t}_i^+ -1}(1-\mu_i)^p/\hat{r}_i$. Substituting $(1-\mu_i)b_{i,min}$ in Eq. (4.1) for $\tilde{b}_{i,\tilde{t}_i^+}$, we have $\tilde{b}_{i,t} = (1-\mu_i)^{t-\tilde{t}_i^+ +1}b_{i,min} + \sum_{p=0}^{t-\tilde{t}_i^+ -1}\frac{(1-\mu_i)^p}{\hat{r}_i}$. However, $\tilde{b}_{i,t}$ is bounded by the upper limit of battery capacity $b_{i,max}$, which implies $\tilde{b}_{i,t} \leq b_{i,max}$. Substituting $(1-\mu_i)$ with $\hat{\mu_i}$, we obtain the expression stated in the proposition. □

Note that when the battery has 100% storage efficiency and no leakage, i.e., $\eta_i = 1$ and $\mu_i = 0$, respectively, Eq. (4.6) is reduced to

$$\tilde{b}_{i,t} = \mathbf{min}(b_{i,max}, b_{i,min} + (t - \tilde{t}_i^+)/r_i) \tag{4.7}$$

Proposition 4.5 computes the charging time interval $\tilde{\tau}_i = \tilde{t}_i^- - \tilde{t}_i^+$ of the battery at a node v_i, i.e., the number of slots needed to charge the battery to its maximum level $b_{i,max}$ starting from its minimum level $b_{i,min}$.

Proposition 4.5. *The charging time interval for the battery of a node v_i is computed as*

$$\tilde{\tau}_i = \begin{cases} r_i(b_{i,max} - b_{i,min}), & \eta_i = 1 \ and \ \mu_i = 0 \\ \lceil \frac{log \ (\frac{1-\hat{r}_i \mu_i b_{i,max}}{1-\hat{r}_i \mu_i \hat{\mu}_i b_{i,min}})}{log \ \hat{\mu}_i} \rceil, & 0 < \eta_i < 1 \ and \ 0 < \mu_i < 1 \end{cases} \tag{4.8}$$

Proof. We set $t = \tilde{t}_i^-$ in Eq. (4.6) to compute the maximum energy level of the battery at a node v_i, i.e., $b_{i,max}$. Thus, we have

$$b_{i,max} = b_{i,min} \times \hat{\mu_i}^{\tilde{\tau}_i + 1} + \sum_{p=0}^{\tilde{\tau}_i - 1} \frac{\hat{\mu_i}^p}{\hat{r}_i} \tag{4.9}$$

For case (i): $\eta_i = 1$ and $\mu_i = 0$, we set $\hat{\mu}_i = 1$ and $\hat{r}_i = r_i$ in Eq. (4.9) to yield $b_{i,max} = b_{i,min} + \tilde{\tau}_i / r_i$. Thus, $\tilde{\tau}_i = r_i(b_{i,max} - b_{i,min})$ as shown in Eq. (4.8). For case (ii): $0 < \eta_i < 1$ and $0 < \mu_i < 1$, i.e., $\hat{\mu}_i \neq 1$, we use the geometric series [94] to produce $\sum_{p=0}^{\tilde{\tau}_i - 1} \frac{\hat{\mu_i}^p}{\hat{r}_i} = \frac{1}{\hat{r}_i} \frac{\hat{\mu}_i^{\tilde{\tau}_i} - 1}{\hat{\mu}_i - 1}$. Thus, Eq. (4.9) becomes

$$b_{i,max} = b_{i,min} \times \hat{\mu_i}^{\tilde{\tau}_i + 1} + \frac{1}{\hat{r}_i} \frac{\hat{\mu}_i^{\tilde{\tau}_i} - 1}{\hat{\mu}_i - 1} \tag{4.10}$$

Solving Eq. (4.10) for $\tilde{\tau}_i$, we obtain Eq. (4.8). □

The amount of energy that leaks from the battery of a node v_i per slot, i.e., $\hat{r}_i \mu_i$, and the battery's leakage rate μ_i in case (ii) of Eq. (4.8), must be less than $\frac{1}{b_{i,max}}$ and $\frac{1}{\hat{r}_i \hat{\mu}_i b_{i,min}}$, respectively. Otherwise, the battery will never be able to charge to its maximum level.

We first present Eq. (4.11) and (4.12) that are used in *Propositions 4.6* and *4.7*. Consider a battery of a node v_i with an energy level of x at time t_1, i.e., $b_{i,t_1} = x$. As the battery leaks, the energy level of the battery at time $t_2 \geq t_1$ is reduced to

$$b_{i,t_2} = x\hat{\mu}_i^{t_2-t_1} \tag{4.11}$$

Eq. (4.11) is used to compute the amount of energy that has leaked from the battery of a node v_i from time t_1 to t_2, i.e., $\Delta_{i,t_1}^{t_2} = b_{i,t_1} - b_{i,t_2}$ for $b_{i,t_1} = x$ as

$$\Delta_{i,t_1}^{t_2} = x(1 - \hat{\mu}_i^{t_2-t_1}) \tag{4.12}$$

Propositions 4.6 to *4.11* relate to a battery in discharging mode. *Proposition 4.6* computes the energy level of the discharging battery at time t, for $t_i < t \leq t_i^-$, where t_i is the most recent time the battery was used. From time t_i to t, the energy level decreases due to battery leakage *only*. Thus, *Proposition 4.6* is valid only for batteries with a non-negative leakage rate, i.e., $\mu_i > 0$.

Proposition 4.6. *The energy level (in ϵ) of the discharging battery at a node v_i at timeslot t, for $t_i < t \leq t_i^-$ is*

$$b_{i,t} = \mathbf{max}(b_{i,min}, b_{i,max} \times \hat{\mu}_i^{t-t_i^+ +1} - \hat{\mu}_i^{t-t_i}) \tag{4.13}$$

Proof. Following Eq. (4.2), the battery level at time t_i^+ is $b_{i,t_i^+} = b_{i,max} \times \hat{\mu}_i$. Using Eq. (4.12), the amount of energy leaked from time t_i^+ to t_i, for $x = b_{i,t_i^+}$ is

$$\Delta_{i,t_i^+}^{t_i} = b_{i,t_i^+} \times (1 - \hat{\mu}_i^{t_i - t_i^+}) \tag{4.14}$$

Thus, after spending 1ϵ of energy at time t_i, the remaining energy of the battery at the end of slot t_i is

$$b_{i,t_i} = b_{i,t_i^+} - \Delta_{i,t_i^+}^{t_i} - 1 \tag{4.15}$$

Now, as per Eq. (4.12), the energy leaked from time t_i to t, for $x = b_{i,t_i}$, is

$$\Delta_{i,t_i}^{t} = b_{i,t_i} \times (1 - \hat{\mu}_i^{t-t_i}) \tag{4.16}$$

Thus, the remaining energy at time t is

$$b_{i,t} = b_{i,t_i} - \Delta_{i,t_i}^{t} \tag{4.17}$$

Using (4.2) in (4.14), (4.2) and (4.14) in (4.16), (4.15) in (4.16), and (4.15) and (4.16) in (4.17), we obtain

$$b_{i,t} = b_{i,max} \times \hat{\mu}_i^{t-t_i^{+}+1} - \hat{\mu}_i^{t-t_i} \tag{4.18}$$

As the energy level is lower bounded by $b_{i,min}$, we thus obtain Eq. (4.13). □

Note that when the leakage rate is $\mu_i = 0$, the energy level of a battery at a node v_i at time slot t is $b_{i,t} = b_{i,t_i} - 1$. This is because the energy level decreases only due to packet transmission/reception.

Let $\delta_{i,b_1}^{b_2}$ be number of timeslots needed to discharge the battery of a node v_i from level $b_1 \leq b_{i,max}$ to $b_2 \geq b_{i,min}$ due to battery leakage *only*. The following *Proposition 4.7* computes $\delta_{i,b_1}^{b_2}$, which is applicable only when each battery has a non-negative leakage rate of $\mu_i > 0$.

Proposition 4.7. *The discharging time interval, due to battery leakage only, for the battery of a node v_i, to decrease from $b_1 \leq b_{i,max}$ to $b_2 \geq b_{i,min}$ is given as*

$$\delta_{i,b_1}^{b_2} = \lfloor \frac{log(b_2) - log(b_1)}{log(\hat{\mu}_i)} \rfloor \tag{4.19}$$

Proof. First, we set $\Delta_{i,t_1}^{t_2} = b_1 - b_2$ and $x = b_1$ in Eq. (4.12). As a result, we have

$$b_1 - b_2 = b_1(1 - \hat{\mu}_i^{\delta_{i,b_1}^{b_2}}) \tag{4.20}$$

Then we solve Eq. (4.20) for $\delta_{i,b_1}^{b_2}$ to obtain Eq. (4.19). □

Proposition 4.8 computes the next earliest time when the battery at a node v_i can be used to transmit/receive a packet.

Proposition 4.8. *Consider the battery at a node v_i is last used at time $t_i \geq \tilde{\tau}_i + 1$. The next earliest timeslot when the battery at a node v_i can be used to transmit/receive a packet is*

$$T_i = \begin{cases} t_i + \sigma_{i,t_i} \times \tilde{\tau}_i + 1, & \mu_i = 0 \\ t_i + \sigma_{i,t_i} \times (\delta_{i,b_1}^{b_2} + \tilde{\tau}_i) + 1, & \mu_i > 0 \end{cases} \tag{4.21}$$

Proof. The next earliest time the battery at a node v_i can be used depends on the remaining battery level at time t_i, i.e., b_{i,t_i}. For Case (i): $\mu_i = 0$, Eq. (4.21) considers two sub-cases: (a) $b_{i,t_i} = b_{i,min}$, and (b) $b_{i,t_i} > b_{i,min}$. For sub-case (a), the battery needs to be recharged. This sub-case requires a charging time interval of $\tilde{\tau}_i$, computed by Eq. (4.8). Thus, we have $T_i = t_i + \tilde{\tau}_i + 1$ because the harvested energy needs to be stored first before it can be used. For this sub-case, σ_{i,t_i} in Eq. (4.21) is set to 1. For sub-case (b), the battery at node v_i can still be discharged to transmit/receive another packet at time $t + 1$, i.e., $T_i = t_i + 1$, and thus σ_{i,t_i} in Eq. (4.21) is set to 0.

For Case (ii): $\mu_i > 0$, there are two sub-cases: (a) $b_{i,t_i} < (b_{i,min} + 1)$, and (b) $b_{i,t_i} \geq (b_{i,min} + 1)$. For sub-case (a), when the remaining energy is less than $(b_{i,min} + 1)$, the battery needs to be recharged. However, the battery cycle constraint requires the energy level of the battery to reach $b_{i,min}$ first before it can be recharged. Using Eq. (4.19), it takes $\lfloor\frac{log(b_{i,min})-log(\ b_{i,t_i})}{log(\hat{\mu}_i)}\rfloor$ slots to discharge the battery (due to leakage) from level $b_{i,t_i} = b_1$ to $b_{i,min} = b_2$. Then, we use Eq. (4.8) to compute the charging time interval, $\tilde{\tau}_i$. Thus, we have $T_i = t_i + (\delta^{b_2}_{i,b_1} + \tilde{\tau}_i) + 1$ because the harvested energy needs to be stored first before it can be used. For this sub-case, we have $\sigma_{i,t_i} = 1$. For sub-case (b), the battery at a node v_i can still be discharged to transmit/receive another packet at time t_i. Thus, the next earliest time the battery at a node v_i can be discharged to transmit/receive a packet is slot $T_i = t_i + 1$. For this sub-case, we have $\sigma_{i,t_i} = 0$. □

For a given discharging cycle k, let $\mathcal{T}_{i,k} > T_i$ be the time at which the energy level at a node v_i is $b_{min} + 1$. In other words, $\mathcal{T}_{i,k}$ is the latest time the battery can be used in the discharging cycle k.

Proposition 4.9. *The latest time the battery can be used for a given discharging cycle k is*

$$\mathcal{T}_{i,k} = T_i + \lfloor\frac{log(b_{i,min}+1) - log(b_{i,T_i})}{log(\hat{\mu}_i)}\rfloor \tag{4.22}$$

Proof. The energy level at time T_i is b_{i,T_i}. The discharging time interval from level b_{i,T_i} to $b_{i,min}+1$ can be computed using Eq. (4.19) for $b_1 = b_{i,T_i}$ and $b_2 = b_{i,min}+1$. Thus, time $\mathcal{T}_{i,k}$ can then be obtained by computing the sum of time T_i and the discharging time, as given in Eq. (4.22). □

For a given time $\mathcal{T}_{i,k}$, *Proposition 4.10* computes the earliest time T_i at which the battery at a node v_i can be used to transmit/receive a packet. In other words, $T_i = t^+_{i,k+1}$. Figure 4.5 illustrates the relationship between times $\mathcal{T}_{i,k}$ and T_i of *Propositions 4.9* and *4.10*, respectively.

Proposition 4.10. *The earliest time $T_i > \mathcal{T}_{i,k}$ at which the battery at a node v_i can be used is*

$$T_i = \mathcal{T}_{i,k} + \lfloor\frac{log\ b_{i,min} - log\ b_{i,\mathcal{T}_{i,k}}}{log\ \hat{\mu}_i}\rfloor + \tilde{\tau}_i + 1 \tag{4.23}$$

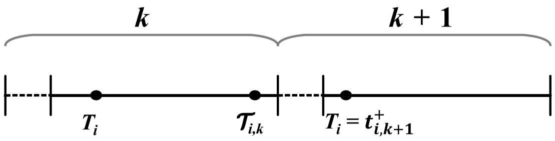

Figure 4.5 An illustration for *Propositions 4.9* and *4.10*. The dashed (solid) lines represent charging (discharging) cycles.

Proof. At time $\mathcal{T}_{i,k}$, a node v_i's energy level is $b_{i,min} + 1$. We need to discharge it first to energy level $b_{i,min}$ before it can be recharged. The discharging time is computed using Eq. (4.19), for $b_1 = b_{i,\mathcal{T}_{i,k}} = b_{i,min} + 1$ and $b_2 = b_{i,min}$, shown as the second term of the right hand side of Eq. (4.23). Then, we need to charge the battery from $b_{i,min}$ to $b_{i,max}$ before it can be used. We use Eq. (4.8) to compute the charging time interval, $\tilde{\tau}_i$. After its fully charged, as per the HSU model, the battery can be discharged in the next slot, which explains the +1 in Eq. (4.23). □

Let α_i be the duration from time $\mathcal{T}_{i,k}$ to $t^+_{i,k+1}$, i.e., $\alpha_i = t^+_{i,k+1} - \mathcal{T}_{i,k}$; see Figure 4.6. Recall that $t^+_{i,k}$ is the starting time of a discharging cycle k of the battery at a node v_i at which time the battery has energy level $b_{i,max} \times \mu_i$. The time duration α_i includes (i) time to discharge 1ϵ of energy, i.e., from $b_{i,min} + 1$ to $b_{i,min}$ at cycle k, before the battery can start charging at cycle $k + 1$, (ii) time to charge the battery from level $b_{i,min}$ to $b_{i,max}$ at cycle $k + 1$, and (iii) a one slot delay before the stored energy can be used at time $t^+_{i,k+1}$, as required by the HSU model. One can use Eq. (4.19) with $b_1 = b_{i,min} + 1$ and $b_2 = b_{i,min}$ to compute (i), and Eq. (4.8) to compute (ii). Thus, we have

$$\alpha_i = \lfloor \frac{log(b_{i,min}) - log(b_{i,min} + 1)}{log(\hat{\mu}_i)} \rfloor + \tilde{\tau}_i + 1 \tag{4.24}$$

Let β_i denote time duration from $t^+_{i,k}$ to $\mathcal{T}_{i,k}$, i.e., $\beta_i = \mathcal{T}_{i,k} - t^+_{i,k}$; see Figure 4.6. In other words, the battery takes β_i slots to discharge all its stored energy (due to leakage only) from level $b_{i,t^+_{i,k}} = b_{i,max} \times \hat{\mu_i}$ to $b_{i,min} + 1$. Using Eq. (4.19), we have

$$\beta_i = \lfloor \frac{log\ (b_{i,min} + 1) - log\ (b_{i,max} \times \hat{\mu_i})}{log\ \hat{\mu_i}} \rfloor \tag{4.25}$$

The following proposition computes $t^+_{i,k+m}$ and $\mathcal{T}_{i,k+m}$ for the battery at a node v_i in a discharging cycle $k + m$, for integer $m = 0, 1, \ldots$.

Proposition 4.11. *Consider the battery of a node v_i in a discharging cycle k, and the battery is not used from time $t^+_{i,k}$ to $\mathcal{T}_{i,k+m}$, for any integer $m = 0, 1, \ldots$. For a given $\mathcal{T}_{i,k}$, the value of $t^+_{i,k+m}$ and $\mathcal{T}_{i,k+m}$ can be computed as*

$$t^+_{i,k+m} = \mathcal{T}_{i,k} + m\alpha_i + (m-1)\beta_i \tag{4.26}$$

$$\mathcal{T}_{i,k+m} = \mathcal{T}_{i,k} + m\alpha_i + m\beta_i \tag{4.27}$$

Proof. For $m = 0$, we have $t^+_{i,k} = \mathcal{T}_{i,k} - \beta_i$, which is true by definition. For $m = 1$, we have $t^+_{i,k+1} = \mathcal{T}_{i,k} + \alpha_i$, which is also true by the definition of α_i or Eq. (4.24). To compute $t^+_{i,k+2}$, we must include the number of slots required to discharge the battery from the energy level at time $t^+_{i,k+1}$ to that at time $\mathcal{T}_{i,k+1}$, and the time duration from time $\mathcal{T}_{i,k+1}$ to time $t^+_{i,k+2}$. Thus, $t^+_{i,k+2} = \mathcal{T}_{i,k+1} + \alpha_i + \beta_i = \mathcal{T}_{i,k} + 2\alpha_i + \beta_i$. Similarly, for $m = 3$, we have $t^+_{i,k+3} = \mathcal{T}_{i,k+2} + \alpha_i + \beta_i = \mathcal{T}_{i,k} + 3\alpha_i + 2\beta_i$. Repeating the steps to compute $t^+_{i,k}$ and $\mathcal{T}_{i,k}$ for $m = 4, 5, \ldots$, we obtain Eq. (4.26) and Eq. (4.27), respectively. Note that for each pair of $\mathcal{T}_{i,k}$ and $t^+_{i,k}$ at any discharging cycle k, we have $\beta_i = \mathcal{T}_{i,k} - t^+_{i,k}$. □

Figure 4.6 illustrates the relationship between α_i, β_i, $t^+_{i,k}$, and $\mathcal{T}_{i,k}$ used in Eq. (4.24), (4.25), (4.26), and (4.27), respectively. Note that variable $\mathcal{T}_{i,k}$ is used

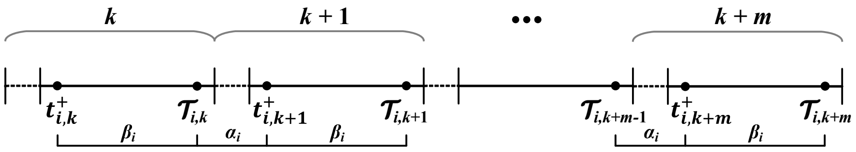

Figure 4.6 An illustration for Eq. (4.24) to Eq. (4.27).

only for batteries with a leakage rate of $\mu_i > 0$. Thus, *Propositions 4.9*, *4.10*, and *4.11* are not relevant for batteries with a leakage rate of $\mu_i = 0$.

We now describe a scenario to schedule a link $l_{i,j}$ in Figure 4.7. Consider a link $l_{i,j}$ and case (i): $t^+_{i,k} < t^+_{j,k}$ in Figure 4.7a. A link $l_{i,j}$ can be activated at timeslot $t_{i,j} = \mathbf{max}\{t^+_{i,k}, t^+_{j,k}\} = t^+_{j,k}$ only if (a) $t_{i,j} \geq t^+_{j,k+n}$, and (b) $t^+_{j,k+n} \leq \mathcal{T}_{i,k+m}$, for $m, n = 0, 1, \ldots$. Similarly, for case (ii): $t^+_{j,k} < t^+_{i,k}$ in Figure 4.7b, a link $l_{i,j}$ can be activated at timeslot $t_{i,j} = t^+_{i,k}$ only if (a) $t_{i,j} \geq t^+_{i,k+m}$, and (b) $t^+_{i,k+m} \leq \mathcal{T}_{j,k+n}$. In other words, we need to compute the two inequalities: (i) $t^+_{j,k+n} \leq \mathcal{T}_{i,k+m}$ and (ii) $t^+_{i,k+m} \leq \mathcal{T}_{j,k+n}$ to determine the time $t_{i,j}$ to schedule each link $l_{i,j}$. Using Eq. (4.26) and (4.27), for inequalities (i) and (ii), we obtain, respectively,

$$n(\alpha_j + \beta_j) - m(\alpha_i + \beta_i) \leq \mathcal{T}_{i,k} - \mathcal{T}_{j,k} + \beta_j \tag{4.28}$$

$$m(\alpha_i + \beta_i) - n(\alpha_j + \beta_j) \leq \mathcal{T}_{j,k} - \mathcal{T}_{i,k} + \beta_i \tag{4.29}$$

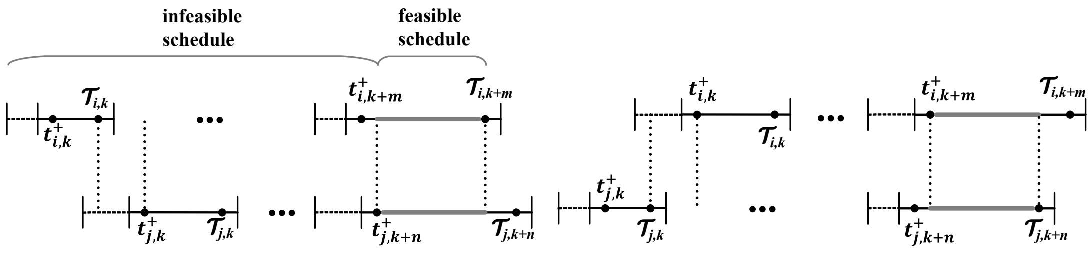

(a) Case (i): $t^+_{i,k} < t^+_{j,k}$.

(b) Case (ii): $t^+_{j,k} < t^+_{i,k}$.

Figure 4.7 Two scenarios to schedule a link $l_{i,j}$.

One can use Satisfiability Modulo Theories (SMT) solver, e.g., Mistral [95], to solve linear inequalities over integers for expressions (4.28) and (4.29). The

Mistral solver implements the Cuts-from-Proofs algorithm [96]. The solver is able to generate solutions for systems of linear inequalities that contain between 10 and 45 variables and between 15 and 50 inequalities per system. For problem **LSME-1**, it is preferable to find a pair (m, n) with the minimum of $\mathbf{max}\{m, n\}$ for inequalities (4.28) and (4.29) to minimise time $t_{i,j}$ so that a link (i, j) can be scheduled earlier. Therefore, in this paper, we propose a simple heuristic function, called $find_{mn}(.)$, to obtain such a pair of (m, n) for inequalities (4.28) and (4.29). Function $find_{mn}$ $(i,\ j,\ \mathcal{T}_{i,k},\ \mathcal{T}_{j,k})$ generates the values of m and n for inequalities (4.28) and (4.29) as follows. Initially, it sets $(m, n) = (0, 0)$. From Eq. (4.26) and (4.27), increasing the value of m results in a larger $t^{+}_{i,k+m}$ and $\mathcal{T}_{i,k+m}$ value. Similarly, a larger n value increases $t^{+}_{j,k+n}$ and $\mathcal{T}_{j,k+n}$. To minimise time $t_{i,j}$, $find_{mn}(.)$ needs to find the minimum integer values for m and n. Consider $t^{+}_{i,k} < t^{+}_{j,k}$, i.e., case (i) in Figure 4.7a, and $t^{+}_{j,k+n} > \mathcal{T}_{i,k+m}$. For this case, a larger value of $\mathcal{T}_{i,k+m}$ is needed. Thus, $find_{mn}(.)$ increases the value of m in (4.28) from $m = 0$ to $m' = 1$ to increase the value of $\mathcal{T}_{i,k+m}$, which also increases $t^{+}_{i,k+m}$. The function $find_{mn}(.)$ also finds the value of n' from (4.28) when it uses $m' = 1$. Next it produces a new value of m in (4.29) using n', e.g., m''. If $m'' \leq m'$, the values $(m' = 1, n')$ satisfy both (4.28) and (4.29), thus it returns (m', n'). However, if $m'' > m'$, it uses m'' in (4.28) to further increase the value of $\mathcal{T}_{i,k+m}$ and obtains a new value for n, e.g., n''. If $n'' \leq n'$, it stops at a feasible solution (m'', n'). However, if $n'' > n'$, it uses n'' in (4.29) to generate an updated value of m, e.g., m''', which is then used to obtain another new value for n in (4.28), namely n'''. Function $find_{mn}(.)$ repeats the iterations until it finds the first feasible solution for m and n. Thus, the link (i, j) can be scheduled at time $t_{i,j} = \mathbf{max}(t^{+}_{i,k+m}, t^{+}_{j,k+n})$.

To illustrate how the function $find_{mn}(.)$ works, consider a link $l_{i,j}$ with $T_i = 22$, $\mathcal{T}_{i,k} = 74$, $T_j = 93$, $\mathcal{T}_{j,k} = 132$, $\alpha_i = 78$, $\alpha_j = 81$, $\beta_i = 90$, and $\beta_j = 39$. In this example, $T_j = t^+_{j,k}$ because $t^+_{j,k} = \mathcal{T}_{j,k} - \beta_j = 132 - 39 = 93$. However, we have $T_i \neq t^+_{i,k}$, in which the battery at node v_i has been used in a discharging cycle k. From (4.28) and (4.29), we respectively have (i) $120n - 168m \leq -19$, and (ii) $168m - 120n \leq 148$. Notice that the link $l_{i,j}$ cannot be activated at time $t_{i,j} = \mathbf{max}(22, 93) = 93$ because $t^+_{j,k} > \mathcal{T}_{i,k}$; see Figure 4.8. Thus, we need to *shift* the discharging cycle of the battery at node v_i to the next cycle by increasing time $\mathcal{T}_{i,k+m}$. To shift one cycle, function $find_{mn}(.)$ sets $m = m' = 1$ in (i) and obtains $n' = 0$. As shown in Figure 4.8, the cycle now starts at $t^+_{i,k+1} = 152$ and ends at $\mathcal{T}_{i,k+1} = 242$, which are obtained by substituting $m = 1$ into Eq. (4.26) and (4.27), respectively. The function then sets $m = m' = 1$ in (ii) and gets $n' = 1 > 0$ that indicates the need for shifting the cycle for the battery at node v_j by one cycle. Otherwise, the link cannot be activated at time $t_{i,j} = \mathbf{max}(152, 93) = 152$ because $t^+_{i,k+1} > \mathcal{T}_{j,k}$; see Figure 4.8. Setting $n = n' = 1$ in (4.29), the function gets a new value of m, i.e., $m'' = 1$. Notice that $m'' \leq m'$, indicating that we do not need to further shift the duration for node v_i, i.e., $(m = 1, n = 1)$ is a feasible solution for (4.28) and (4.29). Thus, the link $l_{i,j}$ can be scheduled at time $t_{i,j} = \mathbf{max}(t^+_{i,k+1}, t^+_{j,k+1}) = \mathbf{max}(152, 213) = 213$.

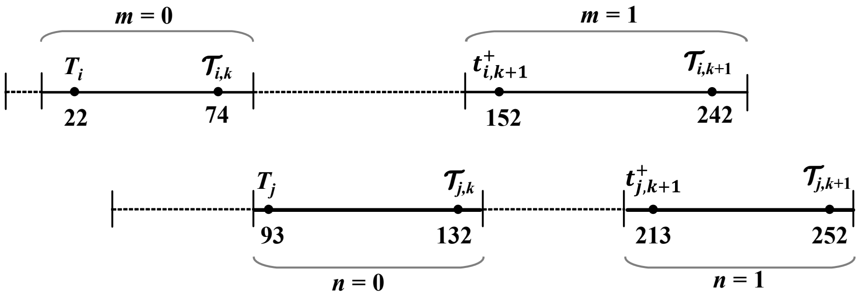

Figure 4.8 A discharging cycle of the battery at node v_i (top) and v_j (bottom).

4.2.2 Problem Solution Feasibility

This section aims to show the feasibility of **LSME-1**. While, in general, two linear inequalities always have a solution, the values of m and n can be non-integers [96]. One can use proof of unsatisfiability in [96] to determine if two linear inequalities have no integer solution. Thus, **LSME-1** for batteries with a leakage rate of $\mu_i > 0$ might not have a feasible solution, i.e., there can be some links $l_{i,j} \in E$ which cannot be scheduled. This is because a link (i, j) can be scheduled only when the batteries at its end nodes are simultaneously in a discharging cycle at the start of the same slot m or n, or different slots m and n. Recall that expressions (4.28) and (4.29) are for case $\mu_i > 0$.

Consider a link (i, j) and slot t at which time the batteries of end nodes v_i and v_j are in a *charging* and *discharging* cycle, respectively. Thus, the link (i, j) at time t cannot be scheduled. We call such a link (i, j) as an *unscheduled* link or u-link at time t, denoted by $(i, j)^t$, if its end nodes' other adjacent links will never be scheduled at or after time t. Let $E^t \subseteq E$ be a set of u-links at time t. Intuitively, when the batteries of the end nodes of each u-link have the same harvesting time, storage efficiency, leakage rate, and minimum and maximum battery levels, the batteries will never reach a discharging cycle at the same time, and thus the link cannot be scheduled. This is because the batteries will have the same charging and discharging intervals. The intuition is one possible necessary condition that prohibits expressions (4.28) and (4.29) having integers m and n as their solution. It is stated and formally proved in the following proposition.

Proposition 4.12. *Each u-link $(i, j)^t \in E^t$ cannot be scheduled if all batteries have the same values of harvesting time r_i, storage efficiency η_i, leakage rate μ_i, minimum battery level $b_{i,min}$, and maximum battery level $b_{i,max}$.*

Proof. The proof considers three cases: (i) set E^t contains only one u-link $(i,j)^t$, (ii) set E^t contains more than one u-links where any pairs of them are not adjacent to each other, and (iii) set E^t contains more than one u-link where some pairs of them are adjacent to each other. For case (i), we show that u-link $(i,j)^t$ cannot be scheduled as follows. For $r_i = r_j$, $\mu_i = \mu_j$, $\eta_i = \eta_j$, $b_{i,min} = b_{j,min}$, $b_{i,max} = b_{j,max}$, Eq. (4.8) obtains $\tilde{\tau}_i = \tilde{\tau}_j$. Thus, for $\tilde{\tau}_i = \tilde{\tau}_j$, $b_{i,min} = b_{j,max}$, and $\mu_i = \mu_j$, Eq. (4.24) produces $\alpha_i = \alpha_j$. Similarly, Eq. (4.25) has $\beta_i = \beta_j$. Let α denote both α_i and α_j, and β denote both β_i and β_j. Further we set $\mathcal{T} = \mathcal{T}_{i,k} - \mathcal{T}_{j,k}$. Thus, we can convert expressions (4.28) and (4.29) into the following two expressions, respectively,

$$n(\alpha + \beta) - m(\alpha + \beta) \leq \mathcal{T} + \beta \tag{4.30}$$

$$m(\alpha + \beta) - n(\alpha + \beta) \leq -\mathcal{T} + \beta \tag{4.31}$$

One necessary condition for (4.30) and (4.31) to have integer solution for m and n is when $m \neq n$. Otherwise, the batteries at node v_i and node v_j cannot be simultaneously in a discharging cycle because both batteries have the same aforementioned parameters, and thus they have the same charging interval and the same discharging interval. Now, we aim to show that any solution for expressions (4.30) and (4.31) cannot have integer values of m and n. Without loss of generality, consider $\mathcal{T}_{i,k} > \mathcal{T}_{j,k}$, and thus $\mathcal{T} > 0$. Multiplying both sides of (4.30) by -1, we have

$$m(\alpha + \beta) - n(\alpha + \beta) \geq -\mathcal{T} - \beta \tag{4.32}$$

Thus, from (4.31) and (4.32), we have

$$-\mathcal{T} - \beta \leq m(\alpha + \beta) - n(\alpha + \beta) \leq -\mathcal{T} + \beta \tag{4.33}$$

or

$$\frac{-(\mathcal{T}+\beta)}{(\alpha+\beta)} \leq m-n \leq \frac{(-\mathcal{T}+\beta)}{(\alpha+\beta)} \tag{4.34}$$

Notice that we have $(-\mathcal{T}+\beta) < (\alpha+\beta)$ because $\mathcal{T}$ is a positive integer. Thus, we have $\frac{(-\mathcal{T}+\beta)}{(\alpha+\beta)} < 1$. Further, $\frac{-(\mathcal{T}+\beta)}{(\alpha+\beta)}$ has a negative value, or we have $\frac{-(\mathcal{T}+\beta)}{(\alpha+\beta)} < 0$. Thus, we have

$$\frac{-(\mathcal{T}+\beta)}{(\alpha+\beta)} < 0 \leq m-n < \frac{(-\mathcal{T}+\beta)}{(\alpha+\beta)} < 1 \tag{4.35}$$

Since $m \neq n$, i.e., $m-n \neq 0$, we have

$$0 < m-n < 1 \tag{4.36}$$

which means the value of $m-n$ is a fraction. Thus, either variable m or n is a fraction.

For case (ii), we repeat the proof for case (i) for each u-link $(i,j)^t \in E^t$. Accordingly, none of the u-links in the set can be scheduled. Finally, for case (iii), arbitrarily consider one u-link $(i,j)^t \in E^t$. Following the proof for case (i), u-link $(i,j)^t$ cannot be scheduled. Next, consider an adjacent link of $(i,j)^t$, e.g., a u-link $(i,k)^t$. We argue that $(i,k)^t$ cannot be scheduled because all of its parameters are unchanged. Note that the expressions (4.30) and (4.31) of u-link $(i,k)^t$ can have integer solutions m and n, and thus the link (i,j) can be scheduled only if the batteries' parameters, i.e., leakage rate μ_i, storage efficiency η_i, minimum battery level $b_{i,min}$, and maximum battery level $b_{i,max}$, change. □

To illustrate *Proposition 4.12*, consider the network in Figure 4.9 in which the link $(1,2)$ is activated first at slot 13. We have $T_1 = T_2 = 93$, $\mathcal{T}_{1,k} = \mathcal{T}_{2,k} = 132$, $T_3 = 13$, and $\mathcal{T}_{3,k} = 52$. Further, $E^t = \{(2,3),(3,1)\}$. We show that u-link $(2,3)^t$ cannot be scheduled as follows. Eq. (4.8) obtains $\tilde{\tau}_2 = \tilde{\tau}_3 = 12$, while Eq. (4.24) and (4.25) produce $\alpha_2 = \alpha_3 = \alpha = 81$ and $\beta_2 = \beta_3 = \beta = 39$, respectively. Further, we have $\mathcal{T} = \mathcal{T}_{2,k} - \mathcal{T}_{3,k} = 132 - 52 = 80$. Thus, we have $-\frac{119}{120} < 0 \leq m - n \leq -\frac{41}{120} < 1$ for (4.35), and $0 < m - n < 1$ for (4.36), meaning either value of m or n is a fraction. Thus, u-link $(2,3)^{t=93}$ cannot be scheduled and the parameters for u-link $(3,1)^t$ remain unchanged. Similarly, u-link $(3,1)^t$ cannot be scheduled because all of its parameters are the same as those of u-link $(2,3)^t$.

While it is important to find all necessary conditions that prohibit expressions (4.28) and (4.29) to have integer values of m and n for their solution, unfortunately, we failed to generate the conditions due to the complexity of the problem.

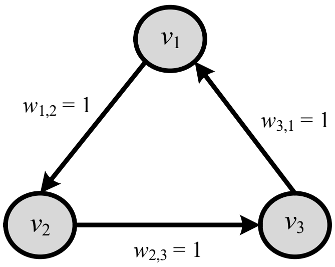

Figure 4.9 A cycle with three nodes: an example for a non-existing solution. Each node v_i has $b_{i,min} = 1$, $b_{i,max} = 3$, $b_i = 3$, $\mu_i = 0.01$, $\eta_i = 1$, and $r_i = 5$.

The following proposition formally shows that **LSME-1** for batteries with $\mu_i = 0$ always has a feasible solution.

Proposition 4.13. *LSME-1 for batteries with a leakage rate of $\mu_i = 0$ will always have a feasible solution, i.e., it is possible to activate each link $l_{i,j} \in E$.*

Proof. For a leakage rate of $\mu_i = 0$, the battery at a node v_i makes a transition from a discharging to a charging cycle *only* after its energy is used to activate at least one incident link at a node v_i. Consider a link $l_{i,j} \in E$. Without loss of generality, assume the battery at a node v_i has a longer discharging cycle than at a node v_j. In other words, the battery at a node v_i is less frequently used than the battery at node v_j. For this case, the battery at a node v_j will transition to a charging cycle earlier than the battery at a node v_i. Thus, the battery at a node v_i remains in a discharging cycle while the battery at a node v_j is being recharged to its maximum level. When the battery at a node v_j is back to a discharging cycle, the link $l_{i,j}$ can be activated. □

4.2.3 A Method to Shorten Superframe Length

The link schedule of a rWSN that complies with the battery cycle constraint will become longer when the batteries of nodes have a smaller leakage rate μ_i. The reason is as follows. Consider a battery of a node v_i that has an energy level of $b_{i,min} + x$, for $x < 1\epsilon$. The battery cycle constraint requires the energy level of the battery to reach $b_{i,min}$ before it can be recharged. However, discharging the non-usable energy from the battery takes longer when its leakage rate is smaller. As an example, consider a battery with $b_{i,min} = 1$ and $x = 0.5$. For a leakage rate of $\mu_i = 0.01$, $b_1 = 1.5$, and $b_2 = 1$, Eq. (4.19) produces 40 timeslots to discharge the 0.5ϵ of energy. The discharging time will significantly increase to 405464 slots when its leakage rate is $\mu_i = 10^{-6}$. The longer discharging time leads to a longer schedule because the battery requires more time before it can be recharged to $b_{i,max}$ so that it can be used to activate links.

To shorten the discharging time, we assume each node is able to discard or *flush* its excess energy x at slot t in the next slot $t + 1$. One way for a node to *flush* excess energy of size x is by using the energy to transmit a *dummy* packet in a given slot. This protocol, henceforth called *energy flush*, is similar to that assumed in [36]. Briefly, the work in [36] used two batteries, called primary and secondary, which were in discharging and charging mode, respectively. When the secondary battery was fully charged, it became the primary battery, while the other became the secondary battery, i.e., it goes into charging mode, even when its energy level had not reached the minimum, i.e., $b_{i,min}$ in our model.

The use of the *energy flush* protocol affects the computation of Eq. (4.19) when it has $b_1 = b_{i,min} + x$ for $x < 1$, and $b_2 = b_{i,min}$. For this case, the value of $\delta^{b_2}_{i,b_1}$ is set to 1 because according to the energy flush protocol the x excess energy can be discharged in one slot. Consequently, for this case, we need to set the value of $\delta^{b_2}_{i,b_1}$ in Eq. (4.21) to 1. Thus, Eq. (4.21) for $\mu_i > 0$, $b_1 = b_{i,min} + x$ for $x < 1$, and $b_2 = b_{i,min}$ becomes

$$T_i = t_i + \sigma_{i,t_i} \times (1 + \tilde{\tau}_i) + 1 \tag{4.37}$$

4.2.4 LSBCC

This section provides the details of our heuristic algorithm to solve **LSME-1**, called **Link Scheduler with Battery Cycle Constraint (LSBCC)**. The algorithm aims to schedule all non-interfering links at the earliest possible timeslot when the battery at its end nodes can be used, i.e., in discharging mode. Further, it uses the conflict graph C_G to check the interference links.

We first describe LSBCC in Algorithm 2 which considers batteries with a leakage rate of $\mu_i > 0$. LSBCC sets time $t = 0$ as the beginning of timeslot and the battery of each node is initially in charging mode. In *Lines 1–3*, LSBCC uses function *INIT*(.) to initialise the following eight parameters for each node v_i. The function initialises the energy level of the battery at each node v_i to $b_{i,min}$, i.e., $\tilde{b}_{i,0} = b_{i,min}$. It uses Eq. (4.8) to compute $\tilde{\tau}_i$, i.e., the charging time interval for the battery at a node v_i. It sets time duration α_i and β_i using Eq. (4.24) and (4.25), respectively. It initialises t_i to the last time the battery at a node v_i is discharged to zero. It also sets T_i to $\tilde{\tau}_i + 1$ and $\mathcal{T}_{i,k}$ to $T_i + \beta_i$. Recall that T_i and $\mathcal{T}_{i,k}$ are the earliest time and the latest timeslot when the battery at a node v_i can be discharged to transmit/receive one packet. Finally, it initialises b_{i,T_i}, the energy level of the battery at a node v_i at time T_i, to $b_{i,max} \times \hat{\mu}_i$, i.e., $b_{i,T_i} = b_{i,max} \times \hat{\mu}_i$.

Algorithm 2 LSBCC

Input: $G(V, E)$, r_i, b_i, $b_{i,max}$, $b_{i,min}$, μ_i, η_i of each node $v_i \in V$, weight $w_{i,j}$ of each link $l_{i,j} \in E$, and conflict graph C_G

Output: Superframe $\mathcal{S}$

```
 1: for each node $v_i \in V$ do
 2:     $INIT(\tilde{b}_{i,0}, \tilde{\tau}_i, \alpha_i, \beta_i, t_i, T_i, \mathcal{T}_{i,k}, b_{i,T_i})$
 3: end for
 4: for each link $l_{i,j} \in E$ do
 5:     $t_{i,j} = COMP\_t_{i,j}(v_i, v_j)$
 6: end for
 7: $K = \{$node $l_{i,j}$ in $C_G$ with $\mathbf{min}\{t_{i,j}\}\}$
 8: $K' = ORDER(K)$
 9: $t \leftarrow \mathbf{min}\{t_{i,j}\}$
10: for each $l_{i,j} \in K'$ do
11:     if NOT $CONFLICT(l_{i,j}, \mathcal{S}[t])$ then
12:         $\mathcal{S}[t] \leftarrow \mathcal{S}[t] \cup l_{i,j}$
13:         $w_{i,j} \leftarrow w_{i,j} - 1$
14:         if $w_{i,j} = 0$ then
15:             remove node $l_{i,j}$ from $C_G$
16:         end if
17:         $t_i \leftarrow t_j \leftarrow t$
18:         $b_{i,t_i} \leftarrow b_{i,T_i} \times \hat{\mu}_i^{t_i - T_i} - 1$
19:         $b_{j,t_j} \leftarrow b_{j,T_j} \times \hat{\mu}_j^{t_i - T_j} - 1$
20:         $T_i \leftarrow COMP\_T_\alpha(i)$
21:         $b_{i,T_i} \leftarrow COMP\_b_\alpha(i)$
22:         $T_j \leftarrow COMP\_T_\alpha(j)$
23:         $b_{j,T_j} \leftarrow COMP\_b_\alpha(j)$
24:         $\mathcal{T}_{i,k} \leftarrow T_i + \lfloor \frac{log\ (b_{i,min}+1) - log\ b_{i,T_i}}{log\ \hat{\mu}_i} \rfloor$
25:         $\mathcal{T}_{j,k} \leftarrow T_j + \lfloor \frac{log\ (b_{j,min}+1) - log\ b_{j,T_j}}{log\ \hat{\mu}_j} \rfloor$
26:     end if
27: end for
28: repeat Lines 4–27 until all $w_{i,j} = 0$
```

Lines 4–6 use function $COMP\_t_{i,j}(.)$ in Algorithm 3 to compute the earliest time each link (i, j) can be activated, i.e., $t_{i,j}$. If the batteries of nodes v_i and v_j are at the same discharging cycle, *Line 2* of $COMP\_t_{i,j}(.)$ sets $t_{i,j}$ to the earliest

Algorithm 3 *COMP_$t_{i,j}$*

```
Input: $v_i, v_j$
Output: $t_{i,j}$
 1: if $T_j \le \mathcal{T}_{i,k}$ or $T_i \le \mathcal{T}_{j,k}$ then
 2:     $t_{i,j} \leftarrow \mathbf{max}(T_i, T_j)$
 3: else
 4:     if $SATISFY(i,j)$ is true then
 5:         $find_{mn}(i, j, \mathcal{T}_{i,k}, \mathcal{T}_{j,k})$
 6:         $t^{+}_{i,k+m} \leftarrow \mathcal{T}_{i,k} + m\alpha_i + (m-1)\beta_i$
 7:         $t^{+}_{j,k+n} \leftarrow \mathcal{T}_{j,k} + n\alpha_j + (n-1)\beta_j$
 8:         $b_{i,t^{+}_{i,k+m}} \leftarrow b_{i,max} \times \hat{\mu}_i$
 9:         $b_{j,t^{+}_{j,k+n}} \leftarrow b_{j,max} \times \hat{\mu}_j$
10:         $\mathcal{T}_{i,k+m} \leftarrow \mathcal{T}_{i,k} + m\alpha_i + m\beta_i$
11:         $\mathcal{T}_{j,k+n} \leftarrow \mathcal{T}_{j,k} + n\alpha_i + n\beta_i$
12:         $t_{i,j} \leftarrow \mathbf{max}(t^{+}_{i,k+m}, t^{+}_{j,k+n})$
13:     else
14:         $t_{i,j} \leftarrow 2^{31} - 1$
15:     end if
16: end if
17: return($t_{i,j}$)
```

time at which both batteries can be discharged. On the other hand, when the two batteries are not at the same discharging cycle, *Lines 4−15* aim to obtain the earliest time that the battery at nodes v_i and v_j can be at the same discharging cycle. More specifically, *Line 4* first uses the proof of unsatisfiability [96] in function *SATISFY*(.) to determine if expressions (4.28) and (4.29) for a link (i, j) have integer solutions. If so, *Line 5* uses function $find_{mn}(.)$ to compute a pair (m, n) that satisfies expressions (4.28) and (4.29). Otherwise, *Line 14* sets $t_{i,j}$ to a large integer value, i.e., $2^{31} - 1$, to denote that the link $l_{i,j}$ can not be scheduled in this iteration. Note that it is possible that the link $l_{i,j}$ can be scheduled in the future. *Lines 6−7* compute the starting time of the next discharging cycle of the battery at nodes v_i and v_j. *Lines 8−9* obtain the battery levels of nodes v_i and v_j. *Lines 10−11* recompute the ending time of the next discharging cycle of the battery at nodes v_i and v_j. *Line 12* computes $t_{i,j}$.

Line 7 of LSBCC creates a set K that stores all links (i, j) that have the same earliest activation time. *Line 8* then uses function $ORDER(K)$ to sort links in set K in order of decreasing weight $w_{i,j}$. Links with equal $w_{i,j}$ are sorted in the decreasing node degree of their end nodes, and for a tie, links are sorted in the increasing order of their node labels.

Line 9 sets t with the earliest slot, i.e., $\mathbf{min}\{t_{i,j}\}$. *Lines 10–27* repeatedly schedule each link $l_{i,j} \in K'$ in order. Each selected link in *Line 12* does not cause interference or is interfered by links that have been scheduled in slot t; see the condition in *Line 11*. Each slot in $\mathcal{S}$ is initially empty. Note that function $CONFLICT(.)$ uses a matrix M of size $|E|^2$ that contains Boolean variables to represent the conflict graph of the network; i.e., $M[a, b]$ is set to "1" if there is an interference between links a and b. *Line 13* decreases the weight of each selected link $l_{i,j}$ by one. Once the weight reaches zero (see *Line 14*), *Line 15* removes the link from contention.

Line *17* sets the last time that batteries at the end nodes of the selected link $l_{i,j}$ is used, i.e., t_i and t_j, to the current time. Further, *Lines 18–19* compute the energy levels of the battery at nodes v_i and v_j at time t_i, after the nodes have transmitted/received one packet. *Line 20* uses function $COMP\_T_\alpha(.)$ that implements Eq. (4.21) to update the next earliest time the battery at node v_i can be discharged. *Line 21* uses function $COMP\_b_\alpha(.)$ to compute the battery's energy level at time T_i, which depends on the remaining energy level at time t_i, i.e., b_{i,t_i}. More specifically, if b_{i,t_i} is greater than or equal to $(b_{i,min} + 1)$, then b_{i,T_i} is set to $b_{i,t_i} \times \hat{\mu}_i$ as the battery can still be used to transmit/receive one packet. Otherwise, b_{i,T_i} is set to $b_{i,max} \times \hat{\mu}_i$ since the battery has been charged to its maximum level. Similarly, LSBCC computes the next earliest time and energy level of the battery at node v_j in *Lines 22–23*. *Lines 24–25* use Eq. (4.22) to obtain the latest time the battery at nodes v_i and v_j can be used. Finally, the steps from *Line 4* are repeated until all links are scheduled, i.e., $w_{i,j} = 0$.

Next, we describe how to adjust LSBCC in Algorithm 2 for use in the case when the battery at each node v_i is leak-free, i.e., for case $\mu_i = 0$. The adjustment comprises the following four changes to Algorithm 2: a) Function $INIT(.)$ in *Line 2* of LSBCC does not initialise parameters α_i, β_i, and $\mathcal{T}_{i,k}$. Recall that these three parameters are used only for batteries with $\mu_i > 0$; b) Replace *Line 5* of Algorithm 2 with $t_{i,j} = \mathbf{max}(T_i, T_j)$. Note that function $COMP\_t_{i,j}(.)$ is applicable only for batteries with $\mu_i > 0$; c) Set b_{i,T_i} to $b_{i,max}$ in *Line 21* if b_{i,t_i} is equal to $b_{i,min}$. Otherwise, set b_{i,T_i} to b_{i,t_i}. Do a similar adjustment in *Line 23* as in *Line 21*; and lastly, d) Omit *Lines 24–25*.

For an example, consider the rWSN and conflict graph C_G shown in Figure 4.3. The function $INIT(.)$ for each node v_i sets the following eight parameters as: (i) $\tilde{b}_{1,0} = \tilde{b}_{2,0} = \tilde{b}_{3,0} = \tilde{b}_{4,0} = b_{1,min} = 1$; (ii) $\tilde{\tau}_1 = 9$, $\tilde{\tau}_2 = 12$, $\tilde{\tau}_3 = 20$, $\tilde{\tau}_4 = 10$; (iii) $\alpha_1 = 78$, $\alpha_2 = 81$, $\alpha_3 = 89$, $\alpha_4 = 79$; (iv) $\beta_1 = 90$, $\beta_2 = \beta_3 = 39$, $\beta_4 = 67$; (v) $t_1 = t_2 = t_3 = t_4 = 0$; (vi) $T_1 = \tilde{\tau}_1 + 1 = 10$, $T_2 = 13$, $T_3 = 21$, $T_4 = 11$; (vii) $\mathcal{T}_{1,k} = T_1 + \beta_1 = 100$, $\mathcal{T}_{2,k} = 52$, $\mathcal{T}_{3,k} = 60$, $\mathcal{T}_{4,k} = 78$; and (viii) $b_{1,T_1} = b_{1,max} \times \hat{\mu}_1 = 5 \times 0.99 = 4.95$, $b_{2,T_2} = 2.97$, $b_{3,T_3} = 2.97$, $b_{4,T_4} = 3.96$. *Lines 4–6* obtain $t_{1,2} = 13$, $t_{2,4} = 13$, and $t_{3,1} = 21$. *Line 7* inserts links $l_{1,2}$ and $l_{2,4}$ into the set K, and thus *Line 8* obtains $K' = \{l_{2,4}, l_{1,2}\}$ because $w_{2,4} > w_{1,2}$, and *Line 9* sets $t = 13$. *Line 11* finds that $l_{2,4}$ has conflict with $l_{1,2}$, and thus *Line 12* inserts only link $l_{2,4}$ into $\mathcal{S}[13]$, and *Line 13* reduces $w_{2,4}$ by one and hence it becomes two. *Line 17* sets $t_2 = t_4 = 13$. *Lines 18–19* compute $b_{2,13} = 1.97$ and $b_{4,13} = 2.88$. *Lines 20–23* obtain $T_2 = 93$, $b_{2,T_2} = 2.97$ and $T_4 = 14$, $b_{4,T_4} = 2.85$. *Lines 24–25* then compute $\mathcal{T}_{2,k} = 132$ and $\mathcal{T}_{4,k} = 49$. *Line 28* repeats the steps from *Line 4* until all links have $w_{i,j} = 0$. Finally, LSBCC produces the link schedule $\mathcal{S}$ in Figure 4.4b, i.e., $\mathcal{S} = [\ \mathcal{S}[13] = \{l_{2,4}\}$, $\mathcal{S}[21] = \{l_{3,1}\}$, $\mathcal{S}[128] = \{l_{2,4}\}$, $\mathcal{S}[152] = \{l_{2,4}\}$, $\mathcal{S}[227] = \{l_{1,2}\}$, $\mathcal{S}[307] = \{l_{1,2}\}\ ]$. The generated schedule contains 303 empty slots as the battery at each node needs time to charge to its maximum level before it can be used to transmit/receive packets.

Proposition 4.14. *The time complexity of LSBCC is* $O(W|E|^2)$*, where* $W = \sum_{(i,j)\in|E|}(w_{i,j})$.

Proof. Lines 1–3 take $O(|V|)$. *Lines 4–6* require $O(|E|)$ because *Lines 1–17* of function $COMP\_t_{i,j}$ take $O(1)$ each and these lines are repeated at most $|E|$ times. *Line 7* takes $O(|E|)$. *Line 8* sorts all links in K using the function $ORDER(K)$ that requires $O(|E|\ log\ |E|)$. *Line 9* takes $O(1)$. *Line 11* requires $O(|E|^2)$ to construct a matrix M which represents the conflict graph C_G. Function $CONFLICT(l_{i,j}, \mathcal{S}[t])$ in *Line 11* uses the matrix at most $|E|$ times. Hence, it takes $O(|E|)$. *Lines 12–25* take $O(1)$ each. The for loop in *Lines 10–27* is repeated at most $|E|$ times, and thus, the loop requires at most $O(|E|^2)$. *Line 28* repeats *Lines 4–27* W times. Thus, the time complexity of LSBCC is $O(W|E|^2)$. □

Notice that the time complexity of LSBCC becomes $O(|E|^3)$ if each link weight has a constant value. For this case, LSBCC runs in polynomial order of the number of links $|E|$. Further, the running time of the algorithm worsens on the networks that contain a high number of links. Nevertheless, since LSBCC runs in polynomial order of $|E|$, it is scalable for use in larger sized networks.

4.3 Evaluation

Section 4.3.1 analyses the schedule length when nodes use a battery that adheres to the battery cycle constraint but with *no leakage*. Section 4.3.2 aims to analyse the effects of parameters r_i, b_i, $b_{i,max}$, and η_i on the feasibility of **LSME-1** when nodes have a battery with a leakage rate of $\mu_i > 0$. Finally, Section 4.3.3 evaluates the impact of the battery cycle constraint on the link schedule length, and on the number of charge/discharge cycles for rWSNs with leak-free batteries and for those with batteries that leak.

Table 4.1 lists the parameter values used in our simulation. We consider arbitrary networks with 10 to 50 nodes randomly deployed on a 40×40 m^2 area. The average number of links $|E|$ are 28, 125, 273, 470, and 758 for networks with 10, 20, 30, 40, and 50 nodes, respectively. Each node has a transmit and interference range of 15 and 30 meters, respectively. We arbitrarily set the range of values of r_i and $w_{i,j}$ to $\{2, 3, \ldots, 17\}$ as in [44] and $\{1, 2, \ldots, 5\}$, respectively.

We use leakage rate μ_i values in the set $\{1, 1.2, 1.4, 1.6, 1.8, 2.0, 2.2, 2.4\} \times 10^{-6}$ per slot since the battery's leakage rate is 20% per 24 hours [97]. We set each slot to one second. Further, we consider batteries with 100% storage efficiency, and arbitrarily set the values of b_i, $b_{i,min}$, and $b_{i,max}$. Note that as reported in Section 3.3.3.1 of Chapter 3, the battery capacity has an insignificant effect on the superframe length $|\mathcal{S}|$. Our results are an average of over 100 random node deployments.

Table 4.1 Parameter values used in our evaluation.

Parameter	***Value (s)***
Network size	40×40 m^2
Transmit range	15 m
Interference range	30 m
$\|V\|$	$\{10, 20, 30, 40, 50\}$
r_i	$\{2, 3, 4, \ldots, 17\}$
μ_i	$\{1, 1.2, 1.4, 1.6, \ldots, 2.4\} \times 10^{-6}$
η_i	1.0
b_i	3ϵ
$b_{i,min}$	1ϵ
$b_{i,max}$	3ϵ
$w_{i,j}$	$\{1, 2, 3, 4, 5\}$

4.3.1 Battery with No Leakage

The aim of this section is to study how the battery cycle constraint affects the superframe length $|\mathcal{S}|$ when each battery has no leakage, i.e., $\mu_i = 0$. Recall that, as stated in *Proposition 4.13*, **LSME-1** always has a feasible solution for $\mu_i = 0$. This section performs two evaluations. First, it compares the performance of LSBCC against LSNBC. Briefly, LSNBC is a version of LSBCC without the battery cycle constraint. Second, it investigates the effect of energy harvesting time r_i on the link schedules produced by LSBCC. All experiments consider 10 to 50 nodes with the following parameter values: $b_i = 3\epsilon$, $b_{i,max} = 3\epsilon$, and $b_{i,min} = 1\epsilon$.

4.3.1.1 LSBCC *versus* LSNBC

This section compares the performance of LSBCC against LSNBC in terms of superframe length $|\mathcal{S}|$ and the total number of charge/discharge cycles. Briefly, LSNBC is similar to LSBCC but without the battery cycle constraint. For this experiment, we consider rWSNs with 10 to 50 nodes with harvesting time $r_i = 5$. We set the battery capacity b_i to 3ϵ of energy, its minimum energy level $b_{i,min}$ to 1ϵ, and maximum energy level $b_{i,max}$ to 3ϵ. Each link weight is randomly fixed to a value between 1 and 5, i.e., $w_{i,j} = [1, 5]$.

LSBCC vs LSNBC on Superframe Length: Figure 4.10 shows that the superframe length $|\mathcal{S}|$ produced by LSBCC is longer than LSNBC. In a rWSN with 10 nodes, LSBCC produces 42 more slots (30.43% longer) as compared to using LSNBC. The results are consistent for other networks, i.e., $|V| = 20$, 30, 40, and 50 nodes. LSBCC produces superframes that are 19.4%, 17.9%, 17.94%, and 17.47% longer than in LSNBC, respectively, with standard deviation values ranging between 56 and 129. The reason for this is that nodes using LSBCC need to wait for their batteries to be fully charged before they can discharge them.

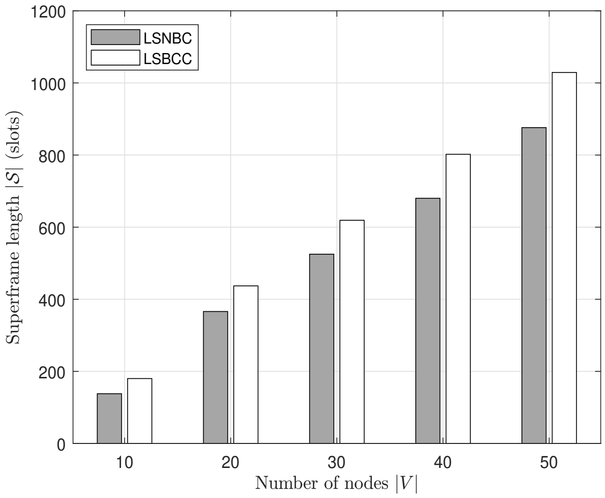

Figure 4.10 LSBCC versus LSNBC in terms of $|\mathcal{S}|$.

LSBCC vs LSNBC on Charge/Discharge Cycles: As shown in Figure 4.11, the number of charge/discharge cycles produced by LSBCC is less than LSNBC. For example, when $|V| = 10$, LSBCC has 64 cycles less than in LSNBC; i.e., 77.11% less. The results are consistent for $|V| = 20, 30, 40$, and 50. More specifically, LSBCC requires 78.86%, 81.03%, 82.62%, and 84.05% fewer cycles than LSNBC, respectively. This is because each battery in LSBCC needs to be charged only when its energy level reaches the minimum. Notice that there is a trade-off between longer link schedules and lesser charge/discharge cycles. For example, for rWSN with $|V| = 30$, the number of cycles is reduced by 81.03% at the expense of a 17.9% longer superframe length $|\mathcal{S}|$. Recall that a battery that has lower number of cycles will have a longer lifetime. In the remaining experiments, we only consider LSBCC.

4.3.1.2 Effect of Harvesting Time

This section investigates the effect of harvesting time r_i on $|\mathcal{S}|$ and charge/discharge cycles. In this simulation, we consider various r_i values, namely $1, 5, 10, 15$, and 20 slots, in a rWSN with 10 to 50 nodes. We set $b_i = 3\epsilon$, $b_{i,min} = 1\epsilon$,

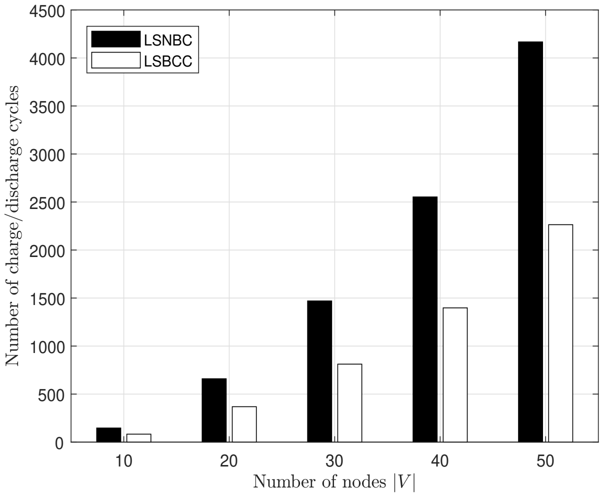

Figure 4.11 LSBCC versus LSNBC on charge/discharge cycles.

$b_{i,max} = 3\epsilon$, and each link has weight $w_{i,j} = 3$.

Effect on Superframe Length: From Figure 4.12, we see that the energy harvesting time of nodes has a significant effect on $|\mathcal{S}|$, i.e., increasing their energy harvesting time results in a longer superframe. Specifically, for a rWSN with 10 nodes, when r_i is increased by 4 slots, i.e., from 1 to 5, $|\mathcal{S}|$ jumps from 68 to 173 slots−an increase of 1.54 times. Similarly, when r_i is increased from 5 to 20 with an interval of 5, i.e., from 5 to 10, 10 to 15, and 15 to 20, $|\mathcal{S}|$ is further increased by 139, 140, and 140 slots, meaning the link schedule increases by 0.8, 0.45, and 0.31 times, respectively. We observe similar trends in rWSN with 20, 30, 40, and 50 nodes. For example, for a rWSN with 50 (100) nodes, when r_i increases from 1 to 20 with an interval of 5, $|\mathcal{S}|$ is increased by 1.33 (1.34), 0.72 (0.72), 0.42 (0.42), 0.3 (0.3) times, respectively. The increase in $|\mathcal{S}|$ is because each battery needs more time to be charged to its maximum level before it can be used to transmit/receive a packet. Also notice that the $|\mathcal{S}|$ for each network size increases almost linearly when r_i is increased from 1 to 20. Further, the rate of increase (in slots) in smaller networks, e.g., $|V| = 10$, is less than that of larger networks, e.g., $|V| = 50$. This is because more nodes mean that more links will need to be scheduled and that more links will have to wait for sufficient energy before they can be activated. Figure 4.12 also shows that the increase in $|\mathcal{S}|$ is more significant in denser networks; see the results for 100 nodes.

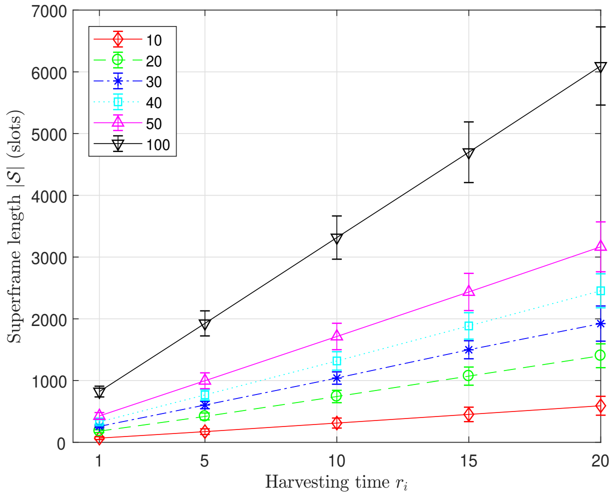

Figure 4.12 Effect of harvesting time r_i on $|\mathcal{S}|$.

Effect on Charge/Discharge Cycles: In our experiment, for $|V| = 10$, 20, 30, 40, and 50, LSBCC produced 86, 377, 821, 1412, and 2276 charge/discharge cycles, respectively, for all values of r_i. The results showed that increasing r_i does not affect the number of battery charge/discharge cycles. This is because charge/discharge cycles depend on the energy level of the battery, not on r_i. Hence, the varying value of r_i does not impact on the cycles.

4.3.1.3 Effect of Battery's DoD

This section studies the effect of Depth of Discharge (DoD) on $|\mathcal{S}|$ and the number of charge/discharge cycles. Recall that DoD corresponds to the percentage of battery capacity that has been discharged. This experiment considers the battery of each node v_i with equal capacity of $b_i = 20\epsilon$, and DoD of 5%, 25%, 50%, 75% and 100%; thus, the usable energy for each discharge cycle is 1ϵ (5% of 20ϵ), 5ϵ,

10ϵ, 15ϵ, and 20ϵ, respectively. For the five DoD values, LSBCC fixes the value of $b_{i,max}$ to 20, and uses five different values of $b_{i,min}$, i.e., 19, 15, 10, 5, and 0, for DoD of 5%, 25%, 50%, 75%, and 100%, respectively. We set $r_i = 5$ and $w_{i,j} = 10$ in a rWSN with 10, 20, 30, 40, and 50 nodes.

Effect on Superframe Length: Figure 4.13 shows that increasing DoD has an insignificant effect on $|\mathcal{S}|$. As an example, when $|V| = 10$ and 20, increasing DoD from 5% to 25% enlarges $|\mathcal{S}|$ by 6.58% (547 to 583) and 0.57% (1394 to 1402), respectively. Similarly, for $|V| = 30$, 40, and 50, there is only a decrease in $|\mathcal{S}|$ of 0.39% (2033 to 2025), 0.12% (2583 to 2580), and 0.12% (3338 to 3334), respectively. Further, when DoD increased from 5% to 100%, the $|\mathcal{S}|$ increased only by 7.03% (583 to 624), 4.21% (1402 to 1461), 1.14% (2025 to 2048), 0.12% (2580 to 2583), and 0.27% (3334 to 3343) for $|V| = 10$, 20, 30, 40, and 50, respectively. This is because the battery's DoD corresponds to the battery's usable capacity, e.g., a battery with a maximum capacity of 20 and DoD of 30% has usable energy of 6, while the same battery with DoD of 80% has a larger usable energy of 16. Thus, increasing a battery's DoD is equivalent to increasing the battery's usable energy or its capacity. Recall that as reported in Section 3.3.3.1 of Chapter 3, battery capacity has an insignificant effect on $|\mathcal{S}|$.

Effect on Charge/Discharge Cycles: As shown in Figure 4.14, increasing DoD decreases the number of charge/discharge cycles. For example, when DoD increased from 5% to 25% in a rWSN with 10 nodes, the number of charge/discharge cycles decreased by 394.78% (from 569 to 115). Similarly, for rWSNs with $|V| = 20$, 30, 40, and 50 nodes, there are 399% (2505 to 502), 399.45% (5469 to 1095), 399.73% (9405 to 1882), and 399.84% (15165 to 3034), respectively, decreases in the number of charge/discharge cycles. In addition, increasing DoD from 25% to 100% reduces the number of charge/discharge cycles from 115 to 29 (a decrease of 74.78%), 502 to 126 (74.9%), 1095 to 274 (74.98%), 1882 to 471

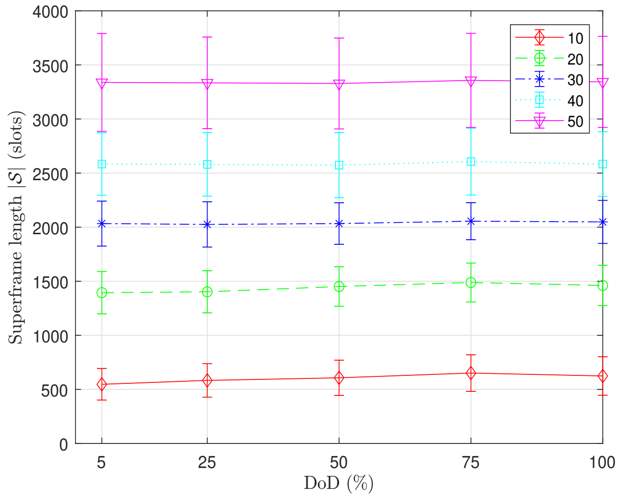

Figure 4.13 Effect of battery's DoD on $|\mathcal{S}|$.

(74.97%), and 3034 to 759 (74.98%) for $|V| = 10$, 20, 30, 40, and 50, respectively. The decrease in the number of charge/discharge cycles when DoD increases is because the battery at each node has more usable energy. Thus, larger DoD values are preferable because the capacity of a battery tends to drop if it has a large number of charge/discharge cycles [98].

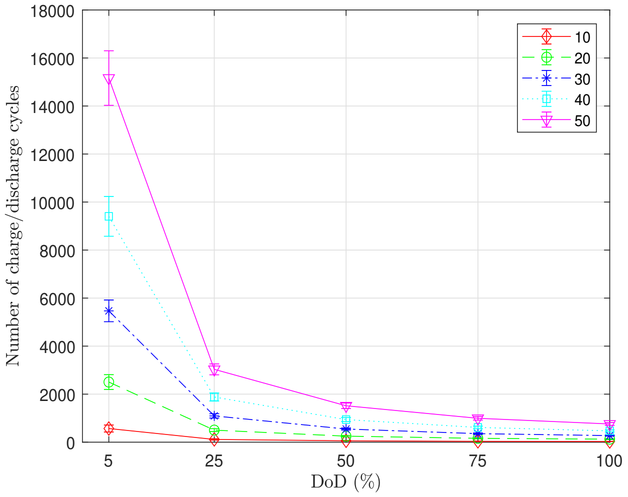

Figure 4.14 Effect of battery's DoD on charge/discharge cycles.

4.3.2 Feasible Solutions of LSME-1

This experiment aims to empirically demonstrate that the **LSME-1**, in general, does not always have a feasible solution, i.e., some links cannot be scheduled for some battery leakage rates $\mu_i > 0$. More specifically, it analyses the impact of parameters r_i, b_i, $b_{i,max}$, η_i, and $\mu_i > 0$ on **LSME-1**'s solution. The experiment considers five cases, i.e., all nodes have: 1) the same parameter values, 2) random parameter values, 3) different values of μ_i, 4) different values of r_i, and 5) different values of pair (r_i, μ_i). Each case considers two different values of link weight, i.e., $w_{i,j} = 1$ and $w_{i,j} = 3$. Table 4.2 summarises the number of scheduled links for each case. The proof of unsatisfiability [96] is used on inequalities (4.28) and (4.29) of each link (i, j) to determine if the link can be scheduled.

Table 4.2 The number of scheduled links (in %).

Various Cases		$\lvert V\rvert$				
		10	**20**	**30**	**40**	**50**
Case (1)	$w_{i,j} = 1$	21.43	7.2	6.59	4.47	3.56
	$w_{i,j} = 3$	8.33	2.4	2.08	1.56	1.19
Case (2)	$w_{i,j} = 1$	78.57	91.20	94.87	97.59	98.68
	$w_{i,j} = 3$	84.52	89.07	94.26	96.81	97.63
Case (3)	$w_{i,j} = 1$	100	100	100	100	100
	$w_{i,j} = 3$	100	100	100	100	100
Case (4)	$w_{i,j} = 1$	100	100	100	100	100
	$w_{i,j} = 3$	100	100	100	100	100
Case (5)	$w_{i,j} = 1$	100	100	99.63	95.53	90.24
	$w_{i,j} = 3$	97.62	100	99.15	95.53	93.18

4.3.2.1 Same Parameter Values

All nodes use the same values of parameters r_i, b_i, $b_{i,max}$, μ_i, and η_i, each of which is selected randomly from sets $\{2, 5\}$, $\{3, 4\}$, $\{3, 4\}$, $\{1, 2.2\} \times 10^{-6}$, and $\{0.9, 1\}$, respectively. For link weight $w_{i,j} = 1$, most links cannot be scheduled, i.e., only 21.43% (6 of 28), 7.2% (9 of 125), 6.59% (18 of 273), 4.47% (21 of 470), and 3.56%

(27 of 758) of the total number of links in networks with 10, 20, 30, 40, and 50 nodes, respectively, can be scheduled; see Case (1) in Table 4.2. Recall that a link (i, j) can be scheduled only if the batteries of its end nodes i and j have an energy level of at least 1ϵ **and** are in the same *discharging* cycle. Alternatively, a link (i, j) cannot be scheduled because one fails to find integer values of m and n that satisfy the expressions (4.28) and (4.29). Similar results are obtained for $w_{i,j} = 3$, where each link needs to be scheduled three times. More specifically, only 8.33% (7 of $3 \times 28 = 84$), 2.4% (9 of 375), 2.08%, 1.56%, and 1.19% of the total link schedules can be generated for networks with 10, 20, 30, 40, and 50 nodes, respectively.

4.3.2.2 Random Parameter Values

Each node is assigned with randomly generated parameters. More specifically, we randomly set $r_i \in \{2, 3, 4, 5\}$, $b_i \in \{3, 4\}$, $b_{i,max} \in \{3, 4\}$, $\mu_i \in \{1, 1.4, 1.8, 2.2\} \times 10^{-6}$, and $\eta_i \in \{0.9, 1\}$. The average number of scheduled links increases when we assign random parameter values at nodes. As an example, Table 4.2 shows that for $w_{i,j} = 3$ and $|V| = 30$, Case (2) produces only 5.74% unscheduled links as compared to 97.92% in Case (1). Notice that the results for $w_{i,j} = 1$ and $w_{i,j} = 3$ for Case (2) are consistent. As an example, for $|V| = 50$ and $w_{i,j} = 1$ ($w_{i,j} = 3$), LSBCC is able to schedule 98.68% (97.63%), i.e., 740 of 758 (2244 of 2274) links.

4.3.2.3 Different Values of μ_i

Each node is set to have the same value of parameters $r_i = 2$, $b_i = 3\epsilon$, $b_{i,min} = 1\epsilon$, $b_{i,max} = 3\epsilon$, and $\eta_i = 1$. Different values of μ_i are assigned to the end nodes of each link as follows: (i) using the *chromatic number* algorithm [99] to compute the minimum number of different values of μ_i for each network; (ii) using the *vertex colouring* algorithm [99] to assign the end nodes of each link with different values of $\mu_i \in \{1, 1.2, 1.4, 1.6, \ldots, 2.4\} \times 10^{-6}$.

As shown in Case (3) of Table 4.2, the average number of scheduled links reaches 100% for all network sizes. However, it does not guarantee the feasibility of **LSME-1**'s link schedule. For example, when $r_i \in \{2, 4\}$ and with other parameters retaining the same value, 99.56% of links can be scheduled for $|V| = 50$ with $w_{i,j} = 3$. Note that this result is not shown in Table 4.2 to reduce space.

4.3.2.4 Different Values of r_i

Each node is assigned with the same value of the following parameters: $b_i = 3\epsilon$, $b_{i,min} = 1\epsilon$, $b_{i,max} = 3\epsilon$, $\mu_i = 1 \times 10^{-6}$, and $\eta_i = 1$. However, the end nodes of each link use different values of harvesting time r_i, each of which is randomly drawn from set $\{2, 3, 4, \ldots, 17\}$. As in Section 4.3.2.3, the chromatic number and vertex colouring algorithms are used to assign different values of r_i to the end nodes of each link. For link weight $w_{i,j} = 1$ and $w_{i,j} = 3$, the total number of links that can be scheduled are 100% for $|V| = 10$, 20, 30, 40, and 50 nodes; see Case (4) in Table 4.2. However, setting the end nodes of each link with a different harvesting time increases the number of scheduled links.

4.3.2.5 Different Values of Pair (r_i, μ_i)

Each node is assigned with the same value of the following parameters: $b_i = 3\epsilon$, $b_{i,min} = 1\epsilon$, $b_{i,max} = 3\epsilon$, and $\eta_i = 1$. However, the end nodes of each link have different values of pair (r_i, μ_i), for harvesting time $r_i \in \{2, 3, 4, 5, 6\}$ and leakage rate $\mu_i \in \{1, 1.2, 1.4, 1.6, \ldots, 2.4\} \times 10^{-6}$. Hence, there are $5 \times 8 = 40$ different $(r_i,\ \mu_i)$ pairs, i.e., $(2, 1 \times 10^{-6})$, $(2, 1.2 \times 10^{-6})$, $(2, 1.4 \times 10^{-6})$, $(2, 1.6 \times 10^{-6})$, $\ldots$, $(2, 2.4 \times 10^{-6})$, $(3, 1 \times 10^{-6})$, $\ldots$, $(6, 2.4 \times 10^{-6})$. As in Section 4.3.2.3, the chromatic number and vertex colouring algorithms [99] are used to assign different pairs of (r_i, μ_i) to the end nodes of each link. As shown in Case (5) of Table 4.2, the average number of links that can be scheduled is 100%, only for networks with 10 ($w_{i,j} = 1$) and 20 nodes. Table 4.2 shows that, for $w_{i,j} = 1$ ($w_{i,j} = 3$), LSBCC is able to schedule 99.63% (99.15%), 95.53% (95.53%), and 90.24% (93.18%) of the links in networks with 30, 40, and 50 nodes, respectively.

The results in Table 4.2 show that except for Case (2), the percentage of links that can be scheduled decreased for networks with a larger number of nodes. This is because larger networks have more links, and hence they have a higher probability that links will have end nodes that do not have the same discharging cycle. Thus, these links cannot be scheduled. Further, assigning the end nodes of each link with different values of μ_i, r_i, or pair (r_i, μ_i), i.e., in Cases (3), (4), and (5), respectively, tends to reduce the number of unscheduled links.

4.3.3 Leak-Free *versus* Leaky Battery

This section aims to compare the impact of the battery cycle constraint on networks where nodes have a leak-free battery and on those where nodes have a battery that leaks. Firstly, it presents the results of a simulation that evaluates the effect of the battery cycle constraint on the link schedule. The results compare the superframe length $|\mathcal{S}|$ generated by LSBCC against LSNBC. Secondly, it aims to see which constraint, *charging* or *discharging*, has a larger effect on the schedule length. Recall that a battery charging constraint forces the battery to be charged only when its capacity reaches the minimum level. On the other hand, a battery discharging constraint imposes a condition on the battery that it can be used only when its energy level reaches maximum. Here, we compare the superframe length $|\mathcal{S}|$ generated by two versions of LSBCC: (i) LSCC that considers only charging constraint, and (ii) LSDC that enforces only discharging constraint. Finally, it provides the results of a simulation that examines the effect of the battery cycle constraint on the number of charge/discharge cycles. Each simulation considers 10 to 50 nodes and uses the following parameter values: $b_i = 3\epsilon$, $b_{i,max} = 3\epsilon$, $b_{i,min} = 1\epsilon$, and $\eta_i = 1$. Note that for all simulations, the parameters r_i and μ_i are set to values that ensure there is a feasible link schedule.

4.3.3.1 LSBCC *versus* LSNBC

In this simulation, we set $r_i \in \{2, 3, 4, 5, 6\}$ and $w_{i,j} = 3$. The leakage rate μ_i of batteries is set to a value in $\{1, 1.2, 1.4, 1.6, 1.8\} \times 10^{-6}$. We first evaluate the effect of using the energy flush method, discussed in Section 4.2.3, on the superframe length $|\mathcal{S}|$. Let LSBCC^f (LSBCC^{nf}) denote LSBCC that does (does not) use energy flush. Then, we compare the $|\mathcal{S}|$ produced by LSBCC^f against that by LSNBC.

Table 4.3 Superframe length $|\mathcal{S}|$ of LSBCC^f and LSBCC^{nf}.

$\lvert \boldsymbol{V} \rvert$	**LSBCC^f**	**LSBCC^{nf}**
10	327	13336041
20	841	38888681
30	1247	54636058
40	1618	116185914
50	2106	149635876

As shown in Table 4.3, all superframes generated by LSBCC^{nf} are significantly longer than LSBCC^f. For example, in networks with $|V| = 10$ nodes, LSBCC^{nf} produced 13335714 more slots (40782 times longer) as compared to those generated by LSBCC^f. Similarly, LSBCC^{nf} generated 46240, 43813, 71807, and 71051 times longer superframes than those by LSBCC^f in networks with $|V| = 20$, 30, 40, and 50 nodes, respectively. As explained in Section 4.2.3, discharging a battery when its energy level is less than $b_{i,min} + 1$ takes vast number of slots when its leakage rate is very small, e.g., 10^{-6}. In the remaining simulations, we use only LSBCC that utilises the energy flush method.

Figure 4.15 shows that the superframe length $|\mathcal{S}|$ produced by LSBCC is longer than LSNBC. As an example, for networks where nodes have a leak-free battery and $|V| = 10$ nodes, LSBCC produced 33 more slots (27.73% longer) as compared to when using LSNBC. The results are consistent for other networks, i.e., $|V| = 20$, 30, 40, and 50 nodes. LSBCC produced superframes that are 24.77%, 25.82%, 28.43%, and 28.36% longer than in LSNBC, respectively, with standard deviation values ranging between 63 and 143. For rWSNs with a battery that leaks, LSBCC generated 206 more slots (1.7 times longer) than LSNBC in $|V| = 10$. Similarly, LSBCC produced 1.43, 1.37, 1.35, and 1.35 times longer superframes than LSNBC when there are $|V| = 20$, 30, 40, and 50 nodes, respectively, with standard deviation values ranging between 61 and 298. This is because LSBCC needs to wait for the battery at each node to be charged (discharged) to its maximum (minimum) level before it can be discharged (charged). These results showed that the battery cycle constraint of each battery results in a negative impact on the schedule length. Note that this experiment produced similar results for link weight $w_{i,j} = 1$; those results are not presented to save space.

Figure 4.15 also showed that networks that use leaky batteries have longer link schedules than those that use leak-free batteries. Specifically, LSNBC with $|V| = 10, 20, 30, 40,$ and 50 nodes produced superframes that are 1.68, 5.81, 7.79, 10.06, and 10.48 times longer, respectively, for networks with a leaky battery as compared to when they use a leak-free battery. This is because with leakage, a battery needs a longer time to accumulate sufficient energy to transmit/receive a packet. The negative impact of using a leaky battery on the schedule length is more apparent in LSBCC. More specifically, for $|V| = 10$ nodes, LSBCC produced 175 more slots (1.15 times longer) when the battery of the nodes leak. Similarly for networks with 20, 30, 40, and 50 nodes, LSBCC generated superframes that are 1.06, 1.03, 1.01, and 1.02 times longer, respectively, for networks with a battery that leaks as compared to when they use a leak-free battery. This is reasonable because a battery that leaks will mean a node will take longer time to be charged to its maximum level and will have a shorter discharging time period than a leak-free battery.

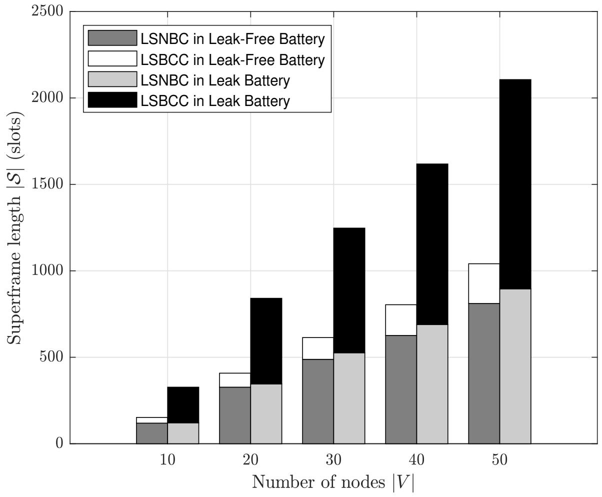

Figure 4.15 LSBCC versus LSNBC in networks where each node has a leak-free or a leaky battery in terms of $|\mathcal{S}|$.

4.3.3.2 Charging *versus* Discharging Constraint

Figure 4.16 shows that in networks with batteries that leak, LSCC generates more slots than LSDC, which means the charging constraint has a greater effect on schedule length than the discharging constraint. More specifically, LSCC produces a superframe 0.67 (111 more slots), 0.65, 0.47, 0.41, and 0.77 times longer than LSDC for networks with 10, 20, 30, 40, and 50 nodes, respectively, with standard deviation values ranging between 52 and 1190. This is because for LSCC, the battery of each node can only be charged if its capacity has reached the minimum level, while LSDC allows the battery to be charged at anytime. In contrast, for a leak-free battery, LSDC produces schedules with more slots than LSCC. For example, LSDC generates a superframe 0.32 (32 more slots), 0.82, 0.92, 0.97, and 1.04 times longer than LSCC for networks with 10, 20, 30, 40, and 50 nodes, respectively, with standard deviation values ranging between 31 and 144. This is because when the battery of a node is leak-free, energy usage is only due to packet transmission/reception. That is, a battery does not reduce to its minimum level from energy loss due to leaking.

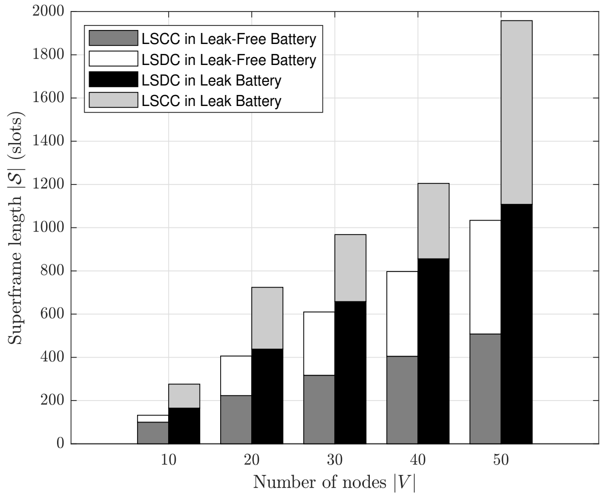

Figure 4.16 LSCC versus LSDC in networks where each node has a leak-free or a leaky battery in terms of $|\mathcal{S}|$.

4.3.3.3 Charge/Discharge Cycles

In this simulation, we set $r_i = 5$ and $w_{i,j} = [1, 5]$; in addition, the leakage rate of the batteries is set to $\mu_i = \{1, 1.2, 1.4, 1.6, \ldots, 2.4\} \times 10^{-6}$. Figure 4.17 shows that the number of charge/discharge cycles produced by LSBCC is significantly less than that for LSNBC, regardless of battery type. As an example, when nodes have a leak-free battery and there are $|V| = 10$, 20, 30, 40, and 50 nodes, LSBCC generates 43.54% or 64 fewer cycles, 44.09%, 44.76%, 45.24%, 45.67% fewer cycles, respectively, than LSNBC, with standard deviation values ranging between 22 and 303. Similarly, when the battery of a node leaks, LSBCC has 45.89%, 46.15%, 46.73%, 47.41%, and 47.11% fewer cycles than LSNBC for 10,

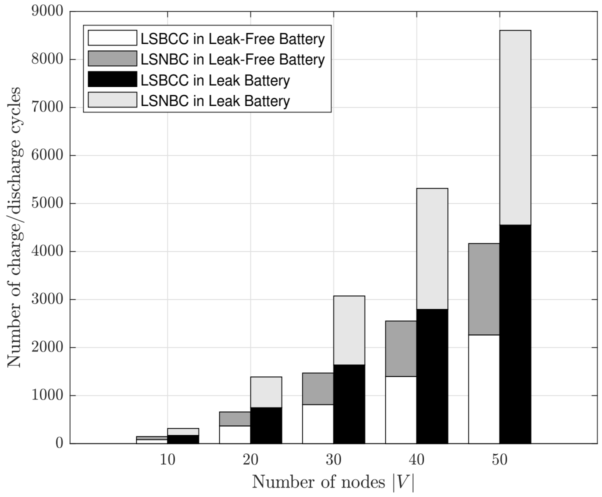

Figure 4.17 LSBCC versus LSNBC in networks where each node has a leak-free or a leaky battery in terms of the number of charge/discharge cycles.

20, 30, 40, and 50 nodes, respectively, with standard deviation values ranging between 66 and 602. Due to the battery cycle constraint, each charge (discharge) occurs only when the battery has reached its minimum (maximum) energy level in LSBCC. On the other hand, when using LSNBC, a node's battery can be charged (discharged) at any slot when it is (is not) used.

Figure 4.17 also shows that the number of charge/discharge cycles for nodes that have a leak-free battery is less than for the case when the battery leaks, for both LSBCC and LSNBC. For example, for $|V| = 10$ nodes, LSBCC requires 51.46% fewer cycles when nodes are equipped with a leak-free battery than when they have a battery that leaks. The results are consistent for networks with 20, 30, 40, and 50 nodes. More specifically, for the leak-free-battery case, there are 50.67%, 50.43%, 49.98%, and 50.25% fewer cycles than when nodes have a battery that leaks. Similarly, LSNBC and nodes with a leak-free battery result in 53.48%, 52.48%, 52.2%, 51.97%, and 51.57% fewer cycles than when they use a leaky battery for $|V| = 10$, 20, 30, 40, and 50 nodes, respectively. This is because a leak-free battery has lesser charging time interval than one that leaks.

4.3.4 Effectiveness of LSBCC

To analyse the performance of LSBCC, we compute the ratio $\mathcal{R} \geq 1$ between its generated $|\mathcal{S}|$ and the optimal bound as per Propositions 4.1, 4.2, and 4.3 for *Line*, *BTree*, and *Grid*, respectively. We set $w_{i,j} = 3$, $b_i = 3$, $b_{i,min} = 0$, $b_{i,max} = 3$, $\hat{b}_i = 3$, and $r_i = 1, 5, 10, 15, 20$. Recall that $\hat{b}_i = b_{i,max} - b_{i,min}$.

As shown in Figure 4.18, LSBCC always produces the optimal superframe for *Line*, for any values of r_i. On the other hand, for $r_i = 1$, *BTree* and *Grid* produce an average of $\mathcal{R} = 1.3$ and $\mathcal{R} = 1.39$, respectively. However, LSBCC has a better performance for larger values of r_i. Specifically, when $r_i \geq 5$, LSBCC has an average performance ratio $\mathcal{R}$ of 1.27 and 1.29 for *BTree* and *Grid*, meaning the superframe lengths are 27% and 29%, respectively, away from the optimal value for rWSNs with 10 to 100 nodes.

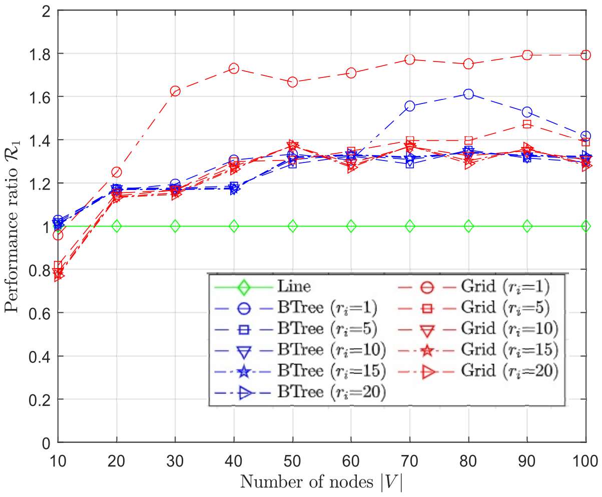

Figure 4.18 The performance of LSBCC in fixed topologies with a various number of nodes for $\mu_i = 0$ and $\eta_i = 1$.

4.4 Chapter Summary

This chapter addressed a new link scheduling problem, called **LSME-1**. It considered the memory effect that degrades the lifetime of a node's battery. The problem was challenging as nodes have a limited battery capacity, different harvesting times, and leakage rates. As a solution, this chapter proposed an algorithm called LSBCC. It also showed, analytically, the impact of enforcing a battery cycle constraint. One main finding was that if nodes' batteries have a non-negative leakage rate, i.e., $\mu_i > 0$, the batteries at some end nodes may never be in the same discharging cycle. Thus, the link of such end nodes cannot be scheduled. This finding was supported by our extensive simulations, whereby the number of unscheduled links can be up to 98.81% of the total number of links in the networks. When all links can be scheduled, enforcing the battery cycle constraint increased the superframe length by up to 1.71 times. However, it reduced the number of charge/discharge cycles by up to 47.41% as compared to cases where nodes do not have the battery cycle constraint. Hence, it can prolong the battery's lifetime. Further, LSBCC in networks with leak-free batteries produced up to 0.54 (0.52) times shorter schedules (fewer charge/discharge cycles) than those with leaky batteries. Our simulations also showed that an increase in energy harvesting time, linearly, increases link schedules. LSBCC produced the optimal superframe length for *Line*, and up to 1.61 and 1.79 times of the theoretical superframe length bounds for *BTree* and *Grid*, respectively, for $r_i \geq 1$. In Chapter 5, we consider the use of a dual-battery system in rWSNs to reduce the schedule length.

Chapter 5

Link Scheduling in rWSNs with a Dual-Battery System

This chapter considers the problem of activating links in an rWSN. It considers: (i) the energy harvesting time of nodes, (ii) the battery cycle constraint that accounts for memory effect, and (iii) nodes with a dual-battery system. It outlines a greedy algorithm that schedules links according to the earliest time in which a battery at the end nodes of each link can be discharged or is full. Figure 5.1 illustrates the dual-battery system. As shown in the figure, while the node is using Battery 1, Battery 2 can be recharged. The node switches the role of its batteries when one battery is fully charged and the other is fully discharged [37]; see the dashed arrows.

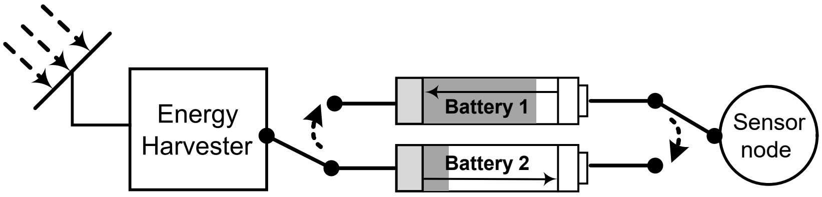

Figure 5.1 A sensor node with a dual-battery system.

To explain the link scheduling problem, consider Figure 5.2, where links (v_1, v_2), (v_1, v_3), (v_1, v_4), and (v_1, v_5) interfere with each other and hence cannot be activated concurrently. We use the HSU battery usage protocol [51]. Recall that in HSU any harvested energy must be stored in a battery before use. For example, node v_1 needs to wait for three timeslots to accumulate one unit of energy, denoted by $v_1|3$, before the energy can be used, no earlier than slot 4. Specifically, we consider the following three scenarios. First, consider Figure 5.2a, where each node has one battery with a capacity of four units and without battery cycle constraint. Node v_1 needs to wait until v_2 can use one unit of energy at time $t = 7 + 1 = 8$ before it transmits a packet to v_2. Its second packet, which is destined for v_3, is transmitted at time $t = 8 + 1 = 9$; this is the earliest time v_3 has sufficient energy. Further, its third and fourth packets can be transmitted no earlier than time 12 and 15, respectively. As a result, the schedule length is 15.

Next, consider Figure 5.2b where each node has one battery with the same capacity as in Figure 5.2a. However, each battery has the battery cycle constraint. Thus, v_1 has to wait until slot $t = 3 \times 4 + 1 = 13$ to fully recharge and use its battery. However, at this time, it cannot transmit because its neighbours' battery is yet to be fully recharged. That is, nodes v_2, v_3, v_4, and v_5 have to wait until slots $t = 7 \times 4 + 1 = 29$, $t = 33$, $t = 37$, and $t = 41$, respectively, before their batteries can be discharged. Thus, the example depicted in Figure 5.2b has a longer schedule, i.e., 41, than that in Figure 5.2a.

Lastly, consider Figure 5.2c, where each node has two batteries with the battery cycle constraint. The total energy available at each node is the same as in Figure 5.2b. Node v_1 needs six slots to fully charge its first battery. Its second battery starts charging after the first battery is fully charged. Therefore, at slot $t = 6 + 6 = 12$, the second battery is full and can be discharged at slot 13. Node v_1 needs to wait until slot $t = 6 + 1 = 7$ before its first battery can be used to transmit a packet. However, it has to wait for its neighbours to fully charge their first batteries. Note that nodes v_2, v_3, v_4, and v_5 require 15, 17, 19, and 21 slots, respectively before their first battery can be discharged. Now, node v_1 can transmit a packet to node v_2, v_3, v_4, and v_5 at slots $t = 15$, $t = 17$, $t = 19$, and $t = 21$, respectively. Thus, the schedule length is 21 versus 41 in Figure 5.2b. This example shows the benefit of employing a dual-battery system at nodes. Note that at $t = 19$ and $t = 21$, node v_1 uses its second battery.

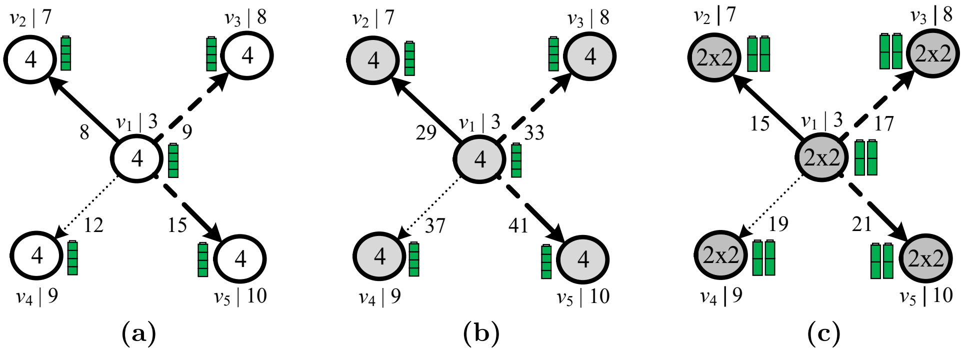

Figure 5.2 An example for (a) single battery without battery cycle constraint, (b) single battery with battery cycle constraint, (c) dual battery with battery cycle constraint.

The layout of this chapter is as follows. Section 5.1 describes the network model and problem. Section 5.2 describes our LSDBS algorithm. Section 5.3 uses simulation to evaluate our proposed algorithm. Finally, Section 5.4 summarises the chapter. Note that the work of this chapter will be presented in [100].

5.1 Preliminaries

Section 5.1.1 discusses our rWSN model and introduces key notations used in this chapter. Section 5.1.2 formally describes the problem at hand.

5.1.1 Network Model

Similar to Chapter 4, in this chapter, nodes use the HSU [51] battery usage protocol. A node v_i is equipped with a harvester and two rechargeable batteries. Let $r_i \geq 1$ (in slots) be the *harvesting time* or the total number of slots required by a node v_i to accumulate 1ϵ of energy. Thus, the harvesting rate of a node is $\frac{\epsilon}{r_i}$ per time slot. Further, we denote the dual battery of a node v_i as B_i^z, for $z \in \{1, 2\}$. For each pair of batteries (B_i^1, B_i^2) at a node v_i, we call the first (second) battery as the *active (reserve)* battery. Let b_i^z (in unit ϵ) be the capacity of battery $z \in \{1, 2\}$ at a node v_i. We assume both batteries have equal capacity, i.e., $b_i^1 = b_i^2$. Further, the capacity of each battery is sufficient to transmit/receive one packet, i.e., $b_i^z \geq 1\epsilon$.

Each battery follows the *battery cycle* constraint. Recall that this constraint requires each battery of a node v_i to be (i) charged to its maximum capacity $b_{i,max}$ before it can be used, and (ii) discharged to its minimum capacity $b_{i,min}$ before it can be recharged. Thus, each battery's *usable* energy is $\hat{b}_i^z = b_{i,max} - b_{i,min}$. Further, each battery can be in one of three modes: (i) *charging (C)*, (ii) *discharging (D)*, or (iii) *idle (I)*, i.e., when the battery is neither being charged nor discharged. Without loss of generality, we assume each battery has an initial energy level of $b_{i,min}$, where $b_{i,min} < b_{i,max}$. Further, we assume $b_{i,min}$ and $b_{i,max}$ are integer values.

We use $\tilde{t}_i^{z+}$ and $\tilde{t}_i^{z-}$ to denote the start and end charging time, respectively, of battery z at a node v_i. Similarly, t_i^{z+} and t_i^{z-} denote the start and end discharging time, respectively. Following the HSU model, we have $t_i^{z+} = \tilde{t}_i^{z-} + 1$ and $\tilde{t}_i^{z+} = t_i^{z-} + 1$. However, only one of the batteries at a node v_i can be charged or discharged at any one time t. Battery B_i^2 will start charging when B_i^1 stops charging. Hence, the start charging time of B_i^2 is equal to the end charging time of B_i^1, i.e., $\tilde{t}_i^{2+} = \tilde{t}_i^{1-}$. The active battery at a node v_i becomes the reserve battery, and vice versa, when the energy level of battery B_i^1 reaches $b_{i,min}$ after packet transmission/reception and that of B_i^2 is fully charged. We assume the time to switch the role of batteries is negligible.

Let $\tilde{\tau}_i^z$ and τ_i^z be the *charging time interval* and *discharging time interval*, respectively, of battery z at a node v_i, which are computed as $\tilde{\tau}_i^z = \tilde{t}_i^{z-} - \tilde{t}_i^{z+}$ and $\tau_i^z = t_i^{z-} - t_i^{z+}$. In other words, B_i^z is being charged during time interval $\tilde{\tau}_i^z$ and discharged during time interval τ_i^z. The value of $\tilde{\tau}_i^z$ is dependent on r_i and $b_{i,max}$, while the length of τ_i^z is affected by $b_{i,min}$ and the number of times the batteries are used in the cycle. We note that the time interval $\tilde{\tau}_i^z$ has equal length in any cycles because r_i and $b_{i,max}$ are constant over all cycles. In contrast, the value of τ_i^z may vary for different cycles due to different energy usage between cycles.

Let $\tilde{b}_{i,t}^z$ and $b_{i,t}^z$ (in unit ϵ) be the amount of energy stored in battery z at a node v_i at the start of slot t for a charging and discharging cycle, respectively. Thus, we have $\tilde{b}_{i,\tilde{t}_i^{z-}}^z = b_{i,max}$ and $b_{i,t_i^{z-}}^z = b_{i,min}$. The battery level of a node v_i at the beginning of each *charging* cycle is given as $\tilde{b}_{i,\tilde{t}_i^{z+}}^z = b_{i,min}$. For each *discharging* cycle, it is $b_{i,t_i^{z+}}^z = b_{i,max}$.

Let T_i be the earliest timeslot a node v_i can transmit/receive a packet, i.e., when B_i^1 can be used to power v_i. The earliest time in which link $l_{i,j}$ can be scheduled is $t_{i,j} = \mathbf{max}(T_i, T_j)$. For each node v_i, we initialise $T_i = \tilde{\tau}_i^1 + 1$. Battery B_i^1 is initially in idle mode and it takes $\tilde{\tau}_i^1$ slots to reach level $b_{i,max}$. Following the HSU protocol, the energy can be used only at one slot later. It is updated when the battery is discharged to transmit/receive a packet.

As an example, Figure 5.3a shows the value of $b_{i,min}$, $b_{i,max}$, b_i^z, and r_i for each node v_i as well as the weight of each link $l_{i,j}$. One can compute the charging time interval for each battery to obtain $\tilde{\tau}_1^z = 4$, $\tilde{\tau}_2^z = 18$, $\tilde{\tau}_3^z = 14$ and $\tilde{\tau}_4^z = 12$; see Section 5.2 for details. Thus, we have $T_1 = \tilde{\tau}_1^1 + 1 = 5$, $T_2 = 19$, $T_3 = 15$, and

$T_4 = 13$. Therefore, the earliest time each link $l_{i,j}$ can be scheduled is computed as $t_{1,2} = \mathbf{max}(5, 19) = 19$, $t_{2,4} = 19$, and $t_{4,3} = 15$. Figure 5.3b shows the conflict graph C_G for the example of the rWSN depicted in Figure 5.3a.

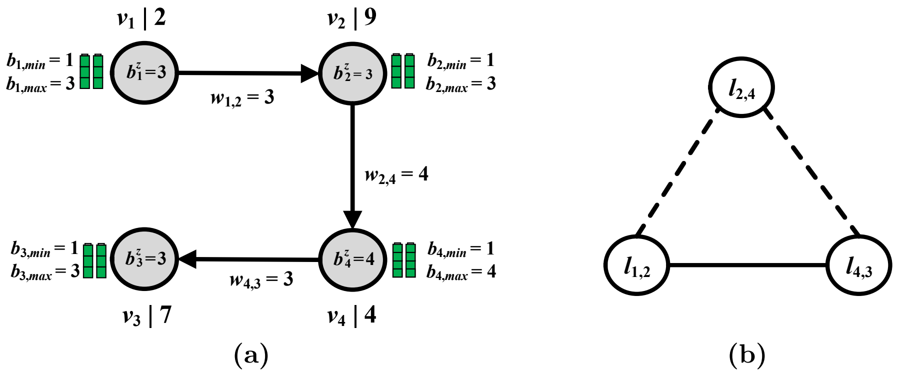

Figure 5.3 A rWSN model: (a) graph G, and its (b) conflict graph C_G.

5.1.2 Problem Statement

Our problem, called **Link Scheduling with Memory Effect-2 (LSME-2)**, is to generate the TDMA link schedule $\mathcal{S}$ with the minimum $|\mathcal{S}|$ for a rWSN such that: (i) each node v_i is equipped with a dual-battery system, (ii) each battery at a node $v_i \in V$ satisfies the *battery cycle* constraint, (iii) each link $l_{ij} \in E$ can be scheduled at time slot t only if a battery of its end nodes is in discharging mode, and (iv) each link $l_{i,j} \in E$ is scheduled at least $w_{i,j}$ times in $\mathcal{S}$.

To illustrate the effect of link scheduling on $|\mathcal{S}|$, consider the example in Figure 5.3. Figure 5.4a shows one *feasible* link schedule with 88 slots. A schedule is *feasible* if it satisfies constraints (i), (ii), (iii), and (iv). The figure shows only non-empty slots, i.e., each empty slot is represented as "…". Figure 5.4b shows a shorter *feasible* schedule of $|\mathcal{S}| = 73$ slots. Our problem aims to generate the shortest *feasible* schedule $\mathcal{S}$. Note that link scheduling in general is known as NP-hard [43]. We remark that our problem is the general version of the link scheduling problem that assumes nodes have no energy constraint. Thus, it is still NP-hard.

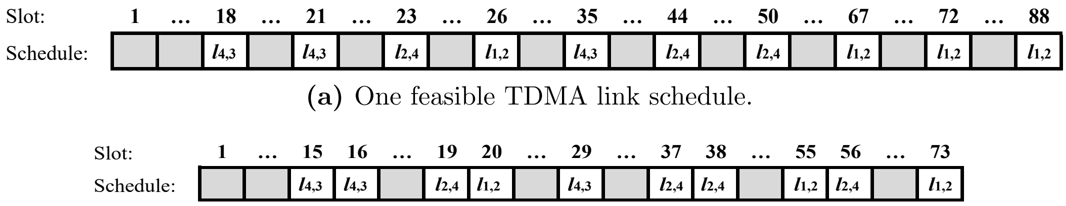
Slot:
1 … 18 … 21 … 23 … 26 … 35 … 44 … 50 … 67 … 72 … 88
Schedule:
$l_{4,3}$ $l_{4,3}$ $l_{2,4}$ $l_{1,2}$ $l_{4,3}$ $l_{2,4}$ $l_{2,4}$ $l_{1,2}$ $l_{1,2}$ $l_{1,2}$
Slot:
1 … 15 16 … 19 20 … 29 … 37 38 … 55 56 … 73
Schedule:
$l_{4,3}$ $l_{4,3}$ $l_{2,4}$ $l_{1,2}$ $l_{4,3}$ $l_{2,4}$ $l_{2,4}$ $l_{1,2}$ $l_{2,4}$ $l_{1,2}$

(a) One feasible TDMA link schedule.

(b) The optimal TDMA link schedule.

Figure 5.4 TDMA link schedules for the rWSN depicted in Figure 5.3. Gray coloured slots show no packet transmissions/receptions.

5.2 Solution

We first describe all possible states of batteries (B_i^1, B_i^2) for a node v_i, and the state transitions of batteries. Then, we present three propositions relied upon by our greedy algorithm.

5.2.1 Battery States and Transitions

There are seven possible battery states at each node v_i. Each state S_k, for $k = 1, 2, \ldots, 7$, takes into account: (i) four of six possible combinations of battery mode, i.e., (I, I), (C, I), (D, I), and (D, C); note that the combination (C, C) and (D, D) are not possible because each node cannot charge or discharge two batteries at the same time, and (ii) the energy level of each battery, i.e., $b_{i,t}^z = b_{i,min}$, $b_{i,t}^z = b_{i,max}$, $b_{i,t}^z > b_{i,min}$, and $b_{i,t}^z < b_{i,max}$. Formally, a state k of batteries (B_i^1, B_i^2) at node v_i is defined as $S_k = (\{\text{mode, energy level}\}, \{\text{mode, energy level}\})$. Table 5.1 shows seven states, i.e., $S_1 = (\{I, b_{i,t}^1 = b_{i,min}\}, \{I, b_{i,t}^2 = b_{i,min}\})$, $S_2 = (\{C, b_{i,t}^1 > b_{i,min}\}, \{I, b_{i,t}^2 = b_{i,min}\})$, $S_3 = (\{I, b_{i,t}^1 = b_{i,max}\}, \{I, b_{i,t}^2 = b_{i,min}\})$, $S_4 = (\{D, b_{i,t}^1 < b_{i,max}\}, \{C, b_{i,t}^2 > b_{i,min}\})$, $S_5 = (\{D, b_{i,t}^1 < b_{i,max}\}, \{I, b_{i,t}^2 = b_{i,max}\})$, $S_6 = (\{I, b_{i,t}^1 = b_{i,max}\}, \{C, b_{i,t}^2 > b_{i,min}\})$, and $S_7 = (\{I, b_{i,t}^1 = b_{i,max}\}, \{I, b_{i,t}^2 = b_{i,max}\})$.

Table 5.1 also shows 17 possible transitions from state S_j to S_k, denoted by $S_j \rightarrow S_k$, between slot t and $t+1$. There is only one transition from S_1, i.e., $S_1 \rightarrow S_2$, because the harvester at node v_i can charge only one battery at a time. Recall that S_1 is the initial state, i.e., the state occurs only at time $t = 0$. There are two alternative transitions from S_2: (i) $S_2 \rightarrow S_2$; if battery B_i^1 is not fully charged, or (ii) $S_2 \rightarrow S_3$; if B_i^1 is fully charged. Similarly, there are two possible transitions from S_3, i.e., $S_3 \rightarrow S_4$ or $S_3 \rightarrow S_6$. The first transition occurs when battery B_i^1 is used to transmit/receive a packet and battery B_i^2 is in charging mode, while the second transition is due to no packet transmission/reception. The followings are four possible transitions from S_4: (i) $S_4 \rightarrow S_2$; when battery B_i^1 becomes empty and battery B_i^2 starts charging, (ii) $S_4 \rightarrow S_3$; when battery B_i^1 becomes empty and battery B_i^2 becomes full, (iii) $S_4 \rightarrow S_5$; when battery B_i^1 is not yet empty and battery B_i^2 is fully charged, or (iv) $S_4 \rightarrow S_4$; when battery B_i^1 is not yet empty and battery B_i^2 is not fully charged. State S_5 can either go to S_3 or remains at S_5. Transition $S_5 \rightarrow S_3$ is when battery B_i^1 becomes empty, while transition $S_5 \rightarrow S_5$ is when battery B_i^1 is not yet empty. Transition $S_6 \rightarrow S_4$ ($S_6 \rightarrow S_5$) occurs when battery B_i^1 becomes empty and battery B_i^2 is fully charged (battery B_i^1 is used to transmit/receive a packet and battery B_i^2 is fully charged). Further, we have $S_6 \rightarrow S_6$ ($S_6 \rightarrow S_7$) when there is no packet transmission/reception and battery B_i^2 is not fully charged yet (there is no packet transmission/reception and battery B_i^2 is fully charged). Finally, transition $S_7 \rightarrow S_5$ is when battery B_i^1 is used to transmit/receive a packet, while $S_7 \rightarrow S_7$ occurs when there is no packet transmission/reception.

Table 5.1 States and transitions of batteries at each node v_i.

Possible States		**Possible Transitions**	
State	(B_i^1, B_i^2)	**Transition**	**Explanation**
S_1	▯▯	$S_1 \rightarrow S_2$	B_i^1 starts charging, B_i^2 is idle.
S_2	◫▯	$S_2 \rightarrow S_2$	B_i^1 is being charged; it is not full.
		$S_2 \rightarrow S_3$	B_i^1 is being charged; it is full.
S_3	▮▯	$S_3 \rightarrow S_4$	B_i^1 is used, B_i^2 starts charging.
		$S_3 \rightarrow S_6$	B_i^1 is not used, B_i^2 starts charging
S_4	▣◫	$S_4 \rightarrow S_2$	B_i^1 is empty, B_i^2 is not full; swap B_i^1 and B_i^2.
		$S_4 \rightarrow S_3$	B_i^1 is empty, B_i^2 is full; swap B_i^1 and B_i^2.
		$S_4 \rightarrow S_4$	B_i^1 is not empty, B_i^2 is not full.
		$S_4 \rightarrow S_5$	B_i^1 is not empty, B_i^2 is full.
S_5	▣▮	$S_5 \rightarrow S_3$	B_i^1 is empty; swap B_i^1 and B_i^2.
		$S_5 \rightarrow S_5$	B_i^1 is not empty.
S_6	▮◫	$S_6 \rightarrow S_4$	B_i^1 is used, B_i^2 is not full.
		$S_6 \rightarrow S_5$	B_i^1 is used, B_i^2 is full.
		$S_6 \rightarrow S_6$	B_i^1 is not used, B_i^2 is not full.
		$S_6 \rightarrow S_7$	B_i^1 is not used, B_i^2 is full.
S_7	▮▮	$S_7 \rightarrow S_5$	B_i^1 is used.
		$S_7 \rightarrow S_7$	B_i^1 is not used.

▯ : Idle ($b_{i,t}^z = b_{i,min}$) ◫ : Charging ($b_{i,t}^z > b_{i,min}$)
▮ : Idle ($b_{i,t}^z = b_{i,max}$) ▣ : Discharging ($b_{i,t}^z < b_{i,max}$)

5.2.2 Key Properties

Propositions 5.1 and *5.2* are concerned with a battery in charging mode, while *Proposition 5.3* is for a battery in discharging mode.

Proposition 5.1. *The energy level of each battery $z \in \{1, 2\}$, in charging mode at a node v_i at timeslot t, for $\tilde{t}_i^{z+} \leq t \leq \tilde{t}_i^{z-}$, is*

$$\tilde{b}_{i,t}^z = \mathbf{min}(b_{i,max}, b_{i,min} + (t - \tilde{t}_i^{z+})/r_i) \tag{5.1}$$

Proof. The maximum amount of energy that can be harvested from $\tilde{t}_i^{z+}$ to t is $\frac{t - \tilde{t}_i^{z+}}{r_i}$. However, $\tilde{b}_{i,t}^z$ is bounded by the upper limit of battery capacity $b_{i,max}$, which implies $\tilde{b}_{i,t}^z \leq b_{i,max}$. □

Proposition 5.2 computes the number of slots required by a node v_i to charge a battery B_i^z from $b_{i,min}$ to $b_{i,max}$, for $z \in \{1, 2\}$.

Proposition 5.2. *The charging time interval of the battery B_i^z at a node v_i is computed as*

$$\tilde{\tau}_i^z = r_i(b_{i,max} - b_{i,min}) \tag{5.2}$$

Proof. We set $t = \tilde{t}_i^{z-}$ in *Proposition 5.1* to generate the maximum energy level of the battery, i.e., $b_{i,max}$. We have $b_{i,max} = b_{i,min} + \tilde{\tau_i}^z / r_i$. Thus, $\tilde{\tau}_i^z$ is as shown in *Proposition 5.2*. □

Proposition 5.3 computes the next earliest time in which a node v_i can transmit/receive another packet.

Proposition 5.3. *Let $t_i \geq \tilde{\tau}_i^1 + 1$ be the time in which a node v_i last transmitted/received a packet. The next earliest timeslot before a node v_i can use its battery again to transmit/receive a packet is*

$$T_i = t_i + \sigma_{i,t_i} \times r_i \times (b_{i,max} - b_{i,t_i}^2) + 1 \tag{5.3}$$

Proof. The next earliest time T_i depends on the remaining energy level of the active battery B_i^1 and the reserve battery B_i^2 at a node v_i at time t_i, i.e., b_{i,t_i}^1 and b_{i,t_i}^2, respectively. We consider two cases: (i) $b_{i,t_i}^1 = b_{i,min}$, and (ii) $b_{i,t_i}^1 > b_{i,min}$. For case (i), the active battery B_i^1 needs to be recharged and a node v_i checks the energy level of the reserve battery B_i^2 at time t_i, i.e., b_{i,t_i}^2. We consider two sub-cases: (i.a) $b_{i,t_i}^2 = b_{i,max}$, and (i.b) $b_{i,t_i}^2 < b_{i,max}$. In both sub-cases, we use Eq. (5.1) to compute b_{i,t_i}^2. For sub-case (i.a), a node v_i switches the role of its batteries from reserve (active) to active (reserve) since the reserve battery B_i^2 is fully charged. Thus, the next earliest time a node v_i can transmit/receive a packet is in the next slot, i.e., $T_i = t_i + 1$. Thus, σ_{i,t_i} in Eq. (5.3) is set to zero. For sub-case (i.b), a node v_i waits for γ_i slots for its reserve battery B_i^2 to be fully charged before it switches the role of its batteries. The next earliest time a node v_i can transmit/receive another packet includes: (i) the last time a node v_i transmitted/received a packet, (ii) time duration γ_i to reach its maximum level $b_{i,max}$ from the battery's level at time t_i, i.e., $\gamma_i = r_i \times (b_{i,max} - b_{i,t_i}^2)$, and (iii) one slot delay before the stored energy in reserve battery B_i^2 can be used as required by the HSU model. Hence, $T_i = t_i + r_i \times (b_{i,max} - b_{i,t_i}^2) + 1$. For this sub-case, σ_{i,t_i} in Eq. (5.3) is set to 1. For case (ii), the active battery B_i^1 at a node v_i has sufficient energy to transmit/receive another packet at time t_i. However, as a node can only transmit/receive one packet at a time, the next earliest time a node v_i can transmit/receive another packet is in the next slot, i.e., $T_i = t_i + 1$. For this case, σ_{i,t_i} in Eq. (5.3) is set to 0. This completes the proof. □

5.2.3 LSDBS

We are now ready to explain **Link Scheduler with a Dual-Battery System (LSDBS)** in Algorithm 4. It aims to schedule all non-interfering links at the earliest possible time slot. Recall that battery B_i^1 (B_i^2) is the active (reserve) battery. At time $t = 0$, batteries B_i^1 and B_i^2 are waiting to be charged. Further, both batteries have an initial energy level of $b_{i,min}$. Finally, the initial charging time of active battery B_i^1, i.e., $\tilde{t}_i^{1+}$ is set to zero.

Lines 1–3 call *INIT*(.) to perform the following: (i) Use Eq. (5.2) to compute the charging time interval for each battery at a node v_i, i.e., $\tilde{\tau}_i^1$ and $\tilde{\tau}_i^2$; (ii) Set the start of the charging time of reserve battery B_i^2, i.e., $\tilde{t}_i^{2+} = \tilde{\tau}_i^1$; (iii) Set $T_i = \tilde{\tau}_i^1 + 1$; Recall that T_i is the earliest time when the active battery B_i^1 at a node v_i can be used to transmit/receive a packet; and (iv) Set the energy level of the active battery B_i^1 at a node v_i at time T_i, i.e., $b_{i,T_i}^1 = b_{i,max}$.

Lines 4–6 compute $t_{i,j}$, i.e., the earliest time a link $l_{i,j}$ can be scheduled. *Line 7* creates a set K that stores links $l_{i,j}$ that have the earliest activation time. *Line 8* then uses function $ORDER(K)$ to store in set K', links in set K in order to decrease weight $w_{i,j}$. Links with equal $w_{i,j}$ are sorted in decreasing degree of their end nodes, and for a tie, links are sorted in increasing order of their node labels. *Line 9* sets t with the earliest slot, i.e., $\mathbf{min}\{t_{i,j}\}$. *Lines 10–29* repeatedly schedule each link $l_{i,j} \in K'$ in order. Each selected link in *Line 12* does not cause interference or is interfered by links that have been scheduled in slot t; see the condition in *Line 11*. Each slot in $\mathcal{S}$ is initially empty. Note that function *CONFLICT()* uses a matrix M of size $|E|^2$ that contains Boolean variables to represent a conflict graph; i.e., $M[a, b]$ is set to 1 if there is an interference between links a and b. *Line 13* decreases the weight of each selected link $l_{i,j}$ by one. Once the link weight is equal to zero, *Line 15* removes the link from contention; see

Algorithm 4 LSDBS: a greedy algorithm that schedules links according to the earliest time when one of the dual battery at its end nodes can be discharged

Input: $G(V, E)$, r_i, b_i^z, $b_{i,max}$, $b_{i,min}$, $w_{i,j}$, and C_G
Output: Superframe $\mathcal{S}$

```
 1: for each node $v_i \in V$ do
 2:     $INIT(\tilde{\tau}_i^1, \tilde{\tau}_i^2, \tilde{t}_i^{2+}, T_i, b^1_{i,T_i})$
 3: end for
 4: for each link $l_{i,j} \in E$ do
 5:     $t_{i,j} = \mathbf{max}(T_i, T_j)$
 6: end for
 7: $K = \{$node $l_{i,j}$ in $C_G$ with $\mathbf{min}\{t_{i,j}\}\}$
 8: $K' = ORDER(K)$
 9: $t \leftarrow \mathbf{min}\{t_{i,j}\}$
10: for each $l_{i,j} \in K'$ do
11:     if NOT $CONFLICT(l_{i,j}, \mathcal{S}[t])$ then
12:         $\mathcal{S}[t] \leftarrow \mathcal{S}[t] \cup l_{i,j}$
13:         $w_{i,j} \leftarrow w_{i,j} - 1$
14:         if $w_{i,j} = 0$ then
15:             remove node $l_{i,j}$ from $C_G$
16:         end if
17:         $t_i \leftarrow t_j \leftarrow t$
18:         $b^1_{i,t_i} \leftarrow b^1_{i,T_i} - 1$
19:         $b^1_{j,t_j} \leftarrow b^1_{j,T_j} - 1$
20:         for each node $x \in \{i, j\}$ do
21:             $T_x \leftarrow COMP\_T_\alpha(x)$
22:             $b^1_{x,T_x} \leftarrow COMP\_b^z_\alpha(x)$
23:             if $b^1_{x,T_x} = b_{x,max}$ then
24:                 $SWAP(B^1_x, B^2_x)$
25:                 $\tilde{t}_x^{2+} \leftarrow T_x - 1$
26:             end if
27:         end for
28:     end if
29: end for
30: repeat Lines 4−29 until all $w_{i,j} = 0$
```

Lines 14–16.

Line *17* sets the last time an active battery at the end nodes of a selected link $l_{i,j}$ is used, i.e., t_i and t_j, to the current time t. Further, *Lines 18–19* compute the energy levels of the active battery at nodes v_i and v_j at time t after being used to transmit/receive one packet. *Lines 20-27* compute the following for each node $x \in \{i, j\}$. *Line 21* uses function $COMP\_T_\alpha(.)$ that implements *Proposition 5.3* to update the next earliest time a node x can transmit/receive another packet. *Line 22* uses function $COMP\_b^z_\alpha(.)$ to compute the energy level of the active battery B^1_x at time T_x, which depends on the remaining energy level at time t_x, i.e., b^1_{x,t_x}. More specifically, if b^1_{x,t_x} is larger than $b_{x,min}$, then b^1_{x,T_x} is set to b^1_{x,t_x} since the active battery B^1_x can still be used to transmit/receive one packet. Otherwise, b^1_{x,T_x} is set to $b_{x,max}$. For the latter case, i.e., $b^1_{x,T_x} = b_{x,max}$, *Line 24* switches the role of the batteries at node v_x, i.e., the reserve (active) battery becomes the active (reserve) battery. Then, *Line 25* computes the start charging time of the reserve battery B^2_x, i.e., $\tilde{t}^{2+}_x$. Finally, the steps from *Line 4* are repeated until all links are scheduled, i.e., $w_{i,j} = 0$.

For example, consider Figure 5.3. In *Line 2*, *INIT*(.) obtains $\tilde{\tau}^z_1 = 4$, $\tilde{\tau}^z_2 = 18$, $\tilde{\tau}^z_3 = 14$, and $\tilde{\tau}^z_4 = 12$. It sets $\tilde{t}^{2+}_1 = 4$, $\tilde{t}^{2+}_2 = 18$, $\tilde{t}^{2+}_3 = 14$, and $\tilde{t}^{2+}_4 = 12$. Further, it computes $T_1 = 5$, $T_2 = 19$, $T_3 = 15$, and $T_4 = 13$. Finally, it initialises $b^1_{1,T_1} = 3$, $b^1_{2,T_2} = 3$, $b^1_{3,T_3} = 3$, and $b^1_{4,T_4} = 4$. *Lines 4–6* compute $t_{1,2} = 19$, $t_{2,4} = 19$, and $t_{4,3} = 15$. *Line 7* inserts links $l_{4,3}$ into the set K. *Line 8* obtains $K' = \{l_{4,3}\}$, while *Line 9* sets $t = 15$. *Line 12* inserts $l_{4,3}$ into $\mathcal{S}[15]$. *Line 13* gets $w_{4,3} = 2$. *Line 17* sets $t_4 = t_3 = 15$. *Lines 18–19* compute $b^1_{4,15} = 3$ and $b^1_{3,15} = 2$. *Lines 20–27* obtain $T_4 = 16$, $b^1_{4,T_4} = 3$ and $T_3 = 16$, $b^1_{3,T_3} = 2$. *Line 30* repeats the steps from *Line 4* until all links are scheduled. Finally, LSDBS produces the link schedule $\mathcal{S}$ in Figure 5.4b.

Proposition 5.4. *The time complexity of LSDBS is $O(W|E|^2)$, where $W = \sum\limits_{(i,j)\in|E|}(w_{i,j})$.*

Proof. *Lines 1–3* take $O(|V|)$ and *Lines 4–6* require $O(|E|)$. *Line 7* takes $O(|E|)$. Function *ORDER*(K) at *Line 8* requires $O(|E|\ log\ |E|)$. *Line 9* takes $O(1)$. *Line 11* requires $O(|E|^2)$ to construct a matrix M which represents the conflict graph C_G. Function *CONFLICT*$(l_{i,j}, \mathcal{S}[t])$ in *Line 11* uses the matrix at most $|E|$ times. Hence, it takes $O(|E|)$. *Lines 12–30* take $O(1)$ each. The for loop in *Lines 10–29* is repeated at most $|E|$ times, and thus, the loop requires at most $O(|E|^2)$. *Line 30* repeats *Lines 4–29* W times. Thus, the time complexity of LSDBS is $O(W|E|^2)$. □

5.3 Evaluation

Section 5.3.1 evaluates the impact of battery cycle constraint on the schedule length. Section 5.3.2 studies the effect of battery cycle constraint on the number of charge/discharge cycles. Table 5.2 lists the parameter values used in our simulation.

Table 5.2 Parameter values used in the evaluation.

Parameter	***Value (s)***
Network size	40×40 m^2
Transmit range	15 m
Interference range	30 m
$\|V\|$	$\{10, 20, 30, 40, 50\}$
r_i	$\{1, 5, 10, 15, 20\}$
$w_{i,j}$	$\{1, 2, 3, 4, 5\}$

5.3.1 Effect of Battery Cycle Constraint

To study the effect of battery cycle constraint on the superframe length $|\mathcal{S}|$, we compare LSDBS, LSBCC, and LSNBC. Briefly, LSBCC is a version of LSDBS in which each node is equipped with only one battery. On the other hand, LSNBC is a version of LSBCC without the battery cycle constraint. We consider 10 to 50 nodes with $r_i = 5$. The total usable energy of *two* batteries when nodes use LSDBS is set to be equal to the *single* battery in LSBCC and LSNBC. Specifically, each battery in LSDBS has usable energy of $\hat{b}_i^z = 5\epsilon$, i.e., it has $b_i = 5\epsilon$, $b_{i,min} = 0\epsilon$, and $b_{i,max} = 5\epsilon$. Thus, the total usable energy of each node v_i in LSDBS is $2 \times 5 = 10\epsilon$. On the other hand, the batteries in LSBCC and LSNBC have a capacity of $b_i = 10\epsilon$, $b_{i,min} = 0\epsilon$, and $b_{i,max} = 10\epsilon$, i.e., their usable energy is $\hat{b}_i = 10\epsilon$. Each link weight is randomly fixed to a value between 1 and 5, i.e., $w_{i,j} = [1, 5]$.

Effect on Superframe Length: Figure 5.5 shows that the superframe length $|\mathcal{S}|$ produced by LSDBS is shorter than LSBCC. In a rWSN with 10 nodes, LSDBS produces 82 less slots (35.19% shorter) as compared to when using LSBCC. The results are consistent for other networks with $|V| = 20$, 30, 40, and 50 nodes. LSDBS produces superframes that are 27.85%, 27.45%, 27.03%, and 27.16%, respectively, shorter than those in LSBCC. This is because nodes that use LSDBS only need to wait for one battery, which has half the usable energy of the battery in LSBCC, to be charged to its maximum level before powering their load. Figure 5.5 shows that schedules generated by LSBDS are also shorter than those in LSNBC. Specifically, for $|V| = 10$, 20, 30, 40, and 50, LSDBS produces $|\mathcal{S}|$ that are $9.04\%, 13.41\%, 14.26\%, 14.8\%$, and 15.12%, respectively, shorter than in LSNBC. As shown in Figure 5.5, the differences between the schedule lengths of LSNBC and LSDBS increase when $|V|$ increases from 10 to 50. This is because the superframe length is affected by the number of slots required by each node to accumulate energy as well as the number of links it has to activate. Each node in LSNBC needs $r_i + 1 = 6$ slots before it can activate one link, while that in LSDBS requires $r_i \times \hat{b}_i^z = 25$ slots to charge one battery to its maximum level so that it can be used to activate five links. Note that on average, each node in a network with $|V| = 10, 20, 30, 40$, and 50, has $7, 16, 20, 30$, and 38 links to activate, respectively. Thus, a node that needs to activate 20 (30) links in LSNBC requires at least $20 \times 6 = 120$ (180) slots, which is 15 (25) slots longer than the node in LSDBS that on average requires $25 \times 4 + 5 = 105$ (155) slots.

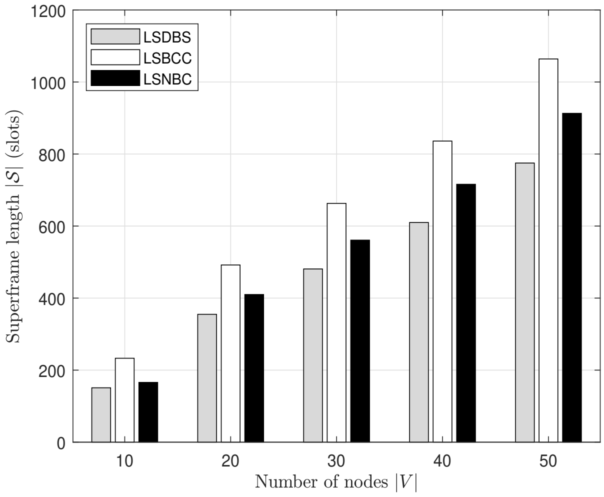

Figure 5.5 LSDBS, LSBCC, LSNBC on $|\mathcal{S}|$.

Effect on Charge/Discharge Cycles: As shown in Figure 5.6, the total number of charge/discharge cycles in LSBCC is larger than that in LSDBS − an average from two batteries. For example, when $|V| = 10$, LSBCC has three cycles more than in LSDBS, i.e., 15% more. The results are consistent for networks with 20, 30, 40, and 50 nodes. Specifically, LSBCC needs 6.17%, 4.62%, 3.4%, and 2.77% more cycles, respectively, than LSDBS. Let $\mathcal{E}_i$ be the amount of energy (in ϵ) used at node v_i to schedule all of its incident links. Thus, each battery of v_i in LSDBS (LSBCC) needs $\lceil \mathcal{E}_i / \hat{b}_i^z \rceil$ ($\lceil \mathcal{E}_i / \hat{b}_i \rceil$) charge/discharge cycles to harvest $\mathcal{E}_i$ of energy. Note that $\hat{b}_i = 2 \times \hat{b}_i^z$, and thus we have $\lceil \mathcal{E}_i / \hat{b}_i^z \rceil / 2 \leq \lceil \mathcal{E}_i / \hat{b}_i \rceil$), i.e., the charge/discharge cycles of each battery in LSDBS are no more than that of the battery in LSBCC. Figure 5.6 also shows that the number of charge/discharge cycles produced by LSDBS is less than LSNBC. More specifically, LSDBS requires $84.38\%, 85.61\%, 86.47\%, 86.92\%$, and 87.13% fewer cycles than LSNBC for $|V| = 10, 20, 30, 40$, and 50, respectively. This is because each battery in LSDBS has to be charged only when its energy is equal to the minimum level. The remaining experiments only use LSDBS.

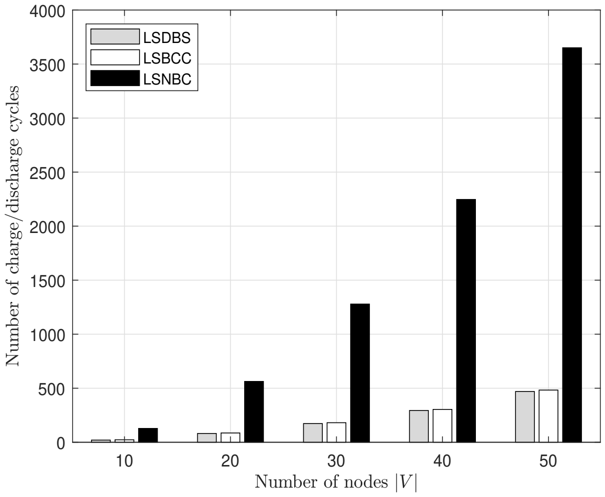

Figure 5.6 LSDBS, LSBCC, LSNBC on charge/discharge cycles.

5.3.2 Effect of Harvesting Time

This section investigates the effect of r_i on $|\mathcal{S}|$ and charge/discharge cycles. In this simulation, we consider various r_i values, namely 1, 5, 10, 15, and 20 slots, in a rWSN with 10 to 50 nodes. We set $b_i^z = 3\epsilon$, $b_{i,min} = 1\epsilon$, $b_{i,max} = 3\epsilon$, and each link has weight $w_{i,j} = 3$.

Effect on Superframe Length: Figure 5.7 shows that increasing r_i produces a longer superframe. Specifically, for 10 nodes, when r_i is increased from 1 to 5, $|\mathcal{S}|$ jumps from 52 to 134 slots $-$ an increase of 1.58 times. Similarly, when r_i increases from 5 to 20, i.e., to 10, 15, and 20, $|\mathcal{S}|$ increases by 0.98, 0.49, and 0.33 times, respectively. We observed similar trends for 20, 30, 40, and 50 nodes. For example, for 50 (100) nodes, when r_i increased from 1 to 20, $|\mathcal{S}|$ increased by

1.54 (1.55), 1.00 (1.00), 0.50 (0.50), 0.33 (0.33) times, respectively. The length of $|\mathcal{S}|$ increased because each node needs more time to charge its battery to the maximum level. Notice that $|\mathcal{S}|$ increases almost linearly when r_i is increased from 1 to 20. Further, the rate in which $|\mathcal{S}|$ increases in smaller networks, e.g., $|V| = 10$, is less than that of larger networks, e.g., $|V| = 50$. This is because more nodes mean more links need to be scheduled.

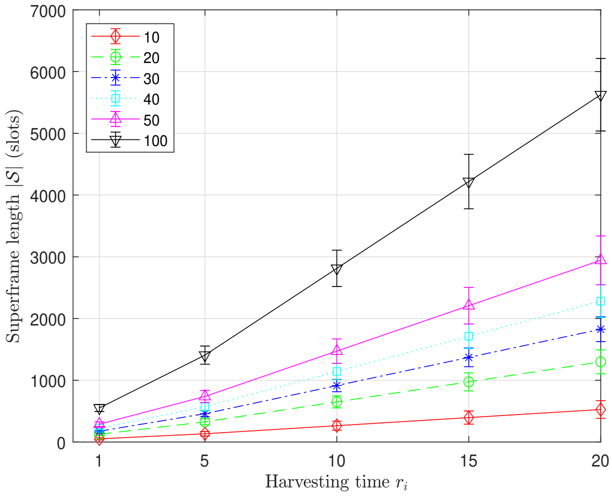

Figure 5.7 Effect of harvesting time r_i on $|\mathcal{S}|$.

Effect on Charge/Discharge Cycles: For $|V| = 10$, 20, 30, 40, and 50, LSDBS produces a total of 95, 396, 850, 1451, and 2325, charge/discharge cycles, respectively, for all values of r_i. In particular, increasing r_i does not affect the number of battery charge/discharge cycles. This is because the number of charge/discharge cycles of a battery at each node v_i that needs to accumulate $\mathcal{E}_i$ of energy, i.e., $\lceil \mathcal{E}_i / \hat{b}_i^z \rceil$, depends only on the size of the battery's usable energy $\hat{b}_i^z$. Thus, different values of r_i will only affect the time duration to harvest $\mathcal{E}_i$ of energy.

5.4 Chapter Summary

This chapter presented a novel link scheduling problem called LSME-2. It proposed a greedy algorithm, LSDBS, that considers nodes with a dual-battery system to solve the problem. Our results showed the benefits of using such a system, in terms of schedule length and charge/discharge cycles. Specifically, compared to using a single battery with the same capacity and cycle constraint, LSDBS produced up to 35.19% (15%) fewer slots (charge/discharge cycles). Interestingly, LSDBS obtained up to 15.12% shorter schedules when compared to nodes that use a single battery, even without cycle constraint, and it had up to 87.13% fewer charge/discharge cycles.

Chapter 6

Conclusion

6.1 Summary

This thesis has proposed three link schedulers, i.e., LS-rWSN, LSBCC, and LS-DBS, to schedule links in rWSNs. Each scheduler solved a link scheduling problem. We have used a greedy heuristic to activate links according to the earliest time in which their end nodes have sufficient energy to transmit/receive a packet. Table 6.1 summarises the works covered in this thesis.

Table 6.1 Three link scheduling problems with proposed solutions, constraints, battery usage protocol, and the number of batteries per node.

Problem	**Solution**	**Constraints**	**Battery usage protocol**	**Number of batteries per node**	**Chapter**
LSHUS	LS-rWSN	- Harvesting time - Battery capacity	HUS	One	Chapter 3
LSME-1	LSBCC	- Harvesting time - Battery capacity - Battery cycle	HSU	One	Chapter 4
LSME-2	LSDBS	- Harvesting time - Battery capacity - Battery cycle	HSU	Two	Chapter 5

Specifically, we have proposed the following three problems and their solutions.

- In Chapter 3, we formulated the link scheduling problem, LSHUS, to generate the shortest TDMA schedule for use in rWSNs with varying energy harvesting times and limited battery capacity constraints. We considered the HUS battery usage protocol. The chapter showed the NP-Complete proof of the problem and analysed the optimal schedule for three fixed topologies. Further, it has proposed LS-rWSN to solve LSHUS. LS-rWSN aimed to activate each non-interfering link with end nodes that have sufficient energy to transmit/receive a packet at the earliest time. We used simulation to show the effect of harvesting time, battery capacity, leakage rate, and storage efficiency on the schedule length, and we described the effectiveness of our algorithm.

- In Chapter 4, we proposed the link scheduling problem, LSME-1, to derive a TDMA link schedule for rWSNs with harvesting time, battery capacity, and battery cycle constraints. We used the HSU battery usage protocol in this problem. The chapter analysed the optimal schedule for three fixed topologies. It presented LSBCC to solve this problem. LSBCC aimed to schedule links according to when their corresponding nodes had sufficient energy. Further, our simulation and analytical results showed that the battery cycle constraint and leaking batteries lead to unscheduled links. We used simulation to show the effect of the battery cycle constraint on the schedule length, and on the number of charge/discharge cycles when nodes were equipped with a leak-free or a leaky battery.

- Finally, in Chapter 5, we addressed the link scheduling problem, LSME-2, to activate links in rWSNs with the dual-battery system. Unlike LSME-1, in which each node only used one battery, LSME-2 considered the use of two batteries at each node, thus it extended LSME-1. We then presented the battery states and transitions. This chapter described LSDBS to solve the problem. LSDBS aimed to schedule links according to the earliest time at which a battery at the end nodes of each link could be discharged, or is full. We used a simulation to show the effect of the battery cycle constraint and harvesting time on the schedule length, and on the number of charge/discharge cycles.

The worst case and the weakness aspect for our proposed solution are as follows:

- LS-rWSN (in Chapter 3): Our solution produced a longer link schedule when the battery of each node has leakage rate of $\mu_i > 0$ and storage efficiency of $\eta_i < 1$.

- LSBCC (in Chapter 4): There can be some links which can not be scheduled for batteries with a leakage rate $\mu_i > 0$ (as discussed in Section 4.2.2) when each node has a battery with the same parameter values of r_i, b_i, $b_{i,max}$, μ_i, and η_i (as discussed in Section 4.3.2.1.).

- LSDBS (in Chapter 5): As in LSBCC, LSDBS can produce results with some unscheduled. However, by using using two batteries, the total number of unscheduled links in LSDBS is expected to be less than in LSBCC.

For real-life implementation, we suggest using either LSBCC or LSDBS for users that require networks with longer lifetime. Recall that both LSBCC and LSDBS aim to prolong each battery's lifetime by enforcing battery cycle constraints. Between LSBCC and LSDBS, we suggest using LSDBS for users that can afford using the more expensive dual batteries. Recall that LSDBS produces shorter link schedule than LSBCC. For users that require higher network capacity for short time network deployment, using LS-rWSN is ideal because the scheduler produces shorter link schedules as compared to LSBCC and LSDBS. Note that without enforcing battery cycle constraint as in LSBCC and LSDBS, the lifetime of batteries when using LS-rWSN is expected to be shorter than using LSBCC and LSDBS, reducing the lifetime of the implemented networks.

6.2 Future Work

There are many possible directions for future research. More specifically, our proposed LSBCC algorithm in Chapter 4 might result in unscheduled links and our proposed LSDBS algorithm in Chapter 5 did not address the battery leakage. We leave these issues for future work. We will design a protocol to ensure all links can be scheduled for battery's leakage rate greater than zero. Further, we plan to convert the proposed algorithms from centralised approach to distributed way. In the distributed approach, each node does not need the entire network topology data because it requires information only from its neighbours. The goals are to reduce the protocol overhead and to achieve the best case in average convergence time. Thus, the distributed algorithm will have more scalability than the centralised algorithm. However, to design the distributed solution is a challenging problem. We believe this is a potential area of future research.

Another research direction is to consider joint routing and link scheduling. This is a cross layer problem. The aim is to achieve a minimum time for packet transmission by choosing the most suitable routing path and link schedule. Since routing in rWSNs is very challenging and has attracted a lot of attention in recent years, we will consider this issue for future work.

This thesis mainly considers superframe length as network performance metrics. Note that the works in this thesis aimed to produce a link schedule with the shortest length. For future works, one can use other metrics, e.g., throughput, duty cycle, and age of information to evaluate the link scheduling algorithms. Further, the works in this thesis can be extended into mobile nodes. Recall that this thesis considers only fixed node model. Different from fixed nodes, mobile nodes need energy for their movement or other computation processes [101]. Thus, they require more energy than the fixed nodes.

Appendix

Copyright Information

The copyright agreements for published papers allow authors to re-use their material in derivative works. Thus, copyright permission is not required. The following copyright information was obtained from IEEE conferences and journals in which the author has published.

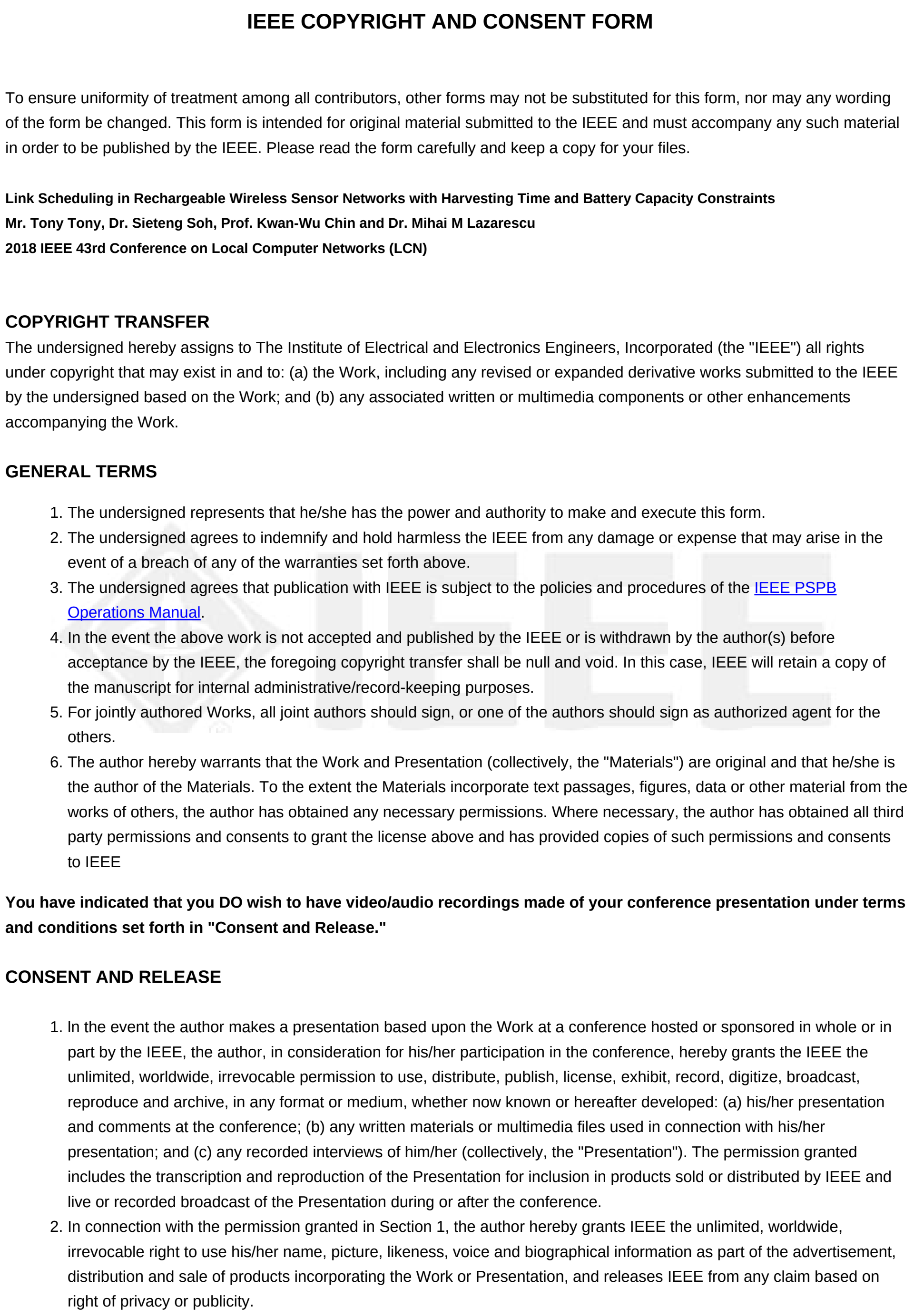

IEEE COPYRIGHT AND CONSENT FORM

To ensure uniformity of treatment among all contributors, other forms may not be substituted for this form, nor may any wording of the form be changed. This form is intended for original material submitted to the IEEE and must accompany any such material in order to be published by the IEEE. Please read the form carefully and keep a copy for your files.

Link Scheduling in Rechargeable Wireless Sensor Networks with Harvesting Time and Battery Capacity Constraints
Mr. Tony Tony, Dr. Sieteng Soh, Prof. Kwan-Wu Chin and Dr. Mihai M Lazarescu
2018 IEEE 43rd Conference on Local Computer Networks (LCN)

COPYRIGHT TRANSFER

The undersigned hereby assigns to The Institute of Electrical and Electronics Engineers, Incorporated (the "IEEE") all rights under copyright that may exist in and to: (a) the Work, including any revised or expanded derivative works submitted to the IEEE by the undersigned based on the Work; and (b) any associated written or multimedia components or other enhancements accompanying the Work.

GENERAL TERMS

1. The undersigned represents that he/she has the power and authority to make and execute this form.
2. The undersigned agrees to indemnify and hold harmless the IEEE from any damage or expense that may arise in the event of a breach of any of the warranties set forth above.
3. The undersigned agrees that publication with IEEE is subject to the policies and procedures of the IEEE PSPB Operations Manual.
4. In the event the above work is not accepted and published by the IEEE or is withdrawn by the author(s) before acceptance by the IEEE, the foregoing copyright transfer shall be null and void. In this case, IEEE will retain a copy of the manuscript for internal administrative/record-keeping purposes.
5. For jointly authored Works, all joint authors should sign, or one of the authors should sign as authorized agent for the others.
6. The author hereby warrants that the Work and Presentation (collectively, the "Materials") are original and that he/she is the author of the Materials. To the extent the Materials incorporate text passages, figures, data or other material from the works of others, the author has obtained any necessary permissions. Where necessary, the author has obtained all third party permissions and consents to grant the license above and has provided copies of such permissions and consents to IEEE

You have indicated that you DO wish to have video/audio recordings made of your conference presentation under terms and conditions set forth in "Consent and Release."

CONSENT AND RELEASE

1. In the event the author makes a presentation based upon the Work at a conference hosted or sponsored in whole or in part by the IEEE, the author, in consideration for his/her participation in the conference, hereby grants the IEEE the unlimited, worldwide, irrevocable permission to use, distribute, publish, license, exhibit, record, digitize, broadcast, reproduce and archive, in any format or medium, whether now known or hereafter developed: (a) his/her presentation and comments at the conference; (b) any written materials or multimedia files used in connection with his/her presentation; and (c) any recorded interviews of him/her (collectively, the "Presentation"). The permission granted includes the transcription and reproduction of the Presentation for inclusion in products sold or distributed by IEEE and live or recorded broadcast of the Presentation during or after the conference.
2. In connection with the permission granted in Section 1, the author hereby grants IEEE the unlimited, worldwide, irrevocable right to use his/her name, picture, likeness, voice and biographical information as part of the advertisement, distribution and sale of products incorporating the Work or Presentation, and releases IEEE from any claim based on right of privacy or publicity.

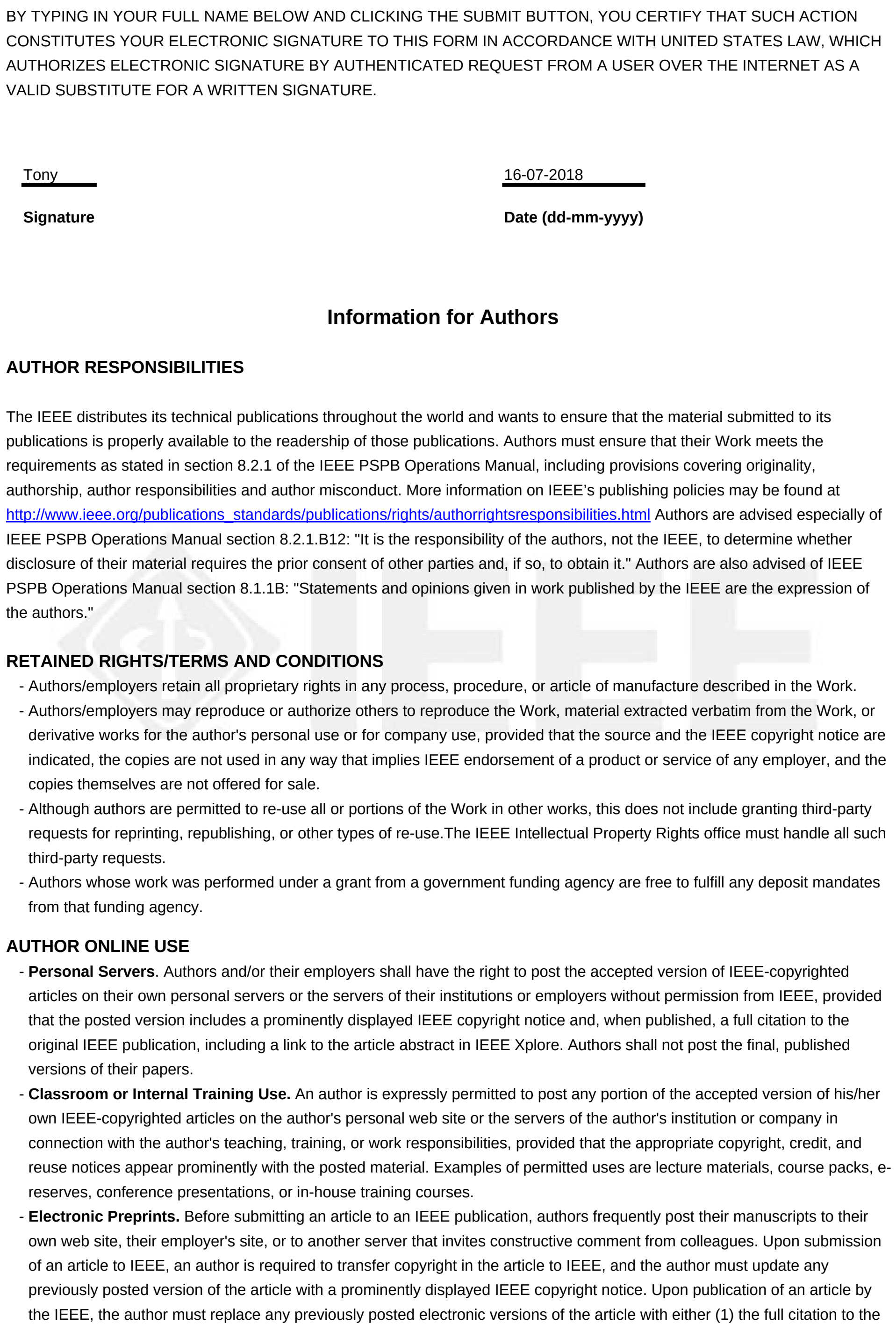

BY TYPING IN YOUR FULL NAME BELOW AND CLICKING THE SUBMIT BUTTON, YOU CERTIFY THAT SUCH ACTION CONSTITUTES YOUR ELECTRONIC SIGNATURE TO THIS FORM IN ACCORDANCE WITH UNITED STATES LAW, WHICH AUTHORIZES ELECTRONIC SIGNATURE BY AUTHENTICATED REQUEST FROM A USER OVER THE INTERNET AS A VALID SUBSTITUTE FOR A WRITTEN SIGNATURE.

Tony	16-07-2018
Signature	**Date (dd-mm-yyyy)**

Information for Authors

AUTHOR RESPONSIBILITIES

The IEEE distributes its technical publications throughout the world and wants to ensure that the material submitted to its publications is properly available to the readership of those publications. Authors must ensure that their Work meets the requirements as stated in section 8.2.1 of the IEEE PSPB Operations Manual, including provisions covering originality, authorship, author responsibilities and author misconduct. More information on IEEE’s publishing policies may be found at http://www.ieee.org/publications_standards/publications/rights/authorrightsresponsibilities.html Authors are advised especially of IEEE PSPB Operations Manual section 8.2.1.B12: "It is the responsibility of the authors, not the IEEE, to determine whether disclosure of their material requires the prior consent of other parties and, if so, to obtain it." Authors are also advised of IEEE PSPB Operations Manual section 8.1.1B: "Statements and opinions given in work published by the IEEE are the expression of the authors."

RETAINED RIGHTS/TERMS AND CONDITIONS

- Authors/employers retain all proprietary rights in any process, procedure, or article of manufacture described in the Work.
- Authors/employers may reproduce or authorize others to reproduce the Work, material extracted verbatim from the Work, or derivative works for the author's personal use or for company use, provided that the source and the IEEE copyright notice are indicated, the copies are not used in any way that implies IEEE endorsement of a product or service of any employer, and the copies themselves are not offered for sale.
- Although authors are permitted to re-use all or portions of the Work in other works, this does not include granting third-party requests for reprinting, republishing, or other types of re-use.The IEEE Intellectual Property Rights office must handle all such third-party requests.
- Authors whose work was performed under a grant from a government funding agency are free to fulfill any deposit mandates from that funding agency.

AUTHOR ONLINE USE

- **Personal Servers**. Authors and/or their employers shall have the right to post the accepted version of IEEE-copyrighted articles on their own personal servers or the servers of their institutions or employers without permission from IEEE, provided that the posted version includes a prominently displayed IEEE copyright notice and, when published, a full citation to the original IEEE publication, including a link to the article abstract in IEEE Xplore. Authors shall not post the final, published versions of their papers.
- **Classroom or Internal Training Use.** An author is expressly permitted to post any portion of the accepted version of his/her own IEEE-copyrighted articles on the author's personal web site or the servers of the author's institution or company in connection with the author's teaching, training, or work responsibilities, provided that the appropriate copyright, credit, and reuse notices appear prominently with the posted material. Examples of permitted uses are lecture materials, course packs, e-reserves, conference presentations, or in-house training courses.
- **Electronic Preprints.** Before submitting an article to an IEEE publication, authors frequently post their manuscripts to their own web site, their employer's site, or to another server that invites constructive comment from colleagues. Upon submission of an article to IEEE, an author is required to transfer copyright in the article to IEEE, and the author must update any previously posted version of the article with a prominently displayed IEEE copyright notice. Upon publication of an article by the IEEE, the author must replace any previously posted electronic versions of the article with either (1) the full citation to the

IEEE work with a Digital Object Identifier (DOI) or link to the article abstract in IEEE Xplore, or (2) the accepted version only (not the IEEE-published version), including the IEEE copyright notice and full citation, with a link to the final, published article in IEEE Xplore.

Questions about the submission of the form or manuscript must be sent to the publication's editor.
Please direct all questions about IEEE copyright policy to:
IEEE Intellectual Property Rights Office, copyrights@ieee.org, +1-732-562-3966

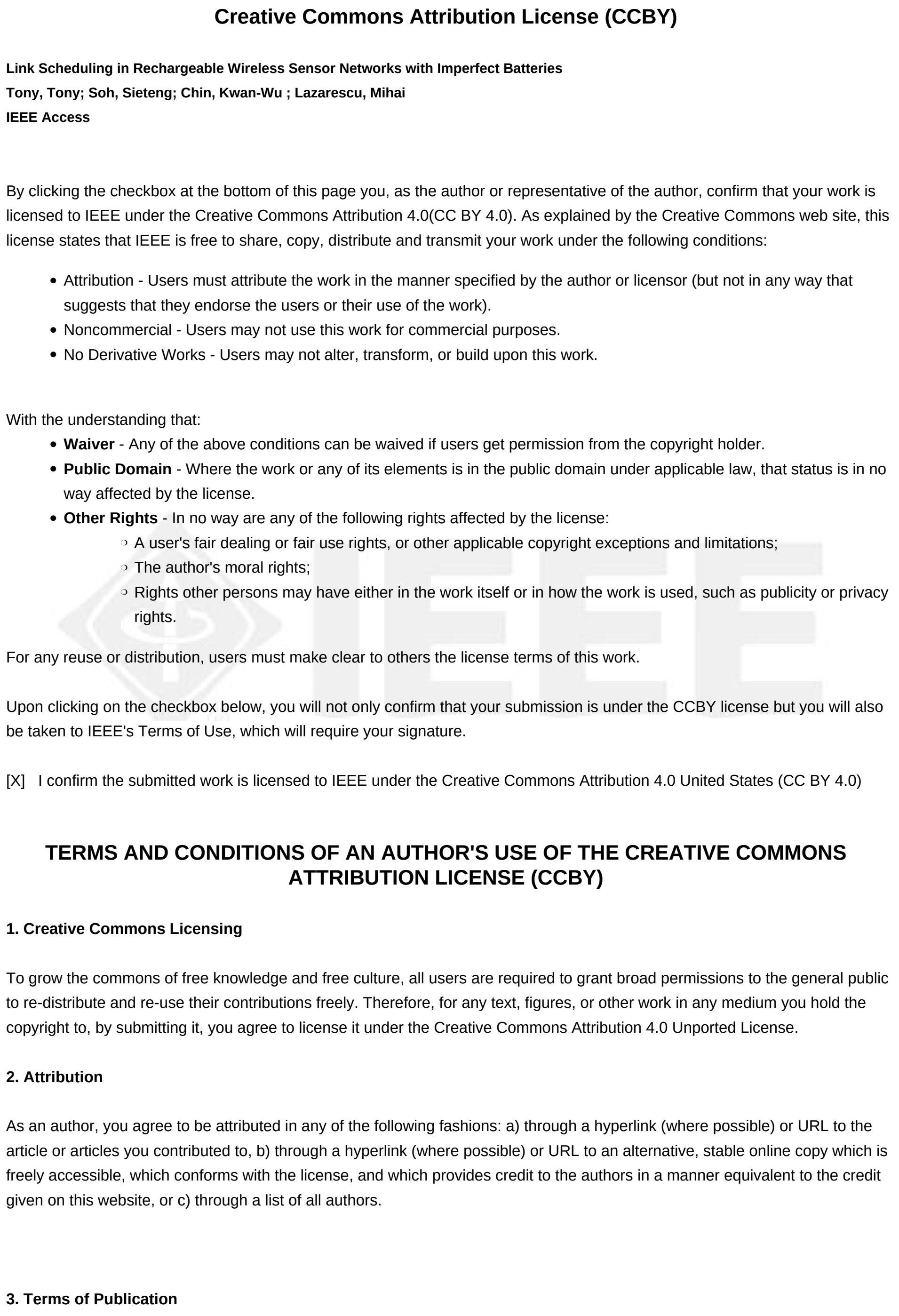

Creative Commons Attribution License (CCBY)

Link Scheduling in Rechargeable Wireless Sensor Networks with Imperfect Batteries
Tony, Tony; Soh, Sieteng; Chin, Kwan-Wu ; Lazarescu, Mihai
IEEE Access

By clicking the checkbox at the bottom of this page you, as the author or representative of the author, confirm that your work is licensed to IEEE under the Creative Commons Attribution 4.0(CC BY 4.0). As explained by the Creative Commons web site, this license states that IEEE is free to share, copy, distribute and transmit your work under the following conditions:

- Attribution - Users must attribute the work in the manner specified by the author or licensor (but not in any way that suggests that they endorse the users or their use of the work).
- Noncommercial - Users may not use this work for commercial purposes.
- No Derivative Works - Users may not alter, transform, or build upon this work.

With the understanding that:

- **Waiver** - Any of the above conditions can be waived if users get permission from the copyright holder.
- **Public Domain** - Where the work or any of its elements is in the public domain under applicable law, that status is in no way affected by the license.
- **Other Rights** - In no way are any of the following rights affected by the license:
    - A user's fair dealing or fair use rights, or other applicable copyright exceptions and limitations;
    - The author's moral rights;
    - Rights other persons may have either in the work itself or in how the work is used, such as publicity or privacy rights.

For any reuse or distribution, users must make clear to others the license terms of this work.

Upon clicking on the checkbox below, you will not only confirm that your submission is under the CCBY license but you will also be taken to IEEE's Terms of Use, which will require your signature.

[X] I confirm the submitted work is licensed to IEEE under the Creative Commons Attribution 4.0 United States (CC BY 4.0)

TERMS AND CONDITIONS OF AN AUTHOR'S USE OF THE CREATIVE COMMONS ATTRIBUTION LICENSE (CCBY)

1. Creative Commons Licensing

To grow the commons of free knowledge and free culture, all users are required to grant broad permissions to the general public to re-distribute and re-use their contributions freely. Therefore, for any text, figures, or other work in any medium you hold the copyright to, by submitting it, you agree to license it under the Creative Commons Attribution 4.0 Unported License.

2. Attribution

As an author, you agree to be attributed in any of the following fashions: a) through a hyperlink (where possible) or URL to the article or articles you contributed to, b) through a hyperlink (where possible) or URL to an alternative, stable online copy which is freely accessible, which conforms with the license, and which provides credit to the authors in a manner equivalent to the credit given on this website, or c) through a list of all authors.

3. Terms of Publication

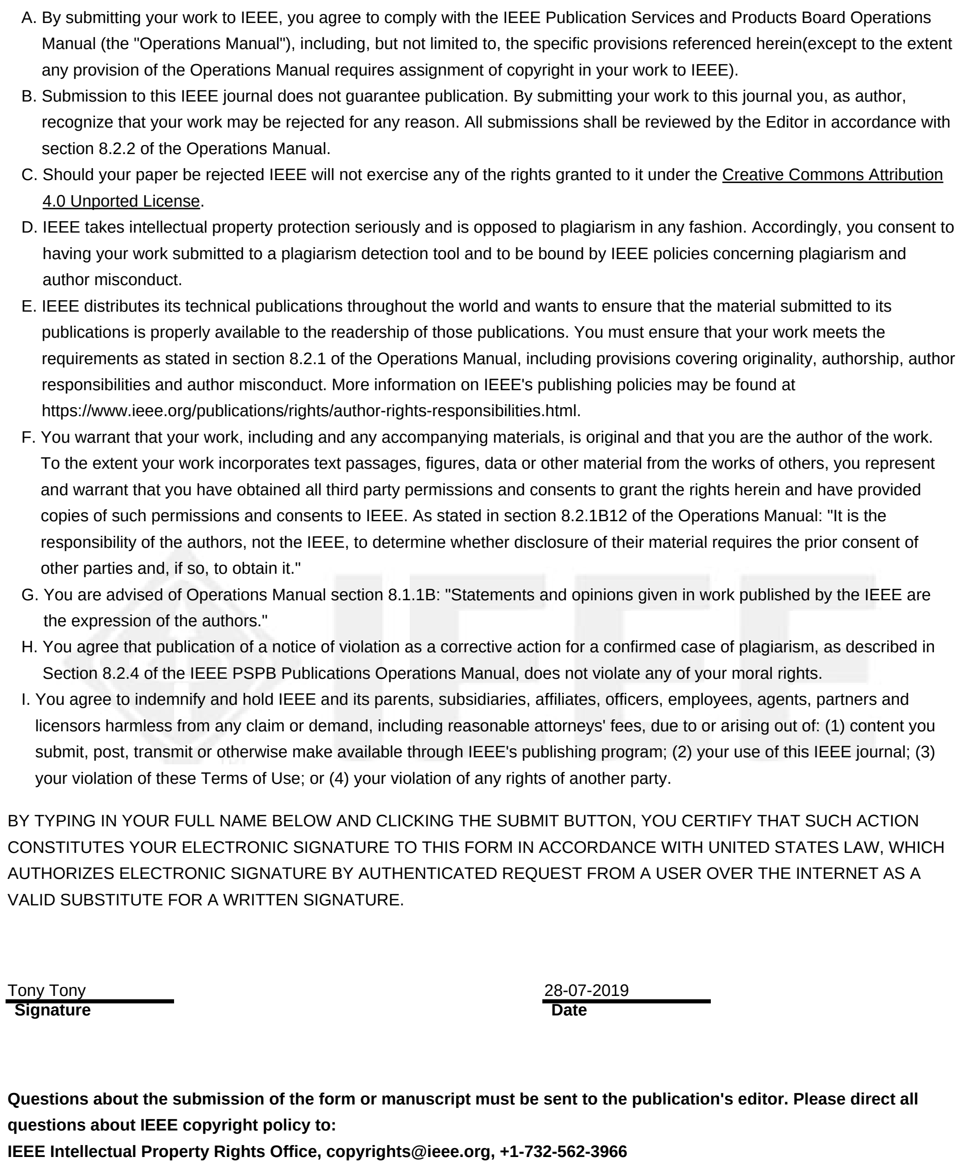

A. By submitting your work to IEEE, you agree to comply with the IEEE Publication Services and Products Board Operations Manual (the "Operations Manual"), including, but not limited to, the specific provisions referenced herein(except to the extent any provision of the Operations Manual requires assignment of copyright in your work to IEEE).
B. Submission to this IEEE journal does not guarantee publication. By submitting your work to this journal you, as author, recognize that your work may be rejected for any reason. All submissions shall be reviewed by the Editor in accordance with section 8.2.2 of the Operations Manual.
C. Should your paper be rejected IEEE will not exercise any of the rights granted to it under the Creative Commons Attribution 4.0 Unported License.
D. IEEE takes intellectual property protection seriously and is opposed to plagiarism in any fashion. Accordingly, you consent to having your work submitted to a plagiarism detection tool and to be bound by IEEE policies concerning plagiarism and author misconduct.
E. IEEE distributes its technical publications throughout the world and wants to ensure that the material submitted to its publications is properly available to the readership of those publications. You must ensure that your work meets the requirements as stated in section 8.2.1 of the Operations Manual, including provisions covering originality, authorship, author responsibilities and author misconduct. More information on IEEE's publishing policies may be found at https://www.ieee.org/publications/rights/author-rights-responsibilities.html.
F. You warrant that your work, including and any accompanying materials, is original and that you are the author of the work. To the extent your work incorporates text passages, figures, data or other material from the works of others, you represent and warrant that you have obtained all third party permissions and consents to grant the rights herein and have provided copies of such permissions and consents to IEEE. As stated in section 8.2.1B12 of the Operations Manual: "It is the responsibility of the authors, not the IEEE, to determine whether disclosure of their material requires the prior consent of other parties and, if so, to obtain it."
G. You are advised of Operations Manual section 8.1.1B: "Statements and opinions given in work published by the IEEE are the expression of the authors."
H. You agree that publication of a notice of violation as a corrective action for a confirmed case of plagiarism, as described in Section 8.2.4 of the IEEE PSPB Publications Operations Manual, does not violate any of your moral rights.
I. You agree to indemnify and hold IEEE and its parents, subsidiaries, affiliates, officers, employees, agents, partners and licensors harmless from any claim or demand, including reasonable attorneys' fees, due to or arising out of: (1) content you submit, post, transmit or otherwise make available through IEEE's publishing program; (2) your use of this IEEE journal; (3) your violation of these Terms of Use; or (4) your violation of any rights of another party.

BY TYPING IN YOUR FULL NAME BELOW AND CLICKING THE SUBMIT BUTTON, YOU CERTIFY THAT SUCH ACTION CONSTITUTES YOUR ELECTRONIC SIGNATURE TO THIS FORM IN ACCORDANCE WITH UNITED STATES LAW, WHICH AUTHORIZES ELECTRONIC SIGNATURE BY AUTHENTICATED REQUEST FROM A USER OVER THE INTERNET AS A VALID SUBSTITUTE FOR A WRITTEN SIGNATURE.

Tony Tony **Signature**	28-07-2019 **Date**

Questions about the submission of the form or manuscript must be sent to the publication's editor. Please direct all questions about IEEE copyright policy to:
IEEE Intellectual Property Rights Office, copyrights@ieee.org, +1-732-562-3966

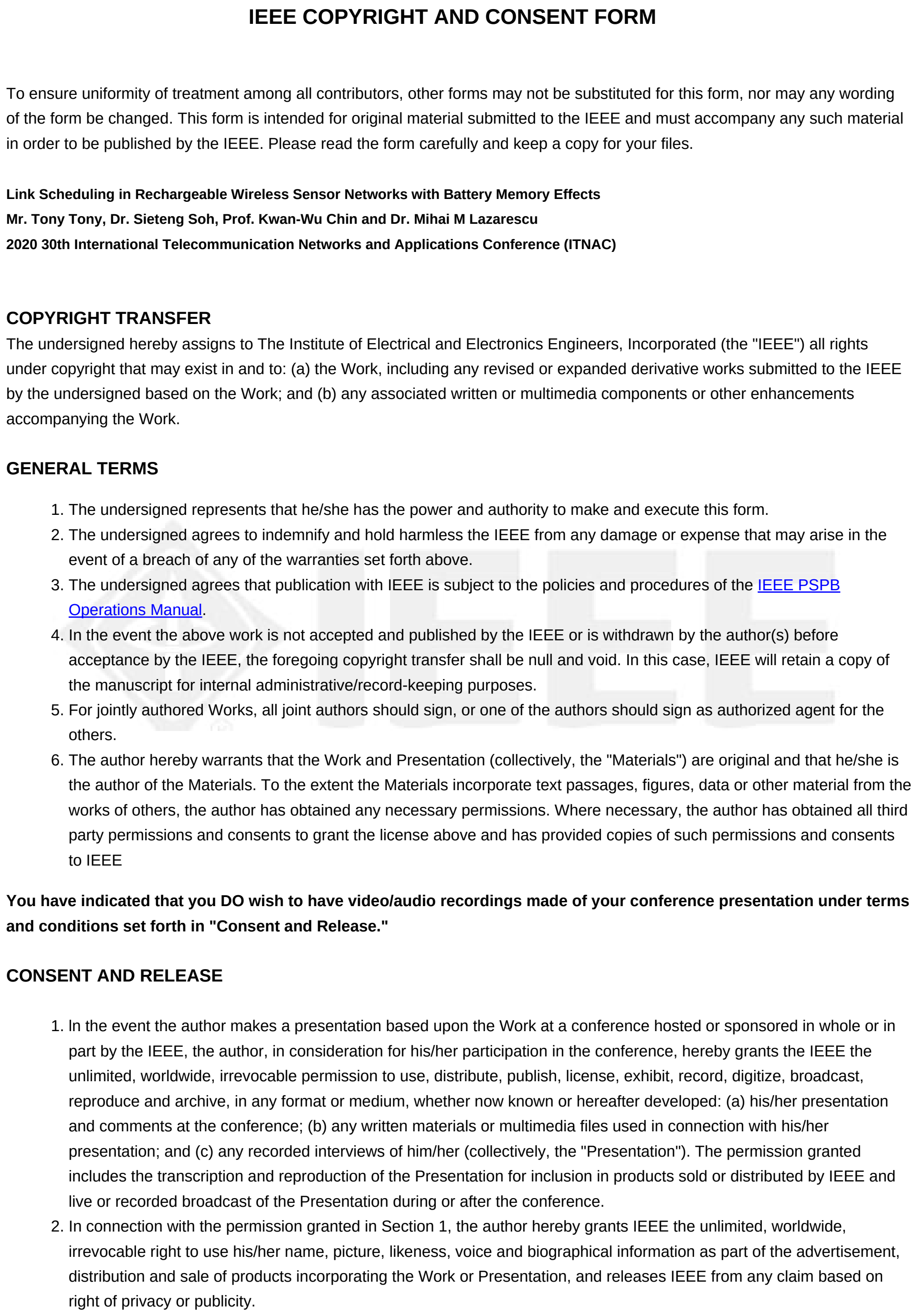

IEEE COPYRIGHT AND CONSENT FORM

To ensure uniformity of treatment among all contributors, other forms may not be substituted for this form, nor may any wording of the form be changed. This form is intended for original material submitted to the IEEE and must accompany any such material in order to be published by the IEEE. Please read the form carefully and keep a copy for your files.

Link Scheduling in Rechargeable Wireless Sensor Networks with Battery Memory Effects
Mr. Tony Tony, Dr. Sieteng Soh, Prof. Kwan-Wu Chin and Dr. Mihai M Lazarescu
2020 30th International Telecommunication Networks and Applications Conference (ITNAC)

COPYRIGHT TRANSFER

The undersigned hereby assigns to The Institute of Electrical and Electronics Engineers, Incorporated (the "IEEE") all rights under copyright that may exist in and to: (a) the Work, including any revised or expanded derivative works submitted to the IEEE by the undersigned based on the Work; and (b) any associated written or multimedia components or other enhancements accompanying the Work.

GENERAL TERMS

1. The undersigned represents that he/she has the power and authority to make and execute this form.
2. The undersigned agrees to indemnify and hold harmless the IEEE from any damage or expense that may arise in the event of a breach of any of the warranties set forth above.
3. The undersigned agrees that publication with IEEE is subject to the policies and procedures of the IEEE PSPB Operations Manual.
4. In the event the above work is not accepted and published by the IEEE or is withdrawn by the author(s) before acceptance by the IEEE, the foregoing copyright transfer shall be null and void. In this case, IEEE will retain a copy of the manuscript for internal administrative/record-keeping purposes.
5. For jointly authored Works, all joint authors should sign, or one of the authors should sign as authorized agent for the others.
6. The author hereby warrants that the Work and Presentation (collectively, the "Materials") are original and that he/she is the author of the Materials. To the extent the Materials incorporate text passages, figures, data or other material from the works of others, the author has obtained any necessary permissions. Where necessary, the author has obtained all third party permissions and consents to grant the license above and has provided copies of such permissions and consents to IEEE

You have indicated that you DO wish to have video/audio recordings made of your conference presentation under terms and conditions set forth in "Consent and Release."

CONSENT AND RELEASE

1. In the event the author makes a presentation based upon the Work at a conference hosted or sponsored in whole or in part by the IEEE, the author, in consideration for his/her participation in the conference, hereby grants the IEEE the unlimited, worldwide, irrevocable permission to use, distribute, publish, license, exhibit, record, digitize, broadcast, reproduce and archive, in any format or medium, whether now known or hereafter developed: (a) his/her presentation and comments at the conference; (b) any written materials or multimedia files used in connection with his/her presentation; and (c) any recorded interviews of him/her (collectively, the "Presentation"). The permission granted includes the transcription and reproduction of the Presentation for inclusion in products sold or distributed by IEEE and live or recorded broadcast of the Presentation during or after the conference.
2. In connection with the permission granted in Section 1, the author hereby grants IEEE the unlimited, worldwide, irrevocable right to use his/her name, picture, likeness, voice and biographical information as part of the advertisement, distribution and sale of products incorporating the Work or Presentation, and releases IEEE from any claim based on right of privacy or publicity.

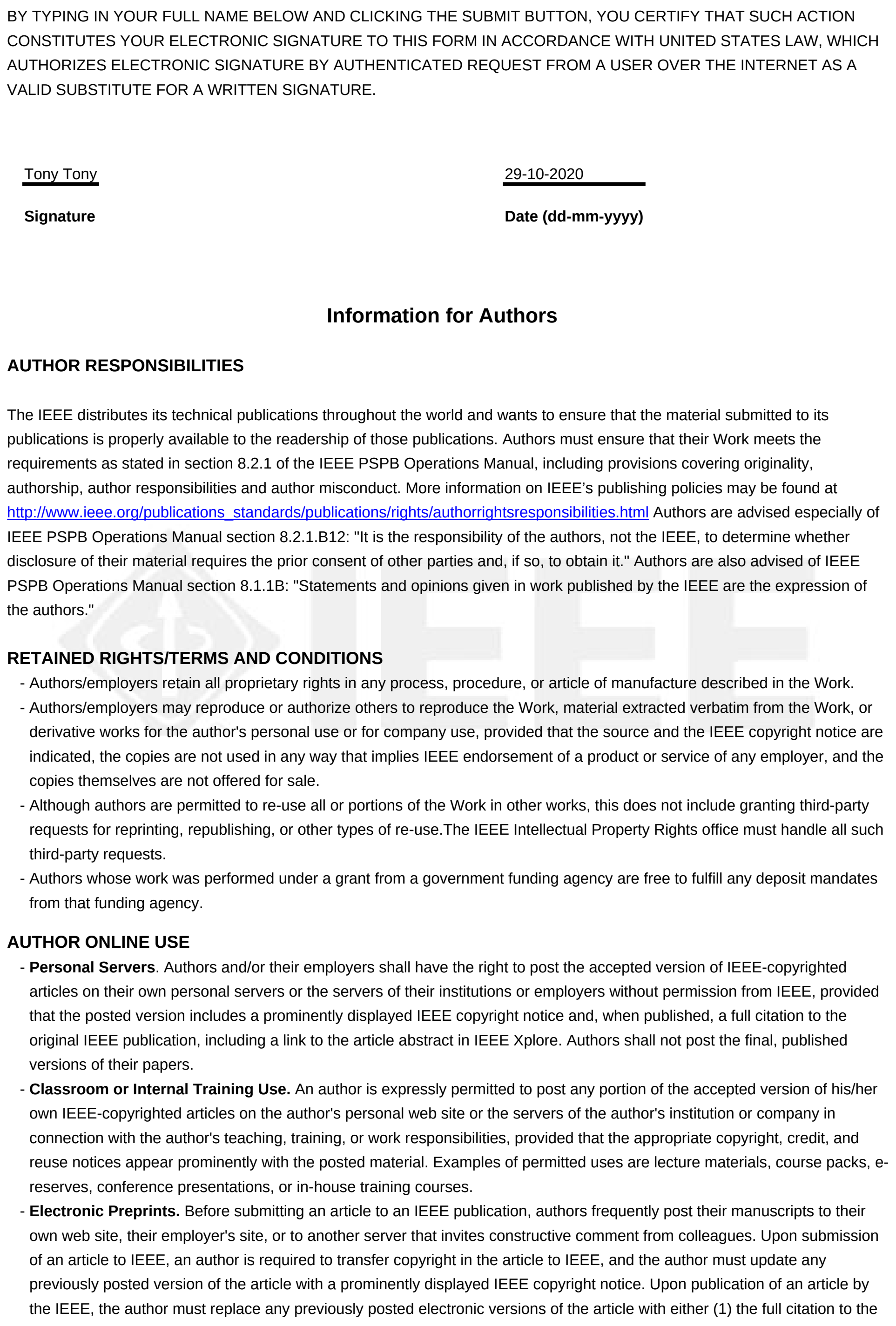

BY TYPING IN YOUR FULL NAME BELOW AND CLICKING THE SUBMIT BUTTON, YOU CERTIFY THAT SUCH ACTION CONSTITUTES YOUR ELECTRONIC SIGNATURE TO THIS FORM IN ACCORDANCE WITH UNITED STATES LAW, WHICH AUTHORIZES ELECTRONIC SIGNATURE BY AUTHENTICATED REQUEST FROM A USER OVER THE INTERNET AS A VALID SUBSTITUTE FOR A WRITTEN SIGNATURE.

Tony Tony	29-10-2020
Signature	**Date (dd-mm-yyyy)**

Information for Authors

AUTHOR RESPONSIBILITIES

The IEEE distributes its technical publications throughout the world and wants to ensure that the material submitted to its publications is properly available to the readership of those publications. Authors must ensure that their Work meets the requirements as stated in section 8.2.1 of the IEEE PSPB Operations Manual, including provisions covering originality, authorship, author responsibilities and author misconduct. More information on IEEE's publishing policies may be found at http://www.ieee.org/publications_standards/publications/rights/authorrightsresponsibilities.html Authors are advised especially of IEEE PSPB Operations Manual section 8.2.1.B12: "It is the responsibility of the authors, not the IEEE, to determine whether disclosure of their material requires the prior consent of other parties and, if so, to obtain it." Authors are also advised of IEEE PSPB Operations Manual section 8.1.1B: "Statements and opinions given in work published by the IEEE are the expression of the authors."

RETAINED RIGHTS/TERMS AND CONDITIONS

- Authors/employers retain all proprietary rights in any process, procedure, or article of manufacture described in the Work.
- Authors/employers may reproduce or authorize others to reproduce the Work, material extracted verbatim from the Work, or derivative works for the author's personal use or for company use, provided that the source and the IEEE copyright notice are indicated, the copies are not used in any way that implies IEEE endorsement of a product or service of any employer, and the copies themselves are not offered for sale.
- Although authors are permitted to re-use all or portions of the Work in other works, this does not include granting third-party requests for reprinting, republishing, or other types of re-use.The IEEE Intellectual Property Rights office must handle all such third-party requests.
- Authors whose work was performed under a grant from a government funding agency are free to fulfill any deposit mandates from that funding agency.

AUTHOR ONLINE USE

- **Personal Servers**. Authors and/or their employers shall have the right to post the accepted version of IEEE-copyrighted articles on their own personal servers or the servers of their institutions or employers without permission from IEEE, provided that the posted version includes a prominently displayed IEEE copyright notice and, when published, a full citation to the original IEEE publication, including a link to the article abstract in IEEE Xplore. Authors shall not post the final, published versions of their papers.
- **Classroom or Internal Training Use.** An author is expressly permitted to post any portion of the accepted version of his/her own IEEE-copyrighted articles on the author's personal web site or the servers of the author's institution or company in connection with the author's teaching, training, or work responsibilities, provided that the appropriate copyright, credit, and reuse notices appear prominently with the posted material. Examples of permitted uses are lecture materials, course packs, e-reserves, conference presentations, or in-house training courses.
- **Electronic Preprints.** Before submitting an article to an IEEE publication, authors frequently post their manuscripts to their own web site, their employer's site, or to another server that invites constructive comment from colleagues. Upon submission of an article to IEEE, an author is required to transfer copyright in the article to IEEE, and the author must update any previously posted version of the article with a prominently displayed IEEE copyright notice. Upon publication of an article by the IEEE, the author must replace any previously posted electronic versions of the article with either (1) the full citation to the

IEEE work with a Digital Object Identifier (DOI) or link to the article abstract in IEEE Xplore, or (2) the accepted version only (not the IEEE-published version), including the IEEE copyright notice and full citation, with a link to the final, published article in IEEE Xplore.

Questions about the submission of the form or manuscript must be sent to the publication's editor.
Please direct all questions about IEEE copyright policy to:
IEEE Intellectual Property Rights Office, copyrights@ieee.org, +1-732-562-3966

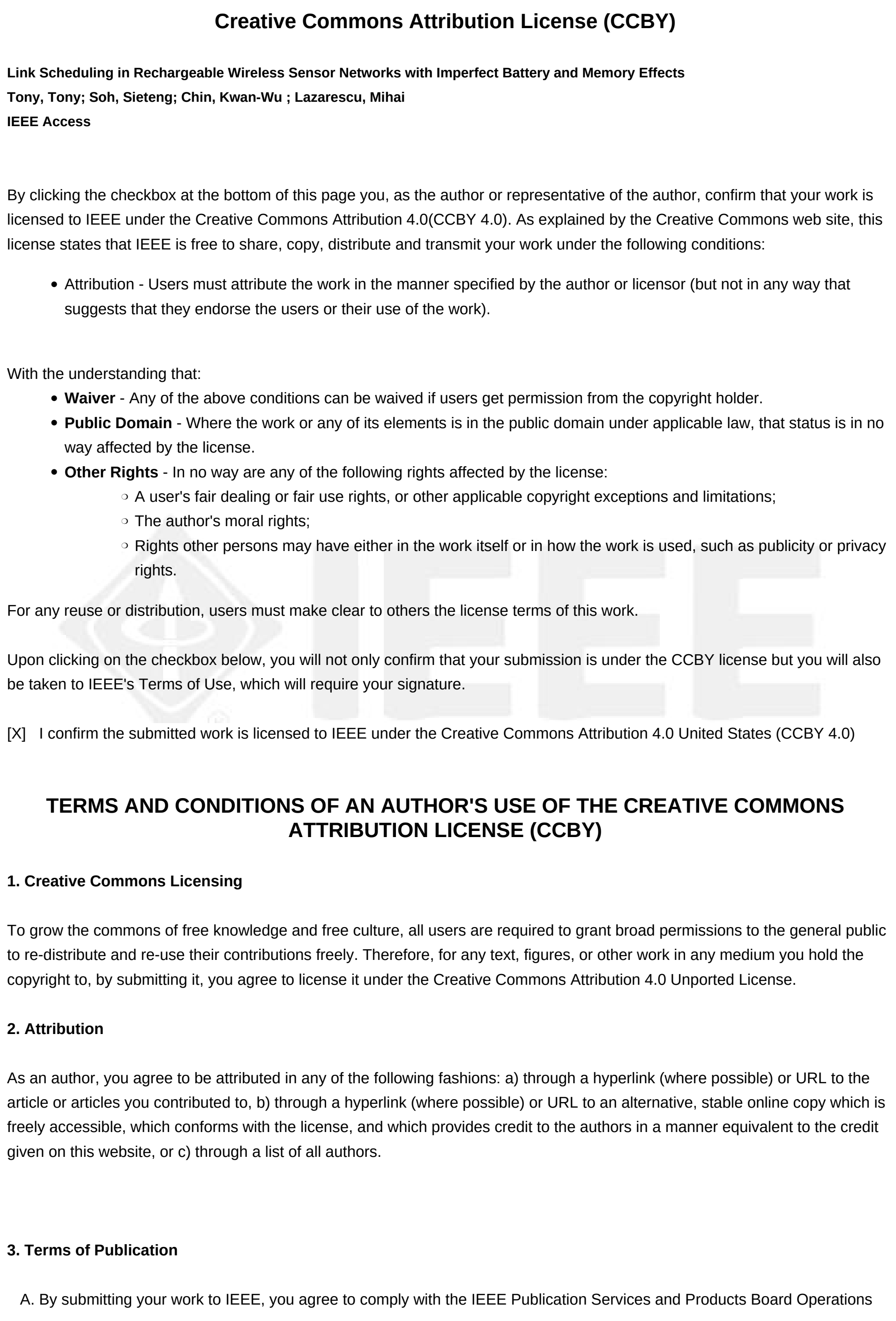

Creative Commons Attribution License (CCBY)

Link Scheduling in Rechargeable Wireless Sensor Networks with Imperfect Battery and Memory Effects
Tony, Tony; Soh, Sieteng; Chin, Kwan-Wu ; Lazarescu, Mihai
IEEE Access

By clicking the checkbox at the bottom of this page you, as the author or representative of the author, confirm that your work is licensed to IEEE under the Creative Commons Attribution 4.0(CCBY 4.0). As explained by the Creative Commons web site, this license states that IEEE is free to share, copy, distribute and transmit your work under the following conditions:

- Attribution - Users must attribute the work in the manner specified by the author or licensor (but not in any way that suggests that they endorse the users or their use of the work).

With the understanding that:

- **Waiver** - Any of the above conditions can be waived if users get permission from the copyright holder.
- **Public Domain** - Where the work or any of its elements is in the public domain under applicable law, that status is in no way affected by the license.
- **Other Rights** - In no way are any of the following rights affected by the license:
    - A user's fair dealing or fair use rights, or other applicable copyright exceptions and limitations;
    - The author's moral rights;
    - Rights other persons may have either in the work itself or in how the work is used, such as publicity or privacy rights.

For any reuse or distribution, users must make clear to others the license terms of this work.

Upon clicking on the checkbox below, you will not only confirm that your submission is under the CCBY license but you will also be taken to IEEE's Terms of Use, which will require your signature.

[X] I confirm the submitted work is licensed to IEEE under the Creative Commons Attribution 4.0 United States (CCBY 4.0)

TERMS AND CONDITIONS OF AN AUTHOR'S USE OF THE CREATIVE COMMONS ATTRIBUTION LICENSE (CCBY)

1. Creative Commons Licensing

To grow the commons of free knowledge and free culture, all users are required to grant broad permissions to the general public to re-distribute and re-use their contributions freely. Therefore, for any text, figures, or other work in any medium you hold the copyright to, by submitting it, you agree to license it under the Creative Commons Attribution 4.0 Unported License.

2. Attribution

As an author, you agree to be attributed in any of the following fashions: a) through a hyperlink (where possible) or URL to the article or articles you contributed to, b) through a hyperlink (where possible) or URL to an alternative, stable online copy which is freely accessible, which conforms with the license, and which provides credit to the authors in a manner equivalent to the credit given on this website, or c) through a list of all authors.

3. Terms of Publication

A. By submitting your work to IEEE, you agree to comply with the IEEE Publication Services and Products Board Operations

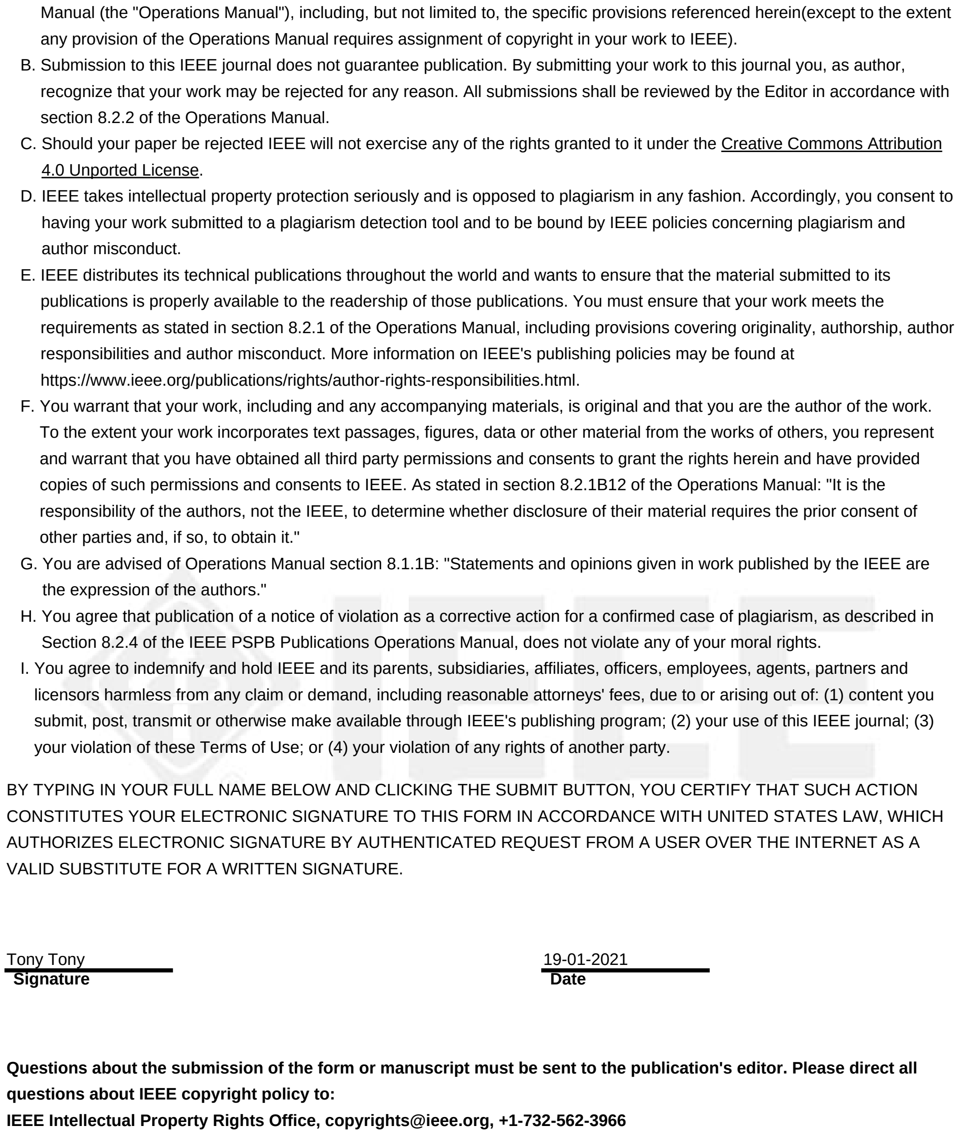

Manual (the "Operations Manual"), including, but not limited to, the specific provisions referenced herein(except to the extent any provision of the Operations Manual requires assignment of copyright in your work to IEEE).

B. Submission to this IEEE journal does not guarantee publication. By submitting your work to this journal you, as author, recognize that your work may be rejected for any reason. All submissions shall be reviewed by the Editor in accordance with section 8.2.2 of the Operations Manual.

C. Should your paper be rejected IEEE will not exercise any of the rights granted to it under the Creative Commons Attribution 4.0 Unported License.

D. IEEE takes intellectual property protection seriously and is opposed to plagiarism in any fashion. Accordingly, you consent to having your work submitted to a plagiarism detection tool and to be bound by IEEE policies concerning plagiarism and author misconduct.

E. IEEE distributes its technical publications throughout the world and wants to ensure that the material submitted to its publications is properly available to the readership of those publications. You must ensure that your work meets the requirements as stated in section 8.2.1 of the Operations Manual, including provisions covering originality, authorship, author responsibilities and author misconduct. More information on IEEE's publishing policies may be found at https://www.ieee.org/publications/rights/author-rights-responsibilities.html.

F. You warrant that your work, including and any accompanying materials, is original and that you are the author of the work. To the extent your work incorporates text passages, figures, data or other material from the works of others, you represent and warrant that you have obtained all third party permissions and consents to grant the rights herein and have provided copies of such permissions and consents to IEEE. As stated in section 8.2.1B12 of the Operations Manual: "It is the responsibility of the authors, not the IEEE, to determine whether disclosure of their material requires the prior consent of other parties and, if so, to obtain it."

G. You are advised of Operations Manual section 8.1.1B: "Statements and opinions given in work published by the IEEE are the expression of the authors."

H. You agree that publication of a notice of violation as a corrective action for a confirmed case of plagiarism, as described in Section 8.2.4 of the IEEE PSPB Publications Operations Manual, does not violate any of your moral rights.

I. You agree to indemnify and hold IEEE and its parents, subsidiaries, affiliates, officers, employees, agents, partners and licensors harmless from any claim or demand, including reasonable attorneys' fees, due to or arising out of: (1) content you submit, post, transmit or otherwise make available through IEEE's publishing program; (2) your use of this IEEE journal; (3) your violation of these Terms of Use; or (4) your violation of any rights of another party.

BY TYPING IN YOUR FULL NAME BELOW AND CLICKING THE SUBMIT BUTTON, YOU CERTIFY THAT SUCH ACTION CONSTITUTES YOUR ELECTRONIC SIGNATURE TO THIS FORM IN ACCORDANCE WITH UNITED STATES LAW, WHICH AUTHORIZES ELECTRONIC SIGNATURE BY AUTHENTICATED REQUEST FROM A USER OVER THE INTERNET AS A VALID SUBSTITUTE FOR A WRITTEN SIGNATURE.

Tony Tony	19-01-2021
Signature	**Date**

Questions about the submission of the form or manuscript must be sent to the publication's editor. Please direct all questions about IEEE copyright policy to:
IEEE Intellectual Property Rights Office, copyrights@ieee.org, +1-732-562-3966

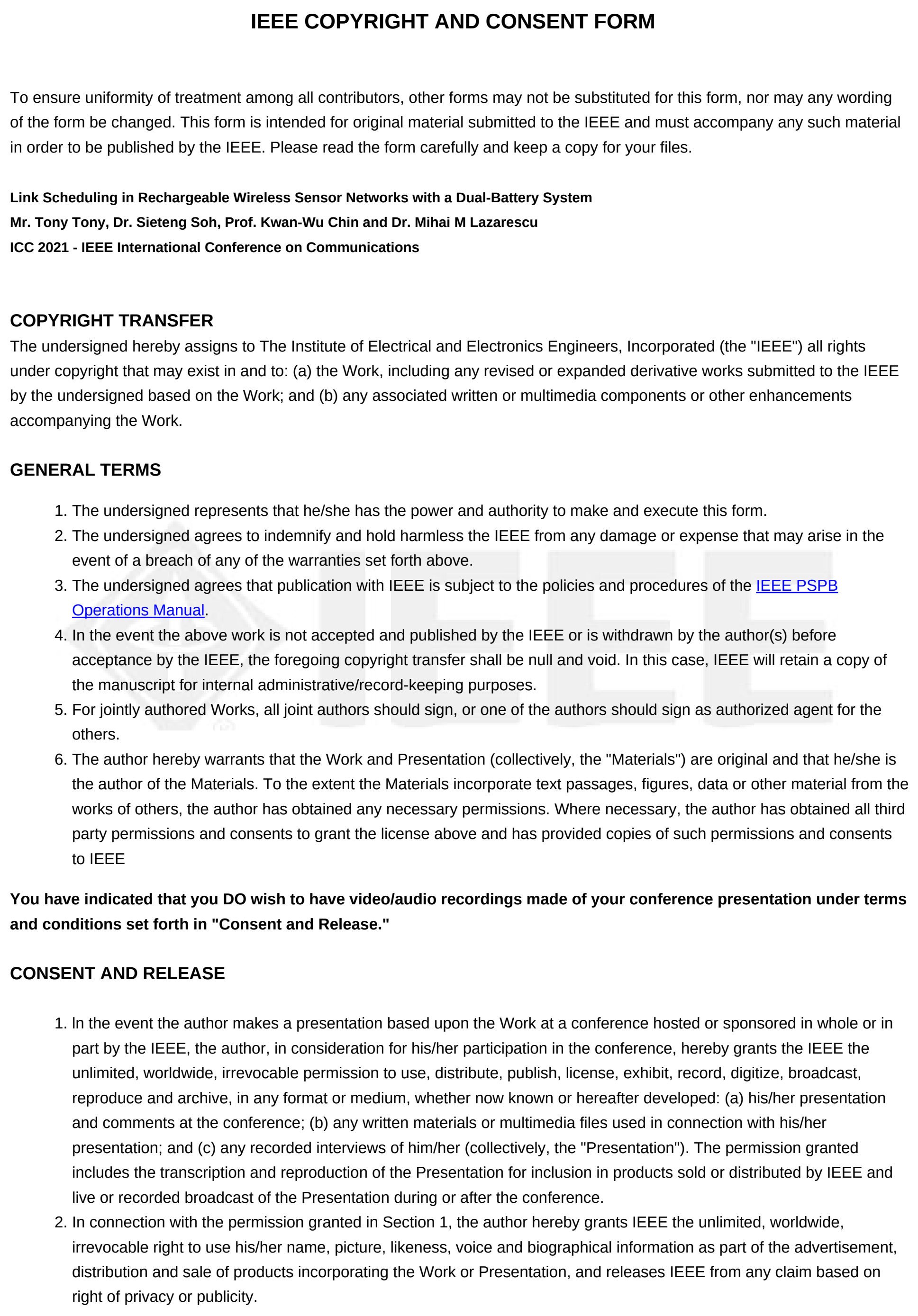

IEEE COPYRIGHT AND CONSENT FORM

To ensure uniformity of treatment among all contributors, other forms may not be substituted for this form, nor may any wording of the form be changed. This form is intended for original material submitted to the IEEE and must accompany any such material in order to be published by the IEEE. Please read the form carefully and keep a copy for your files.

Link Scheduling in Rechargeable Wireless Sensor Networks with a Dual-Battery System
Mr. Tony Tony, Dr. Sieteng Soh, Prof. Kwan-Wu Chin and Dr. Mihai M Lazarescu
ICC 2021 - IEEE International Conference on Communications

COPYRIGHT TRANSFER

The undersigned hereby assigns to The Institute of Electrical and Electronics Engineers, Incorporated (the "IEEE") all rights under copyright that may exist in and to: (a) the Work, including any revised or expanded derivative works submitted to the IEEE by the undersigned based on the Work; and (b) any associated written or multimedia components or other enhancements accompanying the Work.

GENERAL TERMS

1. The undersigned represents that he/she has the power and authority to make and execute this form.
2. The undersigned agrees to indemnify and hold harmless the IEEE from any damage or expense that may arise in the event of a breach of any of the warranties set forth above.
3. The undersigned agrees that publication with IEEE is subject to the policies and procedures of the IEEE PSPB Operations Manual.
4. In the event the above work is not accepted and published by the IEEE or is withdrawn by the author(s) before acceptance by the IEEE, the foregoing copyright transfer shall be null and void. In this case, IEEE will retain a copy of the manuscript for internal administrative/record-keeping purposes.
5. For jointly authored Works, all joint authors should sign, or one of the authors should sign as authorized agent for the others.
6. The author hereby warrants that the Work and Presentation (collectively, the "Materials") are original and that he/she is the author of the Materials. To the extent the Materials incorporate text passages, figures, data or other material from the works of others, the author has obtained any necessary permissions. Where necessary, the author has obtained all third party permissions and consents to grant the license above and has provided copies of such permissions and consents to IEEE

You have indicated that you DO wish to have video/audio recordings made of your conference presentation under terms and conditions set forth in "Consent and Release."

CONSENT AND RELEASE

1. In the event the author makes a presentation based upon the Work at a conference hosted or sponsored in whole or in part by the IEEE, the author, in consideration for his/her participation in the conference, hereby grants the IEEE the unlimited, worldwide, irrevocable permission to use, distribute, publish, license, exhibit, record, digitize, broadcast, reproduce and archive, in any format or medium, whether now known or hereafter developed: (a) his/her presentation and comments at the conference; (b) any written materials or multimedia files used in connection with his/her presentation; and (c) any recorded interviews of him/her (collectively, the "Presentation"). The permission granted includes the transcription and reproduction of the Presentation for inclusion in products sold or distributed by IEEE and live or recorded broadcast of the Presentation during or after the conference.
2. In connection with the permission granted in Section 1, the author hereby grants IEEE the unlimited, worldwide, irrevocable right to use his/her name, picture, likeness, voice and biographical information as part of the advertisement, distribution and sale of products incorporating the Work or Presentation, and releases IEEE from any claim based on right of privacy or publicity.

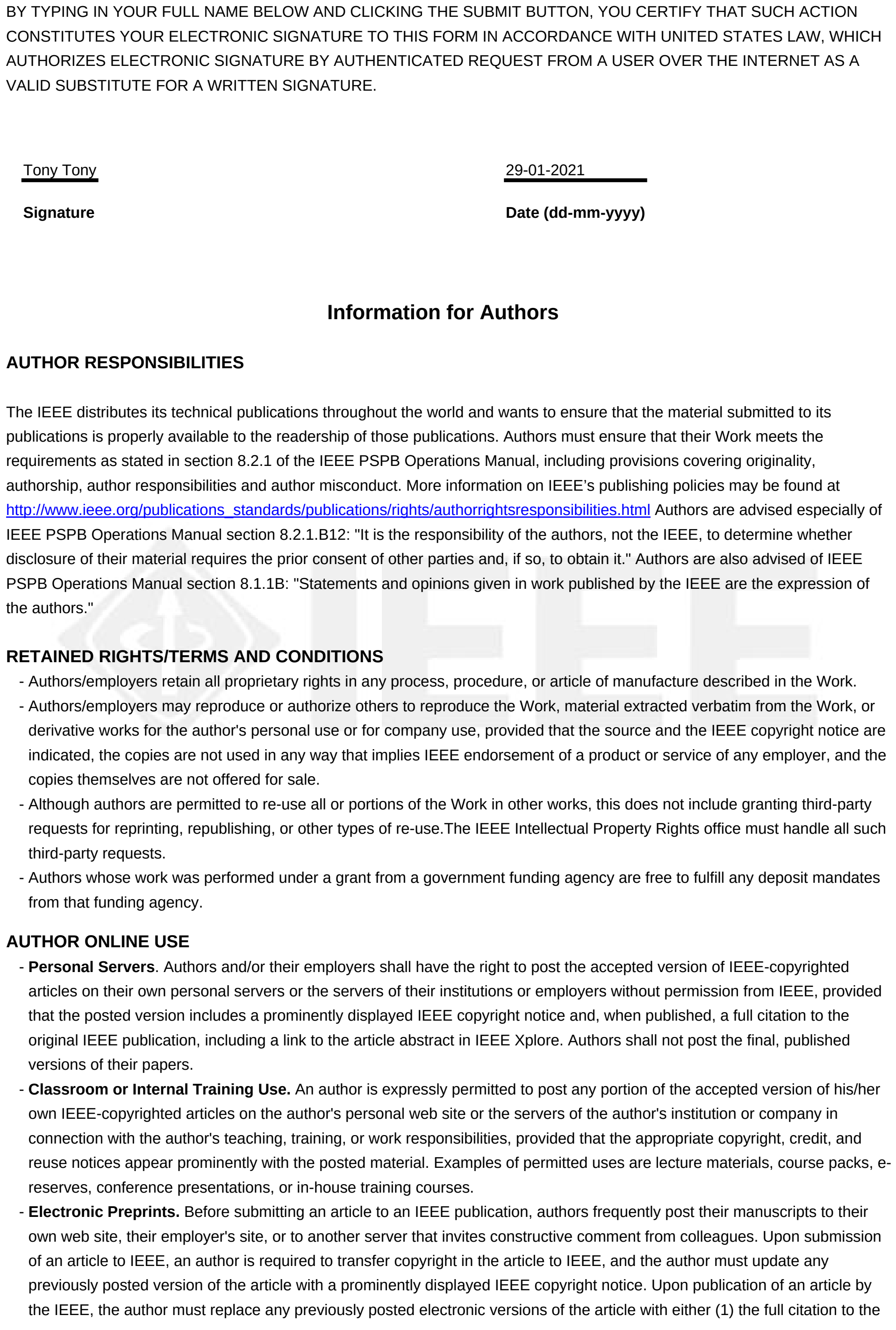

BY TYPING IN YOUR FULL NAME BELOW AND CLICKING THE SUBMIT BUTTON, YOU CERTIFY THAT SUCH ACTION CONSTITUTES YOUR ELECTRONIC SIGNATURE TO THIS FORM IN ACCORDANCE WITH UNITED STATES LAW, WHICH AUTHORIZES ELECTRONIC SIGNATURE BY AUTHENTICATED REQUEST FROM A USER OVER THE INTERNET AS A VALID SUBSTITUTE FOR A WRITTEN SIGNATURE.

Tony Tony	29-01-2021
Signature	**Date (dd-mm-yyyy)**

Information for Authors

AUTHOR RESPONSIBILITIES

The IEEE distributes its technical publications throughout the world and wants to ensure that the material submitted to its publications is properly available to the readership of those publications. Authors must ensure that their Work meets the requirements as stated in section 8.2.1 of the IEEE PSPB Operations Manual, including provisions covering originality, authorship, author responsibilities and author misconduct. More information on IEEE's publishing policies may be found at http://www.ieee.org/publications_standards/publications/rights/authorrightsresponsibilities.html Authors are advised especially of IEEE PSPB Operations Manual section 8.2.1.B12: "It is the responsibility of the authors, not the IEEE, to determine whether disclosure of their material requires the prior consent of other parties and, if so, to obtain it." Authors are also advised of IEEE PSPB Operations Manual section 8.1.1B: "Statements and opinions given in work published by the IEEE are the expression of the authors."

RETAINED RIGHTS/TERMS AND CONDITIONS

- Authors/employers retain all proprietary rights in any process, procedure, or article of manufacture described in the Work.
- Authors/employers may reproduce or authorize others to reproduce the Work, material extracted verbatim from the Work, or derivative works for the author's personal use or for company use, provided that the source and the IEEE copyright notice are indicated, the copies are not used in any way that implies IEEE endorsement of a product or service of any employer, and the copies themselves are not offered for sale.
- Although authors are permitted to re-use all or portions of the Work in other works, this does not include granting third-party requests for reprinting, republishing, or other types of re-use.The IEEE Intellectual Property Rights office must handle all such third-party requests.
- Authors whose work was performed under a grant from a government funding agency are free to fulfill any deposit mandates from that funding agency.

AUTHOR ONLINE USE

- **Personal Servers**. Authors and/or their employers shall have the right to post the accepted version of IEEE-copyrighted articles on their own personal servers or the servers of their institutions or employers without permission from IEEE, provided that the posted version includes a prominently displayed IEEE copyright notice and, when published, a full citation to the original IEEE publication, including a link to the article abstract in IEEE Xplore. Authors shall not post the final, published versions of their papers.
- **Classroom or Internal Training Use.** An author is expressly permitted to post any portion of the accepted version of his/her own IEEE-copyrighted articles on the author's personal web site or the servers of the author's institution or company in connection with the author's teaching, training, or work responsibilities, provided that the appropriate copyright, credit, and reuse notices appear prominently with the posted material. Examples of permitted uses are lecture materials, course packs, e-reserves, conference presentations, or in-house training courses.
- **Electronic Preprints.** Before submitting an article to an IEEE publication, authors frequently post their manuscripts to their own web site, their employer's site, or to another server that invites constructive comment from colleagues. Upon submission of an article to IEEE, an author is required to transfer copyright in the article to IEEE, and the author must update any previously posted version of the article with a prominently displayed IEEE copyright notice. Upon publication of an article by the IEEE, the author must replace any previously posted electronic versions of the article with either (1) the full citation to the

IEEE work with a Digital Object Identifier (DOI) or link to the article abstract in IEEE Xplore, or (2) the accepted version only (not the IEEE-published version), including the IEEE copyright notice and full citation, with a link to the final, published article in IEEE Xplore.

Questions about the submission of the form or manuscript must be sent to the publication's editor.
Please direct all questions about IEEE copyright policy to:
IEEE Intellectual Property Rights Office, copyrights@ieee.org, +1-732-562-3966

Bibliography

[1] P. Djukic and S. Valaee, “Delay aware link scheduling for multi-hop TDMA wireless networks,” *IEEE/ACM Trans. Netw.*, vol. 17, no. 3, pp. 870–883, Jun. 2009.

[2] J. Taneja, J. Jeong, and D. Culler, “Design, modeling, and capacity planning for micro-solar power sensor networks,” in *7th Int. Conf. Inform. Process. Sensor Netw. (IPSN)*, St. Louis, MO, USA, Apr. 2008, pp. 407–418.

[3] M. Kocakulak and I. Butun, “An overview of wireless sensor networks towards internet of things,” in *IEEE 7th Annual Comput. Commun. Workshop Conf. (CCWC)*, Las Vegas, NV, USA, Jan. 2017, pp. 1–6.

[4] D. Kandris, C. Nakas, D. Vomvas, and G. Koulouras, “Applications of wireless sensor networks: an up-to-date survey,” *Applied System Innovation*, vol. 3, no. 1, p. 14, 2020.

[5] M. P. Đurišić, Z. Tafa, G. Dimić, and V. Milutinović, “A survey of military applications of wireless sensor networks,” in *1st Mediterranean Conf. Embedded Comput. (MECO)*, Bar, Montenegro, Jun. 2012, pp. 196–199.

[6] A. M. Mainwaring, D. E. Culler, J. Polastre, R. Szewczyk, and J. Anderson, "Wireless sensor networks for habitat monitoring," in *Proc. 1st ACM Int. Workshop Wireless Sensor Netw. Applicat. (WSNA)*, Atlanta, GA, USA, Sep. 2002, pp. 88–97.

[7] T. Naumowicz, R. Freeman, H. Kirk, B. Dean, M. Calsyn, A. Liers, A. Braendle, T. Guilford, and J. Schiller, "Wireless sensor network for habitat monitoring on Skomer Island," in *35th IEEE Conf. Local Comput. Netw. (LCN)*, Denver, CO, USA, Oct. 2010, pp. 882–889.

[8] A. Tovar, T. Friesen, K. Ferens, and B. McLeod, "A DTN wireless sensor network for wildlife habitat monitoring," in *Proc. 23rd Canadian Conf. Elect. Comput. Eng. (CCECE)*, Calgary, AB, Canada, May 2010, pp. 1–5.

[9] A. Boubrima, W. Bechkit, and H. Rivano, "Optimal WSN deployment models for air pollution monitoring," *IEEE Trans. Wireless Commun.*, vol. 16, no. 5, pp. 2723–2735, May 2017.

[10] K. S. Adu-Manu, C. Tapparello, W. Heinzelman, F. A. Katsriku, and J.-D. Abdulai, "Water quality monitoring using wireless sensor networks: Current trends and future research directions," *ACM Trans. Sensor Netw. (TOSN)*, vol. 13, no. 1, pp. 1–41, Jan. 2017.

[11] G. R. Teja, V. Harish, D. N. M. Khan, R. B. Krishna, R. Singh, and S. Chaudhary, "Land slide detection and monitoring system using wireless sensor networks (WSN)," in *IEEE Int. Adv. Comput. Conf. (IACC)*, Gurgaon, India, Feb. 2014, pp. 149–154.

[12] I. Hakala, M. Tikkakoski, and I. Kivelä, "Wireless sensor network in environmental monitoring-case foxhouse," in *2nd Int. Conf. Sensor Technol. Applicat. (SensorComm)*, Cap Esterel, France, Aug. 2008, pp. 202–208.

[13] F. Walid and T. Ezzedine, "Design of a climate monitoring system based on sensor network," in *13th Int. Wireless Commun. Mobile Comput. Conf. (IWCMC)*, Valencia, Spain, Jun. 2017, pp. 1791–1796.

[14] A. Pantelopoulos and N. G. Bourbakis, "A survey on wearable sensor-based systems for health monitoring and prognosis," *IEEE Trans. Syst. Man Cybern. C, Appl. Rev.*, vol. 40, no. 1, pp. 1–12, Jan. 2010.

[15] J. Ko, C. Lu, M. B. Srivastava, J. A. Stankovic, A. Terzis, and M. Welsh, "Wireless sensor networks for healthcare," *Proc. IEEE*, vol. 98, no. 11, pp. 1947–1960, Nov. 2010.

[16] D. Surie, O. Laguionie, and T. Pederson, "Wireless sensor networking of everyday objects in a smart home environment," in *IEEE Int. Conf. Intell. Sensors Sensor Netw. Inform. Process. (ISSNIP)*, Sydney, NSW, Australia, Dec. 2008, pp. 189–194.

[17] S. Hussain, S. Schaffner, and D. Moseychuck, "Applications of wireless sensor networks and RFID in a smart home environment," in *7th Annual Conf. Commun. Netw. Service Research (CNSR)*, Moncton, NB, Canada, May 2009, pp. 153–157.

[18] N. Vikram, K. Harish, M. Nihaal, R. Umesh, and S. A. A. Kumar, "A low cost home automation system using Wi-Fi based wireless sensor network incorporating Internet of Things (IoT)," in *7th IEEE Int. Adv. Comput. Conf. (IACC)*, Hyderabad, India, Jan. 2017, pp. 174–178.

[19] C. Gomez and J. Paradells, "Wireless home automation networks: A survey of architectures and technologies," *IEEE Commun. Mag.*, vol. 48, no. 6, pp. 92–101, Jun. 2010.

[20] K. Khakpour and M. Shenassa, "Industrial control using wireless sensor networks," in *3^{rd} Int. Conf. Inform. Commun. Technol.: From Theory to Applicat. (ICTTA)*, Damascus, Syria, Apr. 2008, pp. 1–5.

[21] V. J. Hodge, S. O'Keefe, M. Weeks, and A. Moulds, "Wireless sensor networks for condition monitoring in the railway industry: A survey," *IEEE Trans. Intell. Transp. Syst.*, vol. 16, no. 3, pp. 1088–1106, Jun. 2015.

[22] M. Gao, P. Wang, Y. Wang, and L. Yao, "Self-powered ZigBee wireless sensor nodes for railway condition monitoring," *IEEE Trans. Intell. Transp. Syst.*, vol. 19, no. 3, pp. 900–909, Mar. 2018.

[23] A. Wheeler, "Commercial applications of wireless sensor networks using ZigBee," *IEEE Commun. Mag.*, vol. 45, no. 4, pp. 70–77, Apr. 2007.

[24] L. Xie, "Modeling and optimization of rechargeable sensor networks," Ph.D. dissertation, Dept. of Electr. Comput. Eng., Virginia Polytechnic Institute and State University, USA, 2013.

[25] C. Yang, "Link scheduling in multi-transmit-receive wireless mesh networks," Ph.D. dissertation, School of Electron. Comput. Telecommun. Eng., University of Wollongong, Australia, 2015.

[26] M. Aboelaze and F. Aloul, "Current and future trends in sensor networks: a survey," in *2^{nd} IFIP Int. Conf. Wireless Opt. Commun. Netw. (WOCN)*, Dubai, United Arab Emirates, Mar. 2005, pp. 551–555.

[27] F. K. Shaikh and S. Zeadally, "Energy harvesting in wireless sensor networks: A comprehensive review," *Renewable Sustain. Energy Rev.*, vol. 55, pp. 1041–1054, Mar. 2016.

[28] N. A. Pantazis, S. A. Nikolidakis, and D. D. Vergados, “Energy-efficient routing protocols in wireless sensor networks: A survey,” *IEEE Commun. Surveys Tuts.*, vol. 15, no. 2, pp. 551–591, Second Quarter 2013.

[29] S. Bi, Y. Zeng, and R. Zhang, “Wireless powered communication networks: An overview,” *IEEE Wireless Commun.*, vol. 23, no. 2, pp. 10–18, Apr. 2016.

[30] A. Karalis, J. D. Joannopoulos, and M. Soljačić, “Efficient wireless non-radiative mid-range energy transfer,” *Ann. Physics*, vol. 323, no. 1, pp. 34–48, Jan. 2008.

[31] M. K. Watfa, H. Al-Hassanieh, and S. Salmen, “The road to immortal sensor nodes,” in *IEEE Int. Conf. Intell. Sensors Sensor Netw. Inform. Process. (ISSNIP)*, Sydney, NSW, Australia, Dec. 2008, pp. 523–528.

[32] S. Sudevalayam and P. Kulkarni, “Energy harvesting sensor nodes: Survey and implications,” *IEEE Commun. Surveys Tuts.*, vol. 13, no. 3, pp. 443–461, Third Quarter 2011.

[33] H. Kim, Y. Tadesse, and S. Priya, *Piezoelectric Energy Harvesting, in Energy Harvesting Technologies*, S. Priya and D. J. Inman, Eds. New York: Springer, 2009.

[34] Crossbow, *Mica2 Wireless Measurement System*, 2016 (accessed Nov. 1, 2017). [Online]. Available: https://www.iba.edu.pk/trl/News/mica2.pdf

[35] R. A. Huggins, “Mechanism of the memory effect in ”Nickel” electrodes,” *Solid State Ionics*, vol. 177, no. 26-32, pp. 2643–2646, Oct. 2006.

[36] R. V. Bhat, M. Motani, C. R. Murthy, and R. Vaze, "Energy harvesting communications with batteries having cycle constraints," *IEEE Trans. Green Commun. Netw.*, vol. 4, no. 1, pp. 263–276, Mar. 2020.

[37] R. V. Bhat, M. Motani, C. R. Murthy, and R. Vaze, "Energy harvesting communications using dual alternating batteries," *arXiv preprint arXiv:1801.03813*, 2018.

[38] M. I. Hlal, V. K. Ramachandaramurthy, A. Sarhan, A. Pouryekta, and U. Subramaniam, "Optimum battery depth of discharge for off-grid solar PV/battery system," *J. Energy Storage*, vol. 26, Dec. 2019.

[39] J. Yang and J. Wu, "Optimal transmission for energy harvesting nodes under battery size and usage constraints," in *IEEE Int. Symp. Inform. Theory (ISIT)*, Aachen, Germany, Jun. 2017, pp. 819–823.

[40] S. Gandham, M. Dawande, and R. Prakash, "Link scheduling in wireless sensor networks: Distributed edge-coloring revisited," *J. Parallel Distrib. Comput.*, vol. 68, no. 8, pp. 1122–1134, Aug. 2008.

[41] I. Demilkor, C. Ersoy, and F. Alagoz, "MAC protocols for wireless sensor networks: A survey," *IEEE Commun. Mag.*, vol. 4, pp. 115–121, Apr. 2006.

[42] A. D. Gore and A. Karandikar, "Link scheduling algorithms for wireless mesh networks," *IEEE Commun. Surveys Tuts.*, vol. 13, no. 2, pp. 258–273, Second Quarter 2011.

[43] B. Hajek and G. Sasaki, "Link scheduling in polynomial time," *IEEE Trans. Inf. Theory*, vol. 34, no. 5, pp. 910–917, Sep. 1988.

[44] G. Sun, G. Qiao, and L. Zhao, “Efficient link scheduling for rechargeable wireless ad hoc and sensor networks,” *EURASIP J. Wireless Commun. Netw.*, vol. 2013, no. 223, pp. 1–14, 2013.

[45] L. Belkhir and A. Elmeligi, “Assessing ict global emissions footprint: Trends to 2040 & recommendations,” *Journal of Cleaner Production*, vol. 177, pp. 448–463, 2018.

[46] M. A. Razzaque and S. Dobson, “Energy-efficient sensing in wireless sensor networks using compressed sensing,” *Sensors*, vol. 14, no. 2, pp. 2822–2859, Feb. 2014.

[47] J.-P. Vasseur and A. Dunkels, *Smart object hardware and software, in Interconnecting Smart Objects with IP.* San Francisco: Morgan Kaufmann, 2010.

[48] J. Suhonen, M. Kohvakka, V. Kaseva, T. D. Hämäläinen, and M. Hännikäinen, *Low-Power Wireless Sensor Networks: Protocols, Services and Applications.* New York: Springer, 2010.

[49] R. Atallah, M. Khabbaz, and C. Assi, “Energy harvesting in vehicular networks: A contemporary survey,” *IEEE Wireless Commun.*, vol. 23, no. 2, pp. 70–77, Apr. 2016.

[50] C. Knight, J. Davidson, and S. Behrens, “Energy options for wireless sensor nodes,” *Sensors*, vol. 8, no. 12, pp. 8037–8066, Dec. 2008.

[51] M.-L. Ku, W. Li, Y. Chen, and K. J. R. Liu, “Advances in energy harvesting communications: Past, present, and future challenges,” *IEEE Commun. Surveys Tuts.*, vol. 18, no. 2, pp. 1384–1412, Second Quarter 2016.

[52] I. Krikidis, G. Zheng, and B. Ottersten, "Harvest-use cooperative networks with half/full-duplex relaying," in *IEEE Wireless Commun. Net. Conf. (WCNC)*, Shanghai, China, Apr. 2013, pp. 4256–4260.

[53] N. Michelusi, L. Badia, and M. Zorzi, "Optimal transmission policies for energy harvesting devices with limited state-of-charge knowledge," *IEEE Trans. Commun.*, vol. 62, no. 11, pp. 3969–3982, Nov. 2014.

[54] S. Reddy and C. R. Murthy, "Dual-stage power management algorithms for energy harvesting sensors," *IEEE Trans. Wireless Commun.*, vol. 11, no. 4, pp. 1434–1445, Apr. 2012.

[55] X. Kang, Y.-K. Chia, C. K. Ho, and S. Sun, "Cost minimization for fading channels with energy harvesting and conventional energy," *IEEE Trans. Wireless Commun.*, vol. 13, no. 8, pp. 4586–4598, Aug. 2014.

[56] O. Ozel, K. Shahzad, and S. Ulukus, "Optimal energy allocation for energy harvesting transmitters with hybrid energy storage and processing cost," *IEEE Trans. Signal Process.*, vol. 62, no. 12, pp. 3232–3245, Jun. 2014.

[57] P. Cardieri, "Modeling interference in wireless ad hoc networks," *IEEE Commun. Surveys Tuts.*, vol. 12, no. 4, pp. 551–572, Fourth Quarter 2010.

[58] S. Ramanathan, "A unified framework and algorithm for channel assignment in wireless networks," *Wireless Netw.*, vol. 5, no. 2, pp. 81–94, Mar. 1999.

[59] K. Jain, J. Padhye, V. N. Padmanabhan, and L. Qiu, "Impact of interference on multi-hop wireless network performance," *Wireless Netw.*, vol. 11, no. 4, pp. 471–487, Jul. 2005.

[60] Y. Wang, W. Wang, X.-Y. Li, and W.-Z. Song, "Interference-aware joint routing and TDMA link scheduling for static wireless networks," *IEEE Trans. Parallel Distrib. Syst.*, vol. 19, no. 12, pp. 1709–1726, Dec. 2008.

[61] W. Ye, J. Heidemann, and D. Estrin, "An energy-efficient MAC protocol for wireless sensor networks," in *Proc. IEEE INFOCOM, 21st Annual Joint Conf. IEEE Comput. Commun. Societies*, New York, NY, USA, Jun. 2002, pp. 1567–1576.

[62] M. Hadded, P. Muhlethaler, A. Laouiti, R. Zagrouba, and L. A. Saidane, "TDMA-based MAC protocols for vehicular ad hoc networks: a survey, qualitative analysis, and open research issues," *IEEE Commun. Surveys Tuts.*, vol. 17, no. 4, pp. 2461–2492, Fourth Quarter 2015.

[63] L. Wang, "Link scheduling in multi-transmit-receive wireless mesh networks," Ph.D. dissertation, School of. Electron. Comput. Telecommun. Eng., University of Wollongong, Australia, 2015.

[64] A. Sgora, D. J. Vergados, and D. D. Vergados, "A survey of TDMA scheduling schemes in wireless multihop networks," *ACM Comput. Surveys (CSUR)*, vol. 47, no. 3, pp. 1–39, Apr. 2015.

[65] S. C. Ergen and P. Varaiya, "TDMA scheduling algorithms for wireless sensor networks," *Wireless Netw.*, vol. 16, no. 4, pp. 985–997, May 2010.

[66] S. Chilukuri and A. Sahoo, "Delay-aware TDMA scheduling for multi-hop wireless networks," in *Proc. Int. Conf. Distrib. Comput. Netw. (ICDCN)*, Goa, India, Jan. 2015, pp. 1–10.

[67] J. Long, M. Dong, K. Ota, and A. Liu, "A green TDMA scheduling algorithm for prolonging lifetime in wireless sensor networks," *IEEE Syst. J.*, vol. 11, no. 2, pp. 868–877, Jun. 2017.

[68] P. Djukic and S. Valaee, "Distributed link scheduling for TDMA mesh networks," in *Proc. IEEE Int. Conf. Commun. (ICC)*, Glasgow, Scotland, UK, Jun. 2007, pp. 3823–3828.

[69] I. Rhee, A. Warrier, J. Min, and L. Xu, "DRAND: Distributed randomized TDMA scheduling for wireless ad hoc networks," *IEEE Trans. Mobile Comput.*, vol. 8, no. 10, pp. 1384–1396, Oct. 2009.

[70] D. Enqing, Q. Fulong, W. Jiaren, Z. Zongjun, Z. Dejing, and S. Huakui, "An energy efficient distributed link scheduling protocol for wireless sensor networks," in *IEEE 28th Convention Electr. Electron. Engineers in Israel (IEEEI)*, Eilat, Israel, Dec. 2014, pp. 1–4.

[71] Y. Li, X. Zhang, J. Zeng, Y. Wan, and F. Ma, "A distributed TDMA scheduling algorithm based on energy-topology factor in Internet of Things," *IEEE Access*, vol. 5, pp. 10 757–10 768, 2017.

[72] S. Guan, J. Zhang, Z. Song, B. Zhao, and Y. Li, "Energy-saving link scheduling in energy harvesting wireless multihop networks with the non-ideal battery," *IEEE Access*, vol. 8, pp. 144 027–144 038, 2020.

[73] F. Yuan, Q. T. Zhang, S. Jin, and H. Zhu, "Optimal harvest-use-store strategy for energy harvesting wireless systems," *IEEE Trans. Wireless Commun.*, vol. 14, no. 2, pp. 698–710, Feb. 2015.

[74] F. Yuan, S. Jin, K.-K. Wong, Q. T. Zhang, and H. Zhu, “Optimal harvest-use-store design for delay-constrained energy harvesting wireless communications,” *J. Commun. Netw.*, vol. 18, no. 6, pp. 902–912, Dec. 2016.

[75] B. Devillers and D. Gündüz, “A general framework for the optimization of energy harvesting communication systems with battery imperfections,” *J. Commun. Netw.*, vol. 14, no. 2, pp. 130–139, Apr. 2012.

[76] A. Biason and M. Zorzi, “On the effects of battery imperfections in an energy harvesting device,” in *Int. Conf. Comput. Netw. Commun. (ICNC)*, Kauai, HI, USA, Feb. 2016, pp. 1–7.

[77] K. Tutuncuoglu, A. Yener, and S. Ulukus, “Optimum policies for an energy harvesting transmitter under energy storage losses,” *IEEE J. Sel. Areas Commun.*, vol. 33, no. 3, pp. 467–481, Mar. 2015.

[78] J. Liu, H. Dai, and W. Chen, “On throughput maximization of time division multiple access with energy harvesting users,” *IEEE Trans. Veh. Technol.*, vol. 65, no. 4, pp. 2457–2470, Apr. 2016.

[79] S. Kapoor and S. R. B. Pillai, “Distributed scheduling schemes in energy harvesting multiple access,” *IEEE Wireless Commun. Lett.*, vol. 6, no. 1, pp. 54–57, Feb. 2017.

[80] M. R. Lenka, A. R. Swain, and M. N. Sahoo, “Distributed slot scheduling algorithm for hybrid CSMA/TDMA MAC in wireless sensor networks,” in *IEEE Int. Conf. Netw. Archit. Storage (NAS)*, Long Beach, CA, USA, Aug. 2016.

[81] T. He, K. Chin, S. Soh, and C. Yang, "On optimizing max min rate in rechargeable wireless sensor networks with energy sharing," *IEEE Trans. Sustain. Comput.*, vol. 5, no. 1, pp. 107 – 120, 2020.

[82] K. Li, C. Yuen, B. Kusy, R. Jurdak, A. Ignatovic, S. Kanhere, and S. K. Jha, "Fair scheduling for data collection in mobile sensor networks with energy harvesting," *IEEE Trans. Mobile Comput.*, vol. 18, no. 6, pp. 1274 – 1287, Jun. 2019.

[83] Y. Liu, K.-Y. Lam, S. Han, and Q. Chen, "Mobile data gathering and energy harvesting in rechargeable wireless sensor networks," *Inf. Sci.*, vol. 482, pp. 189–209, May 2019.

[84] Y. Gao, X. Li, J. Li, and Y. Gao, "Distributed and efficient minimum-latency data aggregation scheduling for multichannel wireless sensor networks," *IEEE Internet Things J.*, vol. 6, no. 5, pp. 8482–8495, 2019.

[85] R. E. Moraes, W. W. dos Reis, H. R. Rocha, and D. J. Coura, "Power-efficient and interference-free link scheduling algorithms for connected wireless sensor networks," *Wireless Networks*, pp. 1–20, 2019.

[86] K. Yu, Y. Wang, J. Yu, D. Yu, X. Cheng, and Z. Shan, "Localized and distributed link scheduling algorithms in IoT under Rayleigh fading," *Computer Networks*, vol. 151, pp. 232–244, 2019.

[87] J. A. Bondy and U. S. R. Murty, *Graph Theory With Applications.* New York: American Elsevier, 1976.

[88] T. Zhu, Z. Zhong, Y. Gu, T. He, and Z.-L. Zhang, "Leakage-aware energy synchronization for wireless sensor networks," in *Proc. 7th Int. Conf. Mobile Syst. Appl. Services (MobiSys)*, Kraków, Poland, Jun. 2009, pp. 319–332.

[89] Tony, S. Soh, K.-W. Chin, and M. Lazarescu, "Link scheduling in rechargeable wireless sensor networks with harvesting time and battery capacity," in *43rd IEEE Conf. Local Comput. Netw. (LCN)*, Chicago, IL, USA, Oct. 2018, pp. 235–242.

[90] T. Tony, S. Soh, K.-W. Chin, and M. Lazarescu, "Link scheduling in rechargeable wireless sensor networks with imperfect batteries," *IEEE Access*, vol. 7, pp. 104 721–104 736, 2019.

[91] T. Wang and C. G. Cassandras, "Optimal control of multibattery energy-aware systems," *IEEE Trans. Control Syst. Technol.*, vol. 21, no. 5, pp. 1874–1888, Sep. 2013.

[92] T. Tony, S. Soh, K.-W. Chin, and M. Lazarescu, "Link scheduling in rechargeable wireless sensor networks with battery memory effects," in *30th Int. Telecom. Netw. Appl. Conf. (ITNAC)*, Melbourne, Australia, Nov. 2020, pp. 1–8.

[93] T. Tony, S. Soh, K.-W. Chin, and M. Lazarescu, "Link scheduling in rechargeable wireless sensor networks with imperfect batteries and memory effects," *IEEE Access*, vol. 9, pp. 17 803–17 819, 2021.

[94] G. E. Andrews, "The geometric series in calculus," *The American Mathematical Monthly*, vol. 105, no. 1, pp. 36–40, 1998.

[95] T. Dillig, *Mistral SMT Solver*, 2012 (accessed Jul. 30, 2020). [Online]. Available: https://www.cs.utexas.edu/~tdillig/mistral/index.html

[96] I. Dillig, T. Dillig, and A. Aiken, "Cuts from proofs: A complete and practical technique for solving linear inequalities over integers," in *21st Int. Conf. Comput. Aided Verification (CAV)*, Grenoble, France, Jul. 2009, pp. 233–247.

[97] A. Kansal, J. Hsu, S. Zahedi, and M. B. Srivastava, "Power management in energy harvesting sensor networks," *ACM Trans. Embedded Comput. Syst. (TECS)*, vol. 6, no. 4, pp. 32–es, Sep. 2007.

[98] I. Buchmann, *BU-808: How to Prolong Lithium-based Batteries*, 2010 (accessed Feb. 28, 2020). [Online]. Available: https://batteryuniversity.com/learn/article/how_to_prolong_lithium_based_batteries

[99] J. A. Bondy, U. S. R. Murty *et al.*, *Graph Theory with Applications.* Macmillan London, 1976.

[100] T. Tony, S. Soh, K.-W. Chin, and M. Lazarescu, "Link scheduling in rechargeable wireless sensor networks with a dual-battery system," in *IEEE Int. Conf. Commun. (ICC)*, Montreal, QC, Canada, Jun. 2021, pp. 1–6.

[101] X. Liu, M. S. Obaidat, C. Lin, T. Wang, and A. Liu, "Movement-based solutions to energy limitation in wireless sensor networks: State of the art and future trends," *IEEE Netw.*, vol. 35, no. 2, pp. 188–193, 2021.

Every reasonable effort has been made to acknowledge the owners of copyright material. I would be pleased to hear from any copyright owner who has been omitted or incorrectly acknowledged.